Effect of Thiols and Their Aging on Cu Electrodeposition for ULSI Interconnects

Charlie Chunxing Zhi

B.E. Chemical Engineering,
South China University of Technology, Guangzhou, China, 1985
M.S. Chemical Engineering,
South China University of Technology, Guangzhou, China, 1988
M.S. Chemical Engineering,
Oregon State University, Corvallis, Oregon, 1995

A dissertation presented to the faculty of the
OGI School of Science and Engineering
at Oregon Health and Science University
in partial fulfillment of the
requirements for the degree
Doctor of Philosophy
In
Electrical and Computer Engineering

February, 2002

The dissertation "Effect of Thiols and Their Aging on Cu Electrodeposition for ULSI Interconnects" by Charlie Chunxing Zhi has been examined and approved by the following Examination Committee:

Dr. Rajendra Solanki, Thesis Adviser
Professor, Oregon Graduate Institute

Dr. Jack McCarthy
Assistant Professor, Oregon Graduate Institute

Dr. Shankar Rananavare
Associate Professor, Oregon Graduate Institute

Dr. Robert Contolini, Novellus System

TO

My Wife, Qiurong Xu

My Children, Anna and Hudson

Our Parents

Acknowledgements

I would like to express my deepest appreciation to my adviser, Dr. Raj Solanki for his guidance, encouragement, and patient support during the course of this project.

Special thanks to Dr. Rob Contolini for his instruction and in-depth knowledge of electrochemistry to support this project

I also want show my sincere appreciation for Dr. Jack McCarthy and Dr. Dr.Shankar Rananavare for supporting me whenever I asked and reviewing this dissertation.

Special thanks go to Haiming Li, Dr. Jody House, Mike Tidball, and Jinshen Hou for their constant support.

Special thanks also go to Technic Corp. for their generous donation of EG&G M270 Potentiastate instrument. Without this instrument, I can not accomplish this.

Finally, I would like to thank my wife Qiurong Xu and our parents for their support and encouragement of this work. Without them, I don't think I can achieve it.

Table of Contents

ACKNOWLEGEMENTS iv

TABLE OF CONTENTS v

LISTS OF TABLES viii

LISTS OF FIGURES ix

ABSTRACT xvi

Chapter 1 Introduction 1

Reference........ 7

Chapter 2 Copper Electrodeposition for ULSI Interconnects 9

2.1 Copper Electrodeposition Fundamentals 9

2.1.1 Electrochemical Deposition Evolution 9

2.1.2 Electrochemical Deposition Cell 12

2.1.3 Formation of Metal – Solution Interface and Equilibrium Electrode Potential 13

2.2 Kinetics and Mechanism of Electrodeposition 15

2.2.1 Electrochemical Deposition Reaction and Overpotential 16

2.2.2 Relationship between Current and Potential: Butler-Volmer Equation 17

2.2.3 Electrochemical Deposition Kinetic Study 21

2.3 Techniques for study of electrode process and determination of kinetic parameters 22

Reference 25

Chapter 3 The Role of Organic Additives 26

3.1 Common copper electroplating additives and their function 26

3.2 Effect of Additives 32
3.2.1 Effect of Additives on Cu Electrodeposition 32
3.2.2 Effect of Additive on Electrodeposition Superfilling: 36
3.2.3 Effect of Additives on Cu Film Microstructure 37
3.3 Multi-Component Bath Additive characterization 38
Reference 39
Chapter 4 Copper Electrodeposition with Different Thiols 41
4.1 Cu electrodeposition without Organic Additives 41
4.1.1. Electrochemical Characterization of VMS 43
4.1.2. Electrochemical Deposition of Cu and Trench Fill 46
4.1.3. Microstructure of Cu film Electrodeposited without Organic Additives 47
4.2 Cu Electrodeposition with Organic Additives 54
4.2.1 Cu electrodeposition with Cl+PEG+SPS 55
4.2.1.1 Electrochemical Characterization of Cl-PEG-SPS Bath 56
4.2.1.2 Result of Fill Studies of Cl-PEG-SPS Bath 61
4.2.1.3 Microstructure of Cu Film Electroplated with Cl-PEG-SPS Bath 62
4.2.2 Cu Electrodeposition with Cl+PEG+UPS 68
4.2.2.1 Electrochemical Characterization of Cl-PEG-UPS Bath 68
4.2.2.2 Result of Fill Studies of Cl-PEG-UPS Bath 71
4.2.2.3 Microstructure of Cu Film Electroplated with Cl-PEG-UPS Bath 72
4.2.3 Cu Electrodeposition with Cl+PEG+OPX 76
4.2.3.1 Electrochemical Characterization of Cl-PEG-OPX Bath 76
4.2.3.2 Result of Fill Studies of Cl-PEG-OPX Bath 80
4.2.3.3.Microstructure of Cu Film Electroplated with Cl-PEG-OPX Bath 80
4.2.4 Cu Electrodeposition with Cl+PEG+DPS 84
4.2.4.1 Electrochemical Characterization of Cl-PEG-DPS Bath 84

4.2.4.2 Result of Fill Studies of Cl-PEG-DPS Bath 88
4.2.4.3.Microstructure of Cu Film Electroplated with
Cl-PEG-DPS Bath 89
4.2.5 Cu Electrodeposition with Cl-PEG-ZPS 92
4.2.5.1 Electrochemical Characterization of Cl-PEG-ZPS Bath 92
4.2.5.2 Result of Fill Studies of Cl-PEG-ZPS Bath 96
4.2.5.3 Microstructure of Cu Film Electroplated with
Cl-PEG-ZPS Bath 96
4.2.6 Cu Electrodeposition with Cl-PEG-MPS 99
4.2.6.1 Electrochemical Characterization of Cl-PEG-MPS Bath 100
4.2.6.2 Result of Fill Studies of Cl-PEG-MPS Bath 104
4.2.6.3.Microstructure of Cu Film Electroplated with
Cl-PEG-MPS Bath 104
4.3 Mechanism of Thiols 107
4.3.1 Effecs of thiols on the kinetics of Cu electrodeposition 107
4.3.2 Mechanisms from the action of thiols 110
Reference 114
Chapter 5 Influence of Aging of Thiols on Cu Electrodeposition 116
5.1 SPS Degradation Evaluation in Cl-PEG-SPS Bath 116
5.2 UPS Degradation Evaluation in Cl-PEG-UPS Bath 119
5.3 OPX Degradation Evaluation in Cl-PEG-OPX Bath 121
5.4 DPS Degradation Evaluation in Cl-PEG-DPS Bath 123
5.5 ZPS Degradation Evaluation in Cl-PEG-ZPS Bath 125
5.6 MPS Degradation Evaluation in Cl-PEG-MPS Bath 127
5.7 Thiols degradation mechanism in an acid copper electroplating bath 129
Reference 131
Chapter 6 Summary and Conclusions 132
Vita 137

List of Tables

Table 2-1 Relative Standard Electrode Potentials (E^0) with respect to SHE............ 15

Table 4-1 Plating variables for Cu film deposited without organic additives........... 48

Table 4-2 FWHMs of the Cu(111) x-ray diffraction peaks of samples plated under different conditions.. 49

Table 4-3 Roughness and Grain Size of Plated Cu Films.. 52

Table 4-4 Cu electrodeposition reaction kinetic parameters with different thiols... 108

Table 6-1 Roughness of Cu films electrodeposited with various electrolytes......... 133

List of Figures

Fig. 2-1 The evolution chart of copper electroplating 10

Fig. 2-2 Dual damascene process for IC interconnects 12

Fig. 2-3 Cu electrochemical deposition cell 13

Fig. 2-4 Three regions in the general current-overpotential relationship 20

Fig. 3-1 Classification of acid bath additives 27

Fig. 3-2 Brigheners adsorb on the Cu surface and participate in charge transfer reaction 28

Fig.3-3 Brightener stability under different conditions 29

Fig. 3-4 Steady-state current vs. potential for copper deposition in 100 mg/l PEG solution with various molecular weights. 30

Fig.3-5 Cyclic voltammograms of electrodeposition and dissolution of Cu at a Pt electrode in 2M H_2SO_4/0.7M $CuSO_4.5H_2O$ electrolyte. (a) no additive; (b) 10ppm Cl^-; (c) 100 ppm PEG; (d)10 ppm PEG+10 ppm Cl^- 32

Fig. 3-6 Additive surface adsorption behavior 33

Fig. 3-7 Additive effect on *i-E* relationship 35

Fig. 4-1 Linear Sweep Voltammetry (LSV) curves obtained at a rotation speed of 400rpm on a platinum RDE in VMS electrolyte containing 1.8 M H_2SO_4, 0.24 M $CuSO_4$, and 50 mg/l Chloride 44

Fig. 4-2 Tafel plot of Cu electrodeposition without organic additives 45

Fig. 4-3 Cyclic voltammetry curve of additive free copper electrolyte at rotation speed of 400 rpm containing 1.8 M H_2SO_4, 0.24 M $CuSO_4$, and 50 ppm Cl 45

Fig.4-4 Two chronoamperometric transients for deposition at various potentials from the additive-free electrolyte 46

Fig. 4-5 SEM cross section image of fill result from additive free copper electrolyte containing 1.8 M H_2SO_4, 0.24 M $CuSO_4$, and 50 ppm Cl 47

Fig. 4-6 Transmission electron micrographs of the copper films electroplated at a current density of (a) 45 mA/cm^2 and (b) 5 mA/cm^2. In both cases the bath consisted of Cu(g/l)/H^+(g/l)/Cl(mg/l) : 30/250/30 50

Fig. 4-7 AFM views of Cu film surfaces deposited at (a),(b): 45 mA/cm^2 with different bath chemistry, and (c),(d): 5 mA/cm^2 with different bath chemistry, showing the film roughness and grain size difference at two current densities 51

Fig. 4-8 Prediction profile showing the surface roughness dependence on the Cu, acid and Cl concentrations, and the current density. 53

Fig. 4-9 Pareto plot shows the dependence of the surface roughness on the bath parameters and their interactions 53

Fig. 4-10 SPS: Bis-(sodium sulfopropyl)-disulfide(SPS) 56

Fig. 4-11 LVS curves obtained at a rotation speed of 400 rpm on a Pt. RDE in the baths with various combinations of additives. All electrolytes contain 1.8 M H_2SO_4, 0.24 M $CuSO_4$. In addition, the curve labeled Cl^-: 50 ppm Cl^-. PEG: 300 ppm PEG (M.W.4600); SPS: 6 ppm SPS 58

Fig. 4-12 Tafel plot of Cu electrodeposition with various organic additives 58

Fig. 4-13 Cyclic Voltammetry curves of Cl-PEG-SPS electrolyte. The base electrolyte contains 1.8 M H_2SO_4, 0.24 M $CuSO_4$, and 50 ppm. of Cl..... 59

Fig. 4-14 A series of chronoamperometric curves for various electrolytes under overpotential of –0.15 V vs. Ag/AgCl 60

Fig. 4-15 A series of chronoamperometric curves for various electrolytes under overpotential of –0.20 V and –0.25 V vs. Ag/AgCl................................. 61

Fig. 4-16 SEM cross sections of vias deposited with (a) PEG only, (b) PEG/Cl only. The base electrolyte composition is 1.8 M H_2SO_4, 0.24 M $CuSO_4$, 50 ppm Cl- , and 300 ppm PEG (Mw 4600). 62

Fig. 4-17 Fill result of SPS at 12ppm. The base electrolyte composition is 1.8 M H_2SO_4, 0.24 M $CuSO_4$, 50 ppm Cl, 300 ppm PEG (MW: 4600) and

	(a) 12 ppm SPS; (b) 2 ppm SPS. ... 63
Fig. 4-18	Resistance transients during aging of 1 um Cu films at room temperature ... 64
Fig. 4-19	X-ray diffraction pattern of Cu film electrodeposited from VMS, Cl-PEG, and Cl-PEG-SPS bath. ... 65
Fig. 4-20	AFM image of Cu film electrodeposited from VMS ... 66
Fig. 4-21	AFM image of Cu film electrodeposited from Cl-PEG bath. ... 67
Fig. 4-22	AFM image of Cu film electrodeposited from Cl-PEG-SPS bath. ... 67
Fig. 4-23	UPS: 3-[(Amino-iminomethyl)-thio]-1-propanesulfonic acid ... 68
Fig. 4-24	LVS curves obtained at a rotation speed of 400 rpm on a Pt. RDE in the baths with various combinations of additives. All electrolytes contain 1.8 M H_2SO_4, 0.24 M $CuSO_4$. In addition, the curve labeled Cl^-: 50 ppm Cl^-. PEG: 300 ppm PEG (MW.4600); SPS: 6 ppm SPS; ... 69
Fig. 4-25	Tafel plot for Cu electrodeposition in electrolytes with various organic additives ... 70
Fig. 4-26	CV curves obtained at a rotation speed of 400 rpm on a Pt. RDE in the baths with various combination of additives. All electrolytes contained 1.8 M H_2SO_4, 0.24 M $CuSO_4$. The curve labeled Cl^-: 50 ppm Cl^-; PEG: 300 ppm PEG (MW.4600); SPS: 6 ppm SPS ... 71
Fig. 4-27	A series of chronoamperometric curves for various electrolytes under overpotential of –0.15 V vs. Ag/AgCl ... 72
Fig. 4-28	Fill result of UPS. The base electrolyte contains 1.8 M H_2SO_4, 0.24 M $CuSO_4$, 50 ppm Cl, 300 ppm PEG (MW = 4600), (a) 6 ppm UPS; (b) 12 ppm UPS ... 73
Fig. 4-29	Resistance transients during aging of 1 um Cu films at room temperature. ... 74
Fig. 4-30	X-ray diffraction pattern of Cu films electrodeposited from Cl-PEG-UPS bath ... 74
Fig. 4-31	AFM image of Cu film electrodeposited from Cl-PEG-UPS bath ... 75
Fig. 4-32	OPX: (O-Ethyldithiocarbonato)-S-(3-sulfopropyl)-ester, potassium salt. 76

Fig.4-33 LVS curves obtained at a rotation speed of 400 rpm on a Pt RDE in the baths with various combinations of additives. All electrolytes contain 1.8 M H_2SO_4, 0.24 M $CuSO_4$. In addition, the curve labeled Cl^-: 50 ppm Cl^-; PEG: 300 ppm PEG (MW.4600); OPX: 6 ppm OPX 77

Fig. 4-34 Tafel plot of Cu electrodeposition with various electrolytes including OPX 78

Fig. 4-35 Hysteresis curves obtained at a rotation speed of 400 rpm on a Pt. RDE in the bath with various combinations of additives. All electrolytes contain 1.8 M H_2SO_4, 0.24 M $CuSO_4$. In addition, the curve labeled Cl^- has 50 ppm Cl^-. PEG: 300 ppm(MW.4600); SPS or OPX: 6 ppm SPS or OPX 79

Fig. 4.36 Chronoamperometric curves of electrolytes with various combinations of additives under –0.15 V overpotential vs. Ag/AgCl 80

Fig. 4-37 Chronoamperometric curves of electrolytes with various combination of additives under –0.25 V overpotential vs. Ag/AgCl 80

Fig. 4-38 Trench fill result of Cl+PEG+OPX electrolyte with (a) 6 ppm OPX; (b) 12 ppm OPX 81

Fig. 4-39 Resistance transients during aging of 1 um Cu films at room temperature. 82

Fig. 4-40 X-ray diffraction pattern of Cu film electrodeposited from Cl-PEG-OPX bath. 83

Fig. 4-41 AFM image of Cu film electrodeposited from Cl-PEG-OPX bath. 83

Fig. 4-42 DPS: N,N-Dimethyldithiocarbamic acid (3-sulfopropyl) ester, sodium salt 84

Fig. 4-43 LSV curve of electrolytes with various combinations of additives including DPS 85

Fig. 4-44 Tafel plot of Cu electrodeposition with various additives including DPS 85

Fig. 4-45 Hysteresis curves of electrolytes with various combinations of organic additives including DPS 86

Fig. 4-46 Chronoamperometric curves of electrolytes with various combinations of additive under –0.15 V overpotential vs. Ag/AgCl 87

Fig. 4-47 Chronoamperometric curves of electrolytes with various combinations of additives under –0.25 V overpotential vs. Ag/AgCl 88

Fig. 4-48 Via fill result of Cl-PEG-DPX electrolyte with 6ppm DPS 89

Fig. 4-49 Resistance transients during aging of 1 um Cu films at room temperature 90

Fig. 4-50 X-ray diffraction pattern of Cu film electrodeposited from Cl-PEG-DPS bath 90

Fig. 4-51 AFM image of Cu film electrodeposited from Cl-PEG-DPX bath 91

Fig. 4-52 ZPS: of 3-(2-Benzthiazolylthio)-1-propanesulfonic acid, sodium salt 92

Fig. 4-53 LSV curves of electrolytes with various combinations of organic additives including ZPS. 93

Fig. 4-54 Tafel plot of Cu electrodeposition with various combinations of organic additives including ZPS 93

Fig. 4-55 Hysteresis curves of electrolytes with various combinations of organic additives including ZPS 94

Fig. 4-56 Chronoamperometric curves of electrolytes with various combinations of additives under –0.15 V overpotential vs. Ag/AgCl 95

Fig. 4-57 Chronoamperometric curves of electrolytes with various combinations of additives under –0.25 V overpotential vs. Ag/AgCl 95

Fig. 4-58 Fill result of Cl-PEG-ZPS bath with 6ppm ZPS 96

Fig. 4-59 Resistance transients during aging of 1 um Cu films at room temperature 97

Fig. 4-60 X-ray diffraction pattern of Cu film electrodeposited from Cl-PEG-ZPS bath. 98

Fig. 4-61 AFM image of Cu film electrodeposited from Cl-PEG-ZPX bath. 99

Fig. 4-62 MPS: 3-Mercaptopropane sulfonic acid, sodium salt 99

Fig. 4-63 Polarization curves of electrolytes with various combinations of organic additives including MPS 100
Fig. 4-64 Tafel plot of Cu electrodeposition with various combinations of organic additives including MPS. 101
Fig. 4-65 Hysteresis curves of electrolytes with various combinations of organic additives including MPS 102
Fig. 4-66 Chronoamperometric curves of electrolytes with various combinations of additives including MPS under –0.15 V overpotential vs. Ag/AgCl...... 103
Fig. 4-67 Chronoamperometric curves of electrolytes with various combinations of additives including MPS under –0.25 V overpotential vs. Ag/AgCl.. 103
Fig. 4-68 Fill result of Cl-PEG-MPS bath with 6ppm MPS........ 104
Fig. 4-69 Resistance transients during aging of 1 um Cu films at room temperature........ 105
Fig. 4-70 X-ray diffraction pattern of Cu film electrodeposited from Cl-PEG-MPS bath........ 106
Fig. 4-71 AFM image of Cu film electrodeposited from Cl-PEG-MPS bath......... 106
Fig. 5-1 Influence of aging of 12 ppm SPS on the current-potential curves at Pt RDE. The base solution contained 1.8 M H_2SO_4, 0.24 M $CuSO_4$, 50 ppm Cl, and 300ppm PEG (MW 4600) 118
Fig. 5.2 Influence of aging of 12 ppm SPS on the chronoamperometry curves at Pt RDE. The base solution contained 1.8 M H_2SO_4, 0.24 M $CuSO_4$, 50 ppm Cl, and 300ppm PEG (MW 4600) 119
Fig. 5.3 Influence of aging of 12 ppm UPS on the current-potential curves at Pt RDE. The base solution contained 1.8 M H_2SO_4, 0.24 M $CuSO_4$, 50 ppm Cl, and 300ppm PEG (MW 4600) 120
Fig. 5.4 Influence of aging of 12 ppm UPS on the chronoamperometry curves at Pt RDE. The base solution contained 1.8 M H_2SO_4, 0.24 M $CuSO_4$, 50 ppm Cl, and 300ppm PEG (MW 4600) 121
Fig. 5-5 Influence of aging of 12 ppm OPX on the current-potential curves at Pt RDE. The base solution contained 1.8 M H_2SO_4, 0.24 M $CuSO_4$,

50 ppm Cl, and 300ppm PEG (MW 4600) 122

Fig. 5-6 Influence of aging of 12 ppm OPX on the chronoamperometry curves at Pt RDE. The base solution contained 1.8 M H_2SO_4, 0.24 M $CuSO_4$, 50 ppm Cl, and 300ppm PEG (MW 4600) 123

Fig. 5-7 Influence of aging of 12 ppm DPX on the current-potential curves at Pt RDE. The base solution contained 1.8 M H_2SO_4, 0.24 M $CuSO_4$, 50 ppm Cl, and 300ppm PEG (MW 4600) 124

Fig. 5-8 Influence of aging of 12 ppm DPX on the chronoamperometry curves at Pt RDE. The base solution contained 1.8 M H_2SO_4, 0.24 M $CuSO_4$, 50 ppm Cl, and 300ppm PEG (MW 4600) 125

Fig. 5-9 Influence of aging of 12 ppm ZPS on the current-potential curves at Pt RDE. The base solution contained 1.8 M H_2SO_4, 0.24 M $CuSO_4$, 50 ppm Cl, and 300ppm PEG (MW 4600) 126

Fig. 5-10 Influence of aging of 12 ppm ZPS on the chronoamperometry curves at Pt RDE. The base solution contained 1.8 M H_2SO_4, 0.24 M $CuSO_4$, 50 ppm Cl, and 300ppm PEG (MW 4600) 127

Fig. 5-11 Influence of aging of 12 ppm MPS on the current-potential curves at Pt RDE. The base solution contained 1.8 M H_2SO_4, 0.24 M $CuSO_4$, 50 ppm Cl, and 300ppm PEG (MW 4600) 128

Fig. 5-12 Influence of aging of 12 ppm MPS on the chronoamperometry curves at Pt RDE. The base solution contains 1.8 M H_2SO_4, 0.24 M $CuSO_4$, 50 ppm Cl, and 300ppm PEG (MW 4600) 129

ABSTRACT

Effect of Thiols and Their Aging on Cu Electrodeposition for ULSI Interconnects

Charlie Chunxing Zhi, B.S, M.S.

Ph. D., Oregon Graduate Institute of Science and Technology

February, 2002

Thesis Professor: Dr. Rajendra Solanki

Six model thiols, Bis-(3-Sulfopropyl)-disulfide sodium salt (SPS), 3-Mercapto-1-propanesulfonic sodium salt (MPS), (O-Ethyldithiocarbonato)-s-(3-sulfoproplyl)-ester potassium salt(OPX), 3-S-Isothiuronium Propyl Sulfonate(UPS), N, N-Dimethyl-dithiocarbamylpropyl sulfonic sodium salt (DPS), and 3-(Benzothiazolyl-2-mercapto)-propyl-sulfonic sodium salt (ZPS) in an acid-copper plating bath containing chloride ions and polyethylene glycol (PEG) have been systematically evaluated and characterized by electrochemical method and by fill study. These thiols that all have a common thiol and disulfide group ($-SCH_2CH_2CH_2SO_3$) that are commonly used for printed circuit board (PCB) plating baths were evaluated as potential accelerating elements for ULSI Cu plating.

The electrochemical analytical methods employed include linear sweep voltammetry(LSV), chronoamperometry(CA), and cyclic voltammetry (CV) on a rotating disk electrode. Examination of the i-E deposition characteristics of these electrolytes showed that in all cases an analysis of LSV, CA, and CV gives consistent estimates of thiol acceleration capability in an acid copper bath and supplements to one another. It revealed a hysteresis response associated with the acceleration capability of electrolytes containing SPS, OPX, DPS, and MPS that can be employed to monitor and explore

additive efficacy and consumption. In contrast, electrolyte containing UPS and ZPS showed no i-E hysteresis characteristics and retarded copper deposition. Superconformal electrodeposition was observed for a successful trench fill with electrolyte containing SPS.

Thiols are well known for their unstable nature in a plating bath. Examination of i-E characteristics of electrodeposition indicated that DPS and MPS degrade slower than other thiols. The accelerating characteristics of all these thiols disappeared in sixteen days.

Cu film microstructure can be influenced by many factors. This investigation showed organic additives have dominating influence on the film microstructure and self-annealing property. The films deposited from electrolyte containing SPS, UPS, OPX, and DPS exhibited spontaneous recrystallization at room temperature that resulted in a resistivity drop within a few hours of deposition. In contrast, film electrodepositied from ZPS bath showed little resistivity drop and had similar behavior as Cu film from Cl-PEG electrolyte. Microstructure of stabilized Cu films showed that the texture of electroplated Cu film was predominantly (111) oriented. Film roughness was strongly affected by the electrolyte additives, followed by plating current density.

CHAPTER ONE

INTRODUCTION

As devices scale down to deep submicron dimensions, the signal propagation is dominated not by transistor switching speed, but by interconnection performance. The performance of interconnection is dependent on its resistance and capacitance. In order to increase signal propagation speed, low resistivity metallization materials play very important roles in the ultralarge scale integration (ULSI) metallization [1].

Why copper electroplating and how electroplating is integrated in device fabrication

The advantages of Cu relative to Al(Cu) for chip wiring, which include lower resistance, higher allowed current density, and increased scalability[1,2,3], have long been recognized. Copper metallization of chips has thus been the subject of intense investigation for more than a decade [2,4,5]. Copper could be deposited by most conventional methods such as physical vapor deposition (PVD) and chemical vapor deposition (CVD). However, a simple method of electrochemical plating could be used to deposit Cu film as well. This plating technique that includes electroplating and electroless plating has several advantages compared to PVD and CVD due to its low cost, high throughput, low processing temperature, and excellent via/trench filling capability [1]. Electroplating in comparison with electroless deposition is more stable and easy to control. Therefore, electroplating is becoming the leading technique in copper metallization for ULSI interconnection.

In 1997, IBM published results [2] from fully integrated devices with Cu interconnects that showed a 40-45% drop in the resistance of Cu wiring compared to Al(Cu) wiring, and a substantial improvement in electromigration resistance. The transition from Al to Cu interconnects is underway or in development at most major microelectronic companies. The switch from Al to Cu is driven not only by factors such as speed and reliability improvement of semiconductor devices, but use of dual-damascene process which reduces multilevel interconnect fabrication steps by 30%, hence reduced costs as compared to conventional Al-based interconnects [6].

In order for a metal or alloy to be deposited on the surface of a wafer by electroplating, it is first necessary to cover the surface with a seed layer, or plating base, whose function is to conduct the current from a contact at the wafer edge to all points on the wafer where a deposit is desired. The requirement of a seed layer has led to a variety of approaches for the integration of plating. Among these approaches, damascene electroplating is ideally suited for the fabrication of interconnect structures, since it allows inlaying of metal simultaneously in via holes and overlying line trenches [7] by a process called dual damascene. Further, it is compatible with the requirement for a barrier layer between the seed layer and the insulator. The barrier prevents interaction between the metal and the insulator [8]. Further discussion will be present in Chapter 2 for this technique.

Profile evolution in damascene copper plating – Superfilling

The foremost requirement for success of the plating process (as well as for any other process of potential use in the fabrication of damascene copper interconnects) is its ability to fill trenches, vias, and their combinations completely, without any voids or seams. How does electroplating make it possible to obtain void-free and seamless deposits?

A conventional solution for Cu electroplating contains several electrolytes and additives. The roles that these electrolytes and additives play are to control plating process and obtain good deposition quality [1]. There are two possible ways for a profile

of plated copper to evolve in time. In conformal plating, a deposit of equal thickness at all points of a feature leads to the creation of a seam, or, if the shape of the feature is reentrant, a void. For a defect-free filling, a higher deposition rate in the bottom than on the sides of the feature is desired. This mode of plating can be accomplished by the use of additives in the plating bath. The term superfilling, or "bottom-up filling', or "superconformal filling", is used to describe this phenomena. Superfilling produces void-free and seamless deposits inside lithographically defined cavities with vertical walls and high aspect ratios [9]. Electroplating without additives produces conformal plating. The mechanism for copper deposition in the absence of additives has been extensively investigated and generally accepted for some time. A two-step process model has been proposed for copper deposition mechanism without additives, in which the cupric-to-cuprous-ion reduction step is rate controlling for high current densities [10]. However, the understanding for the mechanism of additives, especially superfilling is lacking.

Cu electroplating additives and their understanding

The organic additives in acid copper plating bath are normally categorized into "carrier", "brightener", and "leveler". For acid copper electrodeposition, carriers, sometimes called "suppressors", are usually polyethylene glycols, used alone with chloride to inhibit the deposition reaction. Brighteners, also called "accelerators or anti-suppressors" are often molecules with thiol and disulfide bonds and sulfonic acid groups, while levelers are molecules typically having amine functionality. More discussion of organic additives is presented in Chapter 3.

The successful implementation of copper electroplating technology in ULSI derives from the use of electrolyte additives to affect the local deposition rate, thereby allowing superfilling of trenches and vias in the damascene process. Commercial acid-copper plating baths contain many organic additives [11]. However, detailed knowledge of the function of each additive, as well as the interactions between these additives, is lacking despite the advanced state of the technology. The complexity of the bath

chemistry, coupled with the incomplete understanding of the mechanisms, makes theoretical predictions of the efficacy of an electrolyte difficult with an arbitrary composition [12]. Since electrolyte bath additives are commonly used for the production of thin copper films for printed circuit board (PCB) applications, an empirical understanding of additives for copper deposition does exist.

The first description of this superfilling process was adopted from the theory of additive-induced leveling whereby the electrolyte additives adsorb at the metal electrolyte interface, reducing the active area and inhibiting the metal reduction process [10]. Since the inhibitor concentration is dilute (10^{-3} to 10^{-6} mol/L) the adsorption process is typically considered to be diffusion limited while the copper deposition process proceeds under interfacial charge-transfer control. In order to maintain transport control of the inhibitor flux, the adsorbate must either be incorporated in the growing film or undergo reductive desorption during metal deposition. For the damascene process, the trench or via geometry results in a lower flux of the inhibitor to the bottom of the features than on the external surface. Consequently, the metal deposition kinetics proceeds more rapidly at the bottom of the trench, which results in super-conformal filling. This model also predicts that the slowest growth occurs at the edge demarcating the entrance of the trench or via where the inhibitor flux is expected to be greatest. However, the complexity of additive-electrode interaction was recently highlighted by the observation of "overfill" where the originally concave surface profile becomes convex due to a sustained differential rate of metal deposition that can not be rationalized by the transport-limited inhibition model. Rather, this observation has focused attention on the competition between species that accelerate versus suppress deposition in the multicomponent additive packages, thereby demonstrating the need for detailed information concerning the surface chemistry of copper in solutions containing additives [13].

Another study has dealt with the effect of chloride ions acting alone on copper deposition. Some have proposed that chloride ions affect the behavior of the cuprous intermediates through complexing [11]. J. Kelly and A.C.West [12] studied the mode of action of PEG and chloride ions together, which are often incorporated into industrial plating baths. This work suggested that the adsorption of approximately a monolayer of

spherically packed PEG molecules when chloride ions are present, which inhibits the deposition reaction for cathodic overpotenials. It concluded that adding chloride alone promotes the deposition reaction, while adding PEG alone has a relatively small effect on electrode kinetics.

In addition to influencing the kinetics of metal reduction, electrolyte additives are also known to exert a dramatic effect on the metallurgical microstructure. Specifically, certain additives sharply inhibit epitaxial growth, leading to fine-grained deposits and incorporation of the additives and/or the corresponding breakdown products as impurities within the film [13].

Superfill study for ULSI electroplating

One of the difficulties associated with studying superconformal or superfilling electrodeposition has been the proprietary nature of the chemistry and processing parameters employed throughout the industry. Nonetheless, a brief survey of the literatures suggests that electrolyte formulations that have previously been used for plating throughholes in printed circuit boards may be an effective starting point for exploring submicrometer superconformal deposition [13]. The first complete report of the chemistry and processing conditions used to demonstrate "superfill" in submicrometer dimensions was published in 1999 [14]. The bath chemistry is based on the polyethylene glycol(PEG), thiol[(bits-(3-sulfopropyl) disulfide(SPS)], chloride ions, and diethyl safranine azo dimethyl aniline(Janus Green B) that stems from the patent literature for printed circuit board (PCB). A following report published recently discusses a possible screening and characterizing method as applied to an acid-copper electrolyte package based on this additive cocktail [10]. The second report of the chemistry for the superconformal deposition was published recently for filling a wide range of feature sizes and aspect ratios by using a polyether(polyethylene glycol, PEG), thiol (3-mercapto-1-propanesulfonate, MPSA), and chloride(Cl) electrolyte [13]. Complete filling was observed with this additive package for films grown

potentionstatically in a regime corresponding to mixed kinetic/diffusion control for copper deposition.

The main difference between above two published electrolyte packages with superconformal deposition characteristic is the accelerating agent, also called thiol. Thiols are important additive agents that dictate the superfilling property of an additive package. There are a few commonly used thiols for printed circuit board acid plating bath. However, a systematic evaluation of these thiols for their superfilling characteristics, deposition kinetics, and other effects on ULSI interconnect wiring is lacking. As technology node advances toward 0.1um and below, if electrochemical technology is to remain applicable to fabrication on smaller length scales or very high aspect ratios gaps, further understanding of these thiols is essential to meet the ever-challenging gapfill demand.

The aim of this research was to systematically study all commonly used thiols in a Cl-PEG-Thiol additive package and exam their influence on Cu film microstructure and their aging behavior. The superfilling characteristic of the electrolyte was evaluated by using a rotating disk electrode. Trench and via filling were examined for each additive package. The correlation of i-E measurements of inhibition with superfilling deposition was assessed. The electrodeposition reaction kinetic parameters were extracted from electrochemical characterization of each thiol package, which can be applied to modeling and theoretical prediction of electroplating and its filling capability. These experiments were complemented by resistivity, texture, roughness and grain size measurements of blanket films that provided a preliminary assessment of the extent of thiol's influence on the film microstructure. Finally, this research focused on thiol's aging characteristic.

This thesis contains six chapters including this introduction. In chapter 2, the fundamentals of electrochemical deposition of Cu for ULSI interconnects are discussed. The role of organic additive and electrochemical characterization are described in chapter 3. In chapter 4, the experimental results of electrochemical deposition with different thiols in a multi-components bath are presented. Chapter 5 presents the impact of thiol's aging on Cu electrochemical deposition. Summary and conclusions are presented in chapter 6.

References

[1] W.C. Gau, T.C. Chang. "Copper electroplating for future ultralarge scale integration interconnection," J. Vac. Sci. Technol. A 18(2), 2000, p.656.

[2] D. Edelstein, J. Heidenreich, R. Goldblatt, et al. "Full copper wiring in a sub-0.25 micro-m CMOS ULSI technology," Technical Digest, IEEE International Electron Devices Meeting, 1997, p.773.

[3] D. Edelstein, G.A. Sai-Halasz, Y.J. Mii, "VLSI on-chip interconnection performance simulations and measurements," IBM J. Res. Develop., 39, 1995, p.383.

[4] B. Luther, J.F. White. "Planar copper-polyimide back end of the line interconnections for ULSI devices," Proceeding of the 10th International IEEE VLSI Multilevel Interconnection Conference, 1993, p.15

[5] C.K. Hu, M.B. Small, F. Kaufman, D.J. Pearson. "Copper-polyimide wiring technology for VLSI circuits," Proceeding of the MRS Symposium on VLSI V, 1990, p. 225.

[6] J. Reid, S. Mayer, "Factors influencing fill of IC features using electroplated copper," Advanced Metallization Conf. 1999 Proceedings, MRS, Warrendale, PA, pp. 53-62.

[7] M.M. Chow, J.E. Cronin, "Method for producing coplanar multi-level metal/insulator films on a substrate and for forming patterned conductive lines simultaneously with stud vias," U.S. Patent 4,789,648, December 6, 1988.

[8] C.K. Hu, J.M.E Harper. "Copper interconnections and reliability," Mater. Chem. Phys. 52, 1998, p.5.

[9] P.C. Andricacos, C. Uzoh, J.O. Dukovic, J. Horkans, H. Deligianni. "Damascene copper electroplating for chip interconnections," IBM J. Res. Develop., 42(5), 1998, p.567.

[10] P. Taephaisitphongse, Y. Cao, A.C.West. "Electrochemical and fill study of a multicomponent additive package for copper deposition," J. Electrochem. Soc., 148(7), 2001, pp.492-497.

[11] J. Kelly, C. West, "Copper deposition in the presence of polyethylene glycol, I. quartz crystal microbalance study," J. Electrochem. Soc., 145 (10), 1998, pp.3472–3476.

[12] J. Kelly, A. West. "Copper deposition in the presence of polyethylene glycol II. electrochemical impedance spectroscopy," J. Electrochem. Soc., 45 (10), 1998, pp.3477-3481.

[13] T.P. Moffat, J.E. Bonevich, W.H. Huber, et al. "Superconformal electrodeposition of copper in 500-90 nm features," J. Electrochem. Soc., 147 (12), 2000, pp.4524-4535.

[14] J. Kelly, A. West. "Leveling of 200 nm features by organic additives," Electrochemical and Solid-State Letters, 2 (11), 1999, pp.561-563.

CHAPTER TWO

COPPER ELECTRODEPOSITION FOR ULSI INTERCONNETS

To characterize the impact of thiols on electrochemical deposition, it is necessary to understand electrodeposition mechanism and reaction kinetics first. Thiols can be characterized and analyzed by electrochemical method, and their functions can be explained based on electrochemical deposition mechanism. In this chapter, the history and fundamentals of electrochemical deposition are first reviewed. Electrochemical deposition reaction kinetics is then discussed. Finally, the common electrochemical characterization methods are reviewed for reaction kinetic study and electrodeposition characterization.

2.1 Copper Electrodeposition Fundamentals

2.1.1 Electrochemical Deposition Evolution:

For a better understanding of electrochemical deposition and its evolution towards ULSI Interconnect application, a brief review of electrochemical deposition history would be a good start. An overview of a scientific subject must include at least two parts: retrospect (history) and the present status. Acid copper deposition was referred to as early as 1810 [1]. The evolution chart of copper electroplating is shown in fig. 2.1

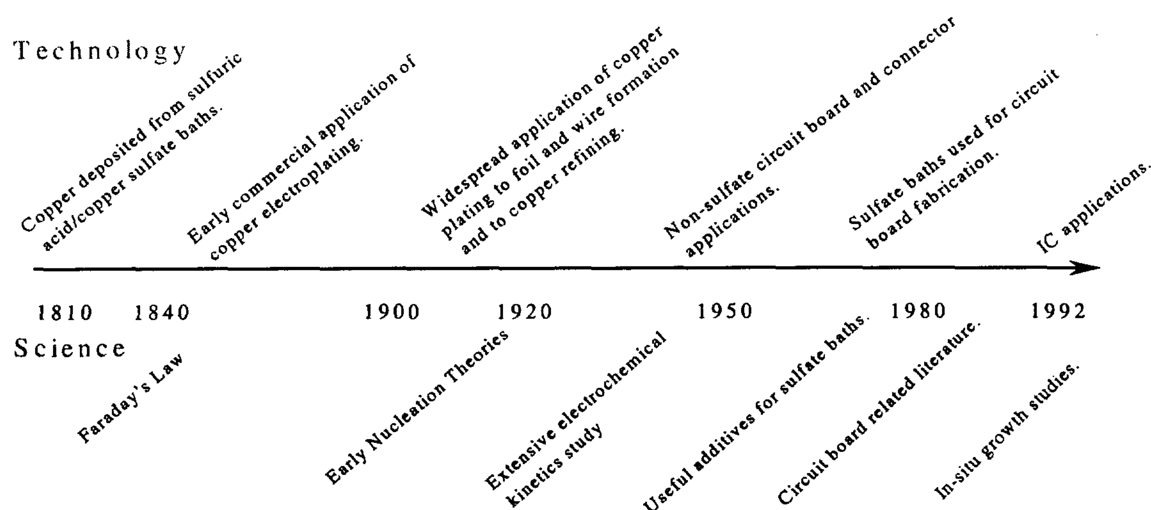

Fig. 2.1 The evolution chart of copper electroplating

This history chart can be divided into three periods:

1905 – 1935: The linear relationship between the overpotential η and log i (logarithm of the current density) was experimentally established in 1905 by Tafel:

$$\eta = a + b \log i \qquad (2.1)$$

Where *a* and *b* are constants.

Erdey-Gruz and Volmer derived the current-potential relationship in 1930 using the Arrhenius equation for the reaction rate constant and introduced the transfer coefficient. Detail of this relationship is discussed in chapter three.

1935 –1965: Work on the development of the modern theory of the electrochemical activation energy (overpotential) started about 30 years after Tafel's formulation of Eq. (2. 1). Frank and Burton [1] realized that the real crystal surfaces (substrates for deposition) have imperfections and a variety of crystal growth sides. This consideration introduced a major change in the theoretical interpretation of deposition process and resulted in a series of new models.

1965 – 1997. Damjanovic et al., [1] treated the optical determination of mechanism of lateral and vertical step propagation. Dickson et al., [1] Studied the nucleation and growth of electrodeposited gold on surfaces of silver by means of electron microscopy.

Rynders and Alkire [1] studied propagation of copper microsteps on platinum surfaces using in situ atomic force microscopy.

Since 1997, there has been an upsurge of interest in electrochemical deposition mainly due to three new technologies: (1) metal deposition for fabrication of integrated circuits, (2) deposition for magnetic recording devices (heads, disks), and (3) deposition of multilayered structures. Electrochemical deposition for integrated circuits can be achieved through either electroless or electrodeposition.

Electrodeposition of Cu for IC fabrication has been successfully used since 1997 for the production of interconnect lines down to 0.20um width. The advantages of Cu relative to Al(Cu) for chip wiring, which include lower resistance, higher allowed current density, and increased scalability have long been recognized [2]. Copper metallization of chips has thus been the subject of intense investigation for more than a decade. In 1989, IBM first demonstrated damascene copper electroplating for chip interconnects [3]. In 1997, IBM published results from fully integrated devices with Cu interconnections. The technology that revolutionized the IC industry is called Dual Damascene process as shown in fig. 2.2. Damascene plating involves deposition of the seed layer over a patterned material, which, in the case of interconnect structures is an insulator. The plated metal covers the entire surface; excess metal must be removed by a planarization step such as chemical-mechanical polishing (CMP).

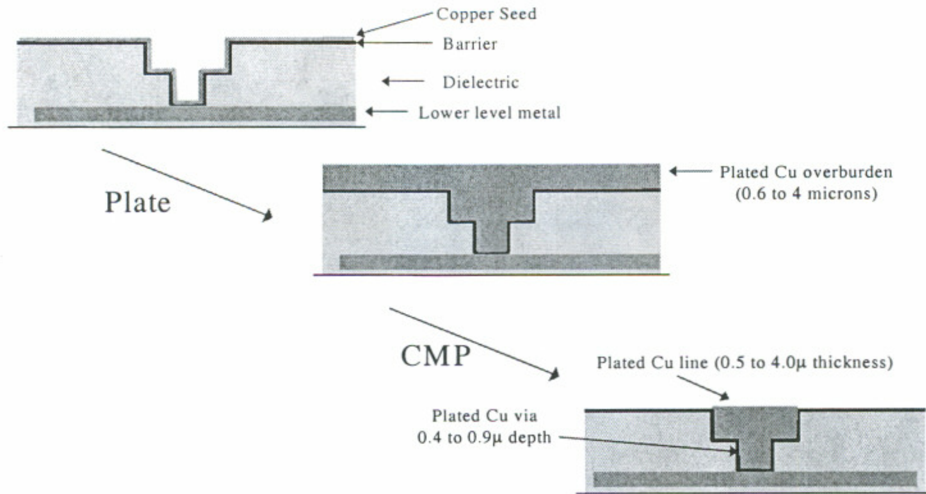

Figure 2.2. Dual Damascene Process for IC interconnects

2.1.2 Electrochemical Deposition Cell

Electrochemical deposition of metals and alloys involves the reduction of metal ions from aqueous, organic, and fused-salt electrolytes. The reduction of metal ions M^{z+} in aqueous solution is represented by

$$M^{z+}_{solution} + ze \rightarrow M_{lattice} \qquad (2.2)$$

This can be accomplished via two different processes: (1) an electrodeposition process in which z electrons (e) are provided by an external power supply and (2) electroless (autocatalytic) deposition process in which a reducing agent in the solution is the electron source (there is not external power supply involved).

There are four types of fundamental subjects involved in the process represented by Eq. (2.2): (1) metal-solution interface as the locus of the deposition process; (2) kinetics and mechanism of the deposition process; (3) nucleation and growth processes of the metal lattice ($M_{lattice}$); and (4) structure and properties of the deposits. A brief review of electrochemical deposition process kinetics and mechanism for Cu electrochemical deposition is the focus of this chapter.

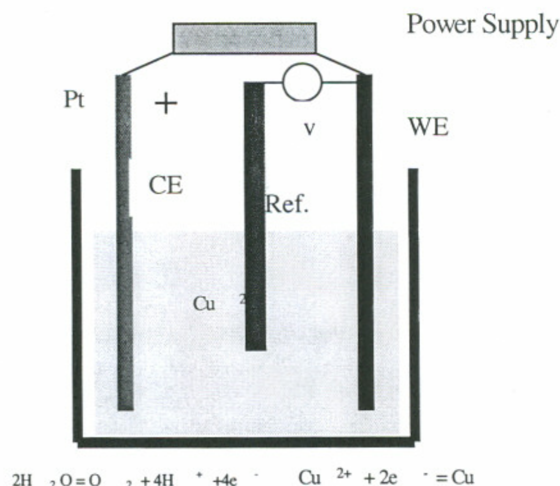

Fig.2.3. Cu electrochemical deposition cell

The basic components of an electrodeopsition cell are, as shown in Fig. 2.3, two metal electrodes (Pt and Cu), water containing dissolved ions, and two metal/solution interfaces: Pt/Solution and Cu/Solution. Successful use of this cell for electrodeposition in the production of desired properties depends on understanding of each component, specifically, components of the metal-solution interface. The metal-solution interface is the locus of the electrodeposition process and thus the most important component of an electrochemical cell. In this research, a standard three-electrode cell with a copper counter electrode and a saturated Ag/AgCl electrode was used for all the i-E measurement. Deposition of patterned wafer coupons was carried out in a modified Hull cell with current waveform controlled by a HP wave generator.

2.1.3 Formation of Metal – Solution Interface and Equilibrium Electrode Potential

When a metal M is immersed in an aqueous solution of its salt MA, there will be an exchange of metal ions M+ at the metal-solution interface (physical boundary). This exchange will cause a charging on the metal side of the interface. In response to this charging, there is a rearrangement of charges on the solution side of the inter-face. In this

case the two sides of the interface acquire opposite and equal charge and reach the equilibrium. The interface region is neutral.

Four models of charge distribution in the solution side of the interface are proposed: Helmholtz, Gouy-Champman, Stern, and Grahame models. The simplest model of the structure of the metal-solution interface is the Helmholtz compact double-layer model (1879). According to this model, all the excess charge on the solution side of the interface is lined up in the same plane at a fixed distance away from the electrode. All excess charge on the metal is located on the metal surface. Grahame modified all other three models by introducing the inner plane of closest approach (IHP; inner Helmholtz plane). IHP is the plane of centers of partially or fully dehydrated, specifically adsorbed ions. The closest approach of the fully hydrated ions is at plane called the outer plane of closest approach (OHP; out Helmholtz plane). The fully hydrated ions cannot approach the electrode closer than the OHP. The OHP is the plane of centers of hydrated ions. Grahame's model differs from the previous models because it involves two distinct planes of closest approach, while only one such plane was postulated by Stern and Helmholtz [1]. Graham's model is widely accepted and used.

The electrical field in the metal-solution interface double layer is very high (eg 10^6 or 10^7 V/cm). Electrodeposition process occurs in this very thin region, where there is a very high electric field. Thus the basic characteristics of the electrodeposition processes are that they proceed in a region of high electric field and that this field can be controlled by an external power source. Rate of deposition varies with the potential and structure of the double layer.

Potential difference across an interface is important for electrodeposition study. There are two types of electrode potentials: metal/metal-ion and red/ox potentials. We can only measure the potential difference when they are two terminals. So it requires two electrodes for a potential difference measurement and this forms an electrochemical cell. The equilibrium potential of an electrode (e.g., M/M^{z+}) is defined as the voltage of the cell, for example, $Pt|H_2(1atm)|H^+(a=1)||M^{z+}|M$, with "a" reference electrode of Pt/H_2, where a stands for activity. There are four types of reference electrodes: hydrogen (0V), calomel (+0.268V), silver-silver chloride (+0.223V), and mercury-mercurous sulfate

electrodes (+0.796V). When standard hydrogen electrode (SHE) is chosen as the reference electrode, the measured cell potential difference is called the relative standard electrode potential and is denoted as E^0. Standard electrode potentials of commonly used materials at 25°C are listed in Table 2.1

In general, an electrode with lower electrode potential will reduce ions of an electrode with higher electrode potential. Or, a high positive standard electrode potential indicates a strong tendency toward reduction; a low negative standard electrode potential indicates a strong tendency toward the oxidized state.

Table 2.1. Relative Standard Electrode Potentials (E^0) with respect to SHE

Reaction	Potential
$Au^+ + e^- = Au$	1.68
$O_2 + 4H^+ + 4e^- = 2H_2O$	1.229
$Pt^{2+} + 2e^- = Pt$	1.2
$Ag^+ + e^- = Ag$	0.799
$Cu^{2+} + 2e^- = Cu$	0.345
$Pb^{2+} + 2e^- = Pb$	-0.126
$Sn^{2+} + 2e^- = Sn$	-0.134
$Ni^{2+} + 2e^- = Ni$	-0.23
$Co^{2+} + 2e^- = Co$	-0.28
$Cd^{2+} + 2e^- = Cd$	-0.403
$Fe^{2+} + 2e^- = Fe$	-0.409
$2H_2O + 2e^- = H_2 + 2OH^-$	-0.827
$Ti^{2+} + 2e^- = Ti$	-1.63
$Al^{3+} + 3e^- = Al$	-1.76

For Cu electrodeposition, a two-stage mechanism was proposed [7]. The standard electrode potential(**E^0**) for Cu/Cu^+ Metal/Metal-ion couple ($Cu^+ + e^- \rightarrow Cu$) is +0.521 V, which is higher than the **E^0**(+0.345V) of overall reaction of Cu/Cu^{2+} ($Cu^{2+} + 2e^- \rightarrow Cu$). Therefore the first reaction step ($Cu^{2+} + e^- \rightarrow Cu^+$) is the slow step of the Cu electrodeposition reaction.

2.2 Kinetics and Mechanisms of Electrodeposition

Electrochemical reactions involve heterogeneous charge transfer processes at electrode surface, their association with materials application is therefore centered on the prediction and control of events occurring at the electronic/ionic interface.

2.2.1 Electrochemical Deposition Reaction and Overpotential

When an electrode is made a part of an electrochemical cell through which current is flowing, its potential will differ from the equilibrium potential. The difference of equilibrium potential (E) and the potential of the same electrode as a result of external current flow (E(*i*)) is called overpotential

$$\eta = E(i) - E \qquad (2.3)$$

Or, in terms of $\Delta\phi$,

$$\eta = \Delta\phi(i) - \Delta\phi_{eq} \qquad (2.4)$$

The overpotential is required to overcome hindrance of the overall electrode reaction, which is usually composed of a sequence of partial reactions. There are four possible partial reactions and thus four types of rate control: charge transfer, diffusion, chemical reaction, and crystallization. Charge-transfer reaction involves transfer of charge carriers, ions or electrons, across the double layer. So it is the only partial reaction directly affected by the electrode potential. Thus, the rate of charge-transfer reaction is determined by the electrode potential.

The slowest partial reaction is the rate-determining reaction for the total overall reaction. However, several partial reactions can have low reaction rates and can be rate-determining. Thus, four different kinds of overpotentials are distinguished and the total overpotential can be considered to be composed of four components.

$$\eta = \eta_{ct} + \eta_d + \eta_r + \eta_c \qquad (2.5)$$

Where η_{ct} , η_d , η_r , and η_c are, as defined above, charge-transfer, diffusion, reaction, and crystallization overpotentials, respectively. The relationship between current density i (in amperes per square centimeter) and overpotential is the focus for electrochemical deposition study since it reflects overall electrode reaction mechanism.

2.2.2 Relationship between Current and Potential: Butler-Volmer Equation

The current-potential relationship for a general electrochemical equation

$$Ox + ze \overset{k}{\longleftrightarrow} Red \qquad (2.6)$$

where Ox is the oxidized form of a species and Red is its reduced form, can be derived in two steps: (1) express the electrochemical rate ν of reaction (2.6) in terms of current density; then (2) introduce the electrode potential E into the rate constant k.

When an electrode is at the equilibrium, $\Delta\phi$ has its equilibrium value $\Delta\phi_{eq}$ and the anodic equilibrium partial current densities i_n and the cathodic partial current density i_p are equal. Equality of i_n and i_p on an atomic scale means that a constant exchange of charge carriers (electrons or ions) takes place across the metal-solution interface. The two equilibrium current densities are designated by one symbol, i_o, called exchange current density.

$$i_o = i_p = i_n \qquad (2.7)$$

The exchange current density can be derived from the partial reaction current-potential relationship (see reference [1] for detail) as;

$$i_o = zFk^o[O]\exp(\frac{-\alpha zF\Delta\phi_{eq}}{RT}) \qquad (2.8)$$

Where z is number of electrons per mole, F is Faraday constant (charge on a mole of electrons), k^o is standard reaction rate constant, which is the value of reaction rate constant k at E_o, [O] is oxidized species concentration, R is gas constant, and α is charge transfer coefficient. The physical interpretation of k^o is straightforward. It simply is a measure of the kinetic facility of a redox couple. A system with large k^o will achieve equilibrium on a short time scale, but a system with small k^o will be sluggish.

The exchange current density i_o is one of the most important parameters of electrochemical kinetics. It defines the kinetic properties of the particular electrochemical reaction with the electrode material.

When the interface is not in equilibrium, a net current density i flows through the electrode (double layer). It is given by the difference between the anodic partial current density i_p (a positive quantity) and the cathodic partial current density i_n (a negative quantity):

$$i = i_p - i_n \qquad (2.9)$$

When current flows through an electrode, its potential and the nonequilibrium potential difference $\Delta\phi(i)$ can deviate from equation (2.4) as:

$$\Delta\phi(i) = \Delta\phi_{eq} + \eta \qquad (2.10)$$

From equation (2.9) and (2.10), assuming that the charge transfer is the slow process and other processes (e.g. mass transport) are fast, and also all steps that precede or follow reaction (2.5) are neglected, Butler-Volmer equation is developed, and gives the relationship between the current density i and the charge-transfer overpotential η in terms of two parameters, the exchange current density i_0 and the charge transfer coefficient α as shown in equation (2.11) (see reference [1] for detail):

Butler-Volmer equation [1]:

$$i = i_o[\exp(\frac{(1-\alpha)zF\eta}{RT}) - \exp(\frac{-\alpha zF\eta}{RT})] \qquad (2.11)$$

Where i_o is equilibrium current density, and η is overpotential.

Equation (2.11) depicts the variation of the partial current densities and the net current density with an overpotential under the condition of no mass transfer effect.

For large cathodic current as was the case of this research, η becomes more negative, and the first exponential term in the equation (corresponding to the anodic partial current) decreases while the second exponential term (corresponding to the cathodic partial reaction) increases. Thus, under these conditions, an approximate new form of the Butler-Volmer equation is shown in equation (2.12):

$$i = -i_o \exp(\frac{-\alpha zF\eta}{RT}) \qquad (2.12)$$

Consider its inverse form, $\eta=f(i)$, we get the **Tafel Equation** for the cathodic process (high mass transfer rate) [1]:

$$\eta = a - b \log |i| \qquad (2.11)$$

Where $a = \frac{2.303RT}{\alpha zF}\log i_o, b = \frac{2.303RT}{\alpha zF}$.

Tafel equation (2.11) shows that there is an exponential relationship between η and i, or a linear relationship between η and $\log(i)$ when η has large cathodic values. This is also true for an anodic process. The derivation given above shows that Tafel equation is a special case of a general Butler-Volmer equation. The Tafel form can be

expect to hold whenever the back reaction (i.e., the anodic process when a net reduction is considered, and vice versa) contributes less than 1% of the current.

When overpotential η is small, Butler-Volmer equation is approximated as current proportional to potential per Ohms law

$$i = i_0 f\eta \qquad (2.12)$$

Where $f = F/RT$

Thus, for small values of η, less than about 0.01V, when the electrode potential is near the reversible potential, the current varies linearly with the overpotential.

Therefore, in the case when electrode reaction rate is determined by the charge-transfer overpotential η_{ct},(not mass-transfer limited) the i-η_{ct} relationship has a linear range (low η), followed by an exponential range (large η). When the mass transport to the electrode is considered for the rate of reaction, a general current-potential relationship is shown Figure 2.4

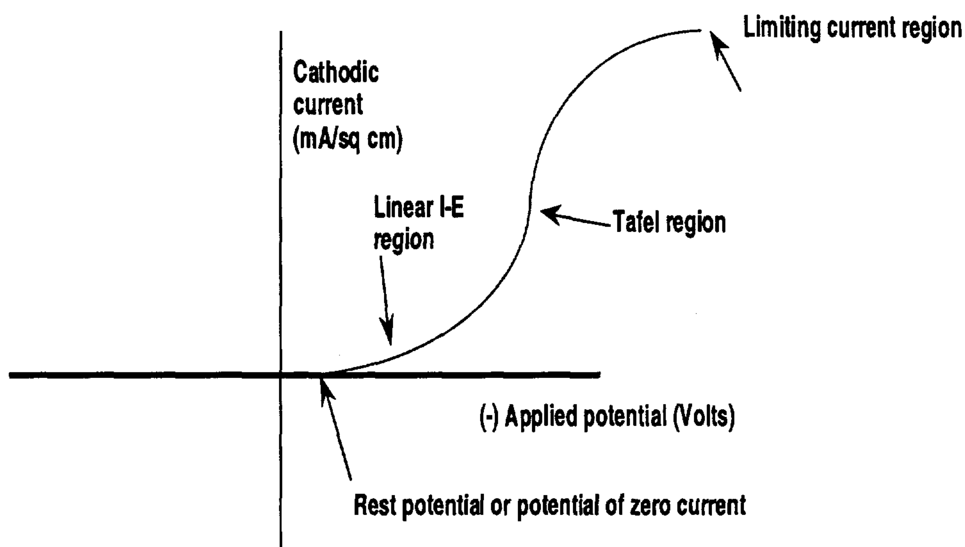

Fig. 2.4 Three regions in the general current-overpotential relationship.

2.2.3 Electrochemical Deposition Kinetic Study

Part of this study is to examine the effect of electrolyte additives on the kinetics of Cu electrodeposition reaction, in particular, the effect of thiols on the kinetics of copper deposition from acidic copper sulfate solutions. Quantification of the kinetic parameters for the reaction aids the selection of thiols and appropriate conditions for the copper electrodeposition. Polarization curves, Tafel Plots, Chronoamperometry, and Cyclic Voltammetry were used to obtain electrodeposition reaction behavior, Tafel slope, charge transfer coefficient, and exchange current density.

The charge transfer coefficient, α, is a measure of the symmetry of the energy barrier to reaction. In most systems α turns out to lie between 0.3 and 0.7 [4]. It is an indicator for the severity of irreversible reaction, which is contributed by reaction surface When electrode kinetics are sluggish and significant activation overpotentials are required, good Tafel relationship can be seen. This point underscores the fact that Tafel behavior is an indicator of totally irreversible kinetics [4]. A Tafel plot of log (i) vs. η is a useful device for evaluating kinetic parameters. In general, there is an anodic branch with slope of $(1-\alpha)zF\eta/2.3RT$ and a cathodic branch with slope $-\alpha zF\eta/2.3RT$. Both linear segments extrapolate to an intercept of log (i_o). The charge transfer coefficient α and the exchange current i_o are readily accessible from this plot.

From the cathodic polarization curve, we obtain the Tafel slope $\vec{b}$ as

$$\vec{b} = \frac{\partial \eta}{\partial \log|i|} = \frac{\Delta \eta}{\Delta \log|i|} = \frac{2.303RT}{\alpha zF} \qquad (2.13)$$

And the plot intercept is $\log(i_o)$ [1].

Detailed techniques and methods used in this research are discussed in following section.

2.3 Techniques for study of electrode process and determination of kinetic parameters

A general Red/Ox electrochemical reaction, Eq. (2.1), proceeds in at least five steps:

1. Transfer of Ox from the bulk solution to the inter-phase
2. Adsorption of Ox onto the electrode surface
3. Charge transfer at the electrode to form Red
4. Desorption of Red from the surface
5. Transport of Red from the inter-phase into the bulk of the solution

For the $M/M+$ electrode as in this research, steps 4 and 5 are absent since the product of the charge transfer M remains incorporated in the metal electrode. Step 1 and step 5 are mass-transfer processes. Study of the charge transfer processes (step 2 and 3), free from the effects of mass transport, is possible by the use of transient techniques. In the transient techniques the interface at equilibrium is changed from an equilibrium state to a steady state characterized by a new potential difference $\Delta\phi$. The analysis of the time dependence of this transition is a basis of transient electrochemical techniques. There are two kinds of methods used by this technique: Galvanostatic technique and Potentiostatic technique. A three–electrode cell is utilized for study of this process.

The complete electrochemical behavior of a system can be obtained through a series of steps of different potentials or current with recording of the current-time curves to yield a three-dimensional i-t-E surface. In the galvanostatic technique the current between the test electrode and the auxiliary (counter-) electrode is held constant with a current source (galvanostat) and the potential between the test electrode, and the reference electrode is determined as a function of time. The potential is the dependent variable, which is recorded.

In the potentiostatic technique the potential of the test electrode is controlled while the current, the dependent variable is measured as a function of time. The potential difference between the test electrode and the reference electrode is controlled by an instrument known as a potentiostat. In this research, electrochemical measurements were

made using an EG&G 270 potentiostat rotating disc electrode system. Following techniques were used for this investigation:

Linear Sweep Voltammetry (LSV)/Polarization Curve: Information about an electrode reaction is often gained by determining current as a function of potential (*i-E* Curves), and certain names are sometimes associated with features of the curves. The departure of the electrode potential (or cell potential) from the reversible (i.e., nernstian or equilibrium) value upon passage of faradaic current is termed polarization. The larger this departure is, the larger the extent of polarization is said to be. The extent of polarization is measured by the overpotential, η, which is the deviation of the potential from the equilibrium value. Current-potential curves, particularly those obtained under steady-state conditions, are sometimes referred to as polarization curves. Linear Sweep Voltammetry method is used to build this curve. This method sweeps the potential with time and records the *i-E* curve directly. The technical name of this potential sweep method is called Linear Potential Sweep Chronoamperometry, most refer to it as linear sweep voltammetry (LSV) [1]. In this research, polarization curves were obtained for electrolyte with different thiols. Two curves are plotted based on polarization curve, one is current-potential polarization curve to compare the electrode reaction with different electrolyte additives under same rotation speed. Another is the Tafel extrapolation plot to determine Tafel slope, charge transfer coefficient and exchange current density for each thiol additive package.

Chronoamperometry Curve (CA): Chronoamperometry curve gives the current change vs. time at constant potential. The current-time curves observed in response to different steps of overpotential can provide useful information of flux of reactant and the depletion effect. It reflects reaction behavior regarding overpotential for each electrolyte electrodeposition.

Cyclic Voltammetry (CV)): Cyclic Voltammetry is a reversal technique and is the potential-scan equivalent of double potential step chronoamperometry. It is a very useful method for obtaining information about fairly complicated electrode reactions. The *i-E* hysteresis from this measurement indicates any irreversible changes of electrode surface chemistry occurred as the metal deposition proceeds. Further more, the hysteresis

associated with the full combination of additives reflects the competition between inhibition provided by the inhibitor and acceleration provided by thiols, which leads to an irreversible change in the reaction dynamics [5]. No hysteresis was found in baths with fewer than three components needed for superfilling, suggesting a correspondence between I-E hysteresis and superfilling [6]. This technique can also be used for the detection of thiol's aging effect, which is reflected in the hysteresis measurement.

Copper electrodeposition has become the process of choice for ULSI interconnect metalliation. Further understanding of this process will enable better process control, process simulation, and process optimization for future generation ULSI. Copper Electrodeposition has a long history with a lot of extensive studies and in-depth theories. However, electrodeposition reaction is a heterogeneous reaction and involves many complex process steps. The application of this process in USLI has brought up a lot of challenges for better understanding and controlling of this process, especially with organic additives. In this research, these basic electrochemical knowledge and techniques have been used for thiol's characterization in chapter 4 and 5.

References

[1]. M. Paunovic, M. Schlesinger. Fundamentals of Electrochemical Deposition. Wiley & Sons, 1998, pp.1-5, pp.39-100.

[2]. D.C. Edelstein. "Advantages of copper interconnects," Proceeding of the 12th International IEEE VLSI Multilevel Interconnection Conference, 1995, p.301.

[3]. P.C. Andricacos, C. Uzoh, J.O. Dukovic, J. Horkans, H. Deligianni. "Damascene copper electroplating for chip interconnections," IBM Journal of Research and Development, 42(5), 1998, p.567.

[4]. A.J. Bard, L.R. Faulkner. Electrochemical Methods. John Wiley & Sons, 1980, p.105-121.

[5]. T.P. Moffat, J.E. Bonevich, W.H. Huber, et al. "Superconformal electrodeposition of copper in 500-90 nm features," J. Electrochem. Soc., 147 (12), 2000, pp.4524-4535.

[6]. K.R. Hebert, "Analysis of current-potential hysteresis during electrodeposition of copper with additives," J. Electrochem. Soc., 148 (11), 2001, p.726-732.

[7] E.E. Farndon, F.C. Walsh, S.A. Campbell. "Effect of thiourea, benzotriazole, and 4,5–dithiaoctane-1,8-disulphonic acid on the kinetics of copper deposition from dilute acid sulphate solutions," J. Appl. Electrochem., 25, 1995, pp.574-583.

CHAPTER THREE

THE ROLE OF ORGANIC ADDITIVES IN ELECTRODEPOSITION

Electrolyte additives are the focus of this research, particularly thiols. In this chapter, common copper electroplating additives are reviewed. Additive characterization and working mechanism are discussed. Additives are the most mysterious part of electrodeposition. Detailed knowledge is lacking in this area. This chapter contains the most up to date information available in this field.

3.1 Common copper electroplating additives and their function

Most solutions used in electrodeposition of metals and alloys contain one or more inorganic or organic additives that have specific functions in the deposition process. These additives affect deposition and crystal building processes as adsorbates at the surface of the cathode [1].

The inorganic components of Cu bath consists of copper cations, sulfate ions, free acid, and chloride ions. A commercial standard copper sulfate solution was used for this research. This base electrolyte contains 0.24 M $CuSO_4$ (17.5 g/l Cu), 1.8 M H_2SO_4 (175 g/l sulfuric acid), and 50 ppm Chloride. Since the acid concentration of this electrolyte is much higher than some other electrolytes used in semiconductor industry (175 g/l vs.10 g/l sulfuric acid), it is called high acid electrolyte. Low acid electrolyte is gaining its popularity due to its high bath resistance, which results in better trench fill capability, better defect performance, and better film uniformity across a wafer, especially for 300mm wafer. However, its fundamental behavior is same as high acid electrolyte. This

research started when high acid electrolyte was still the choice of IC industry. Therefore, low acid electrolyte was not used in this study.

The definition of organic additives in acid plating bath is a mixture of organic molecules and chloride ions which adsorb at the copper surface during plating to enhance thickness distribution and feature fill and to control copper grain structure and thus ductility, hardness, stress, and surface smoothness. There are three types of organic additives as shown in figure 3.1

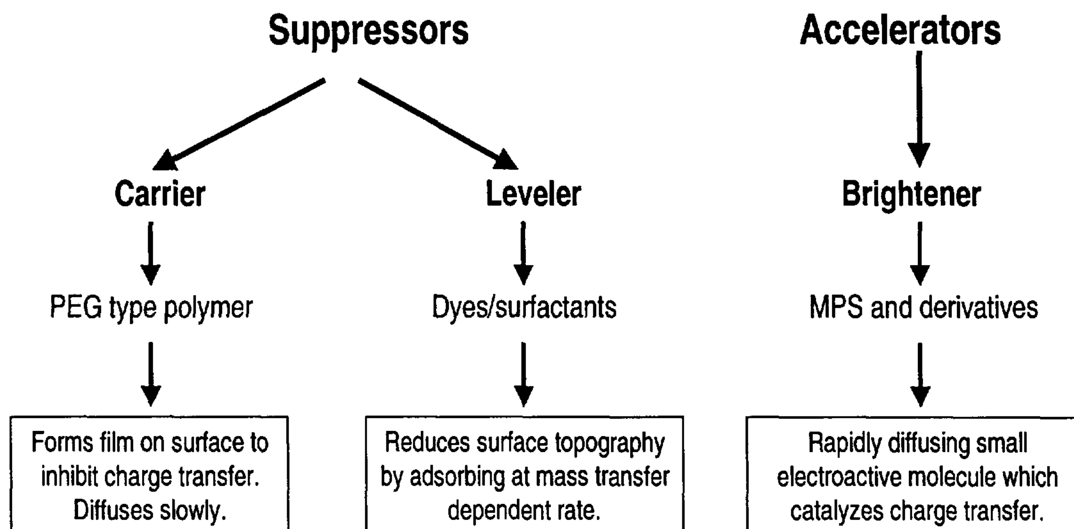

Fig. 3.1 Classification of acid bath additives

It is widely understood that organic additives can influence copper film microstructure and electrodeposition superfilling capability for trenches and vias. Film microstructure has a direct impact on film mechanical and electrical properties. Superfilling guarantees a void free trench and via filling. The potential problems with organic additives are the impurities and aging by-products, especially the process control of them.

Brighteners:

The common brighteners in acid copper bath are organic sulfur compounds in different thiol forms with a sulfinic compound on one end. The generalized molecular structure of thiols is shown as:

$$X\text{-}S\text{-}S\text{-}C\text{-}C\text{-}C\text{-}SO_3^-$$

The chemical characteristics of thiols are water-soluble salts of organic acid containing a mercapto functional group, which present at 1-10 ppm in solution. Its function is to absorb on copper metal surface during plating and participate in charge transfer reaction. Brighteners provide growth sites on the copper interface in the presence of other additives as shown Figure 3.2. It determines Cu growth characteristics with major impact on metallurgy.

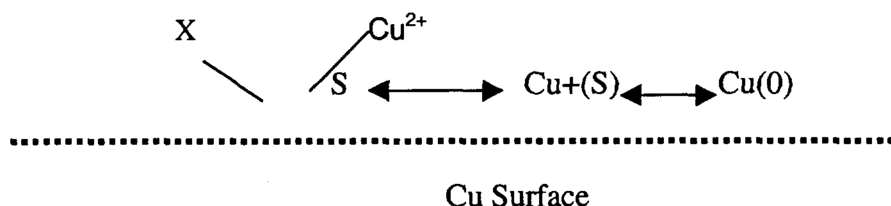

Fig. 3.2 Brigheners absorb on the Cu surface and participate in charge transfer reaction

Brighteners are the least stable additive components in the plating bath, and are subject to oxidation by air (oxygen), electrochemical oxidation at anode, and catalytic decomposition at Cu surface as shown in Figure 3.3 [1]. The by-products from these thiols are often detrimental to deposit properties and filling. However, a systematic evaluation of common thiols and their decomposition speed are lacking. This is one of the focus for this research.

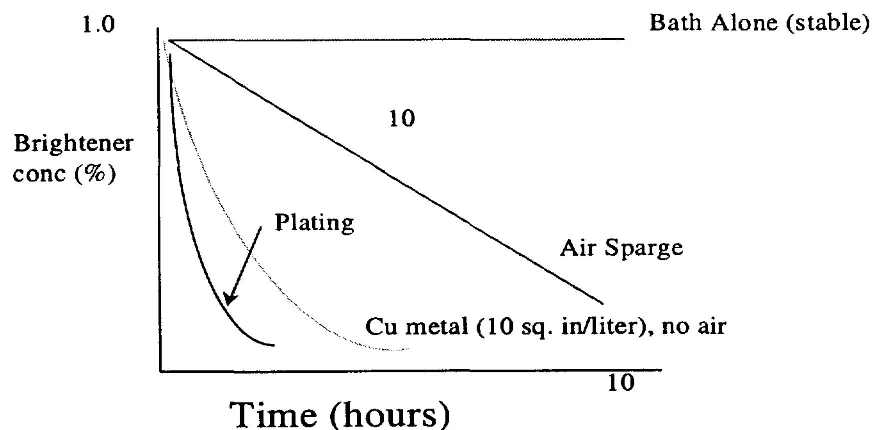

Fig. 3.3 Brightener stability under different conditions

Carrier

The chemical composition of carriers consists of oxygen containing polymers, and no sulfur or nitrogen functional groups. A typical example is polyethylene glycol or polyoxyethylene glycol of 1,000 to 8,000 MW. The function of carriers is to adsorb on the cathode surface to form a relatively thick film during copper plating. Carrier effect on plating is stable over wide concentration (10-1000ppm) and MW (800 - 10000) ranges. Carrier suppresses electrodeposition charge transfer, which is called polarizing effect, by forming a barrier to diffusion of Cu^{2+} ions to the surface [4,5,6].

Carrier alone or with Cl^- only yields good thickness distributions but poor fill and deposit properties. It requires brightener for superfilling property for a good gapfill. The stability of carriers degrades as they are gradually broken into lower MW fragments at both the anode and cathode. Carriers that are below MW of about 750 tend to lose polarization effectiveness. The carrier's electrochemical property is well understood [4,5,6]. Its impact on the i-V relationship is shown in Figure 3.4.

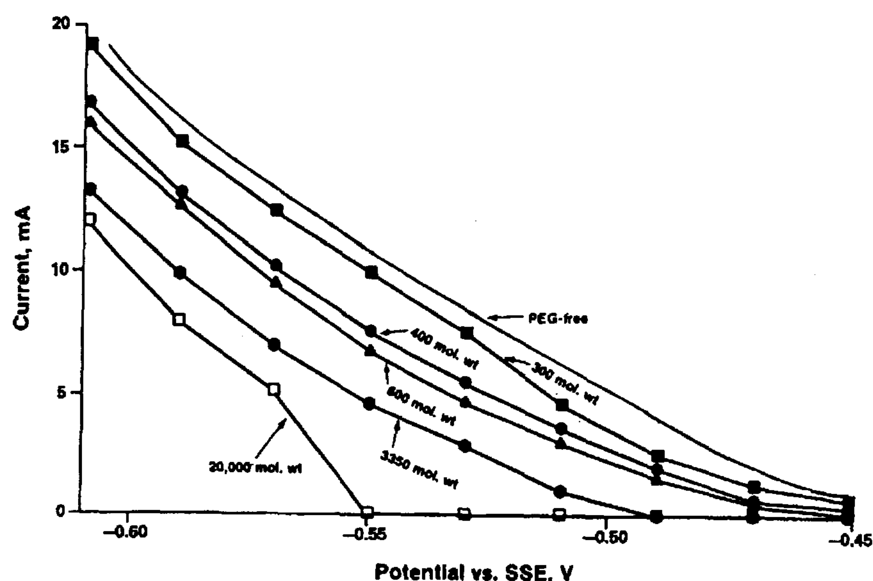

Fig. 3.4 Steady-state current vs. potential for copper deposition in 100 mg/l PEG solution with various molecular weights.

From this graph, we can clearly see the strength of carrier suppressing capability increases with molecular weight of PEG. Kelly and West [4,5] studied the mode of action of PEG and chloride ions together, which is often incorporated into industrial plating baths. Their work suggested the adsorption of approximately a monolayer of spherically packed PEG molecules when chloride ions are present, which inhibits the deposition reaction for cathodic overpotenials. It concluded that adding chloride alone promotes the deposition reaction, while adding PEG alone has a relatively small effect on electrode kinetics. Using of PEG and chloride together gives good polarization effect.

Leveler

The chemical characteristics of levelers are typically high MW monomer or polymer with both sulfonic acid and nitrogen. Chemical choice of leveler varies by user and application requirements. It usually is present at 10 - 100 ppm concentrations.

Function of levelers is to reduce growth rate of copper at protrusions and edges to yield a smooth final deposit surface. It effectively increases polarization resistance

(suppressing the electrodeposition rate) at high growth areas by inhibiting growth to a degree proportional to mass transfer to localized sites. Theories of leveling by additives are based on the correlation between an increase in polarization produced by the leveling agents, and the preferential adsorption of a leveling agent on the high point [3].

Chloride

Chloride is added as HCl and used with nearly all commercially available additive systems. It is normally present at bath concentrations of 30 - 100 ppm. The function of chloride is to adsorb at both cathode and anode and to modify adsorption properties of carrier to influence thickness distribution. It also accumulates in anode film and increases anode dissolution kinetics.

Chloride does not decompose or complex irreversibly with bath components. The electrochemical characterization of chloride has been studied extensively by researchers [4,5,6]. Its impact on electrodeposition i-E relationship is shown in Figure 3.5

From this plot, we can see when chloride is present together with PEG, it provides higher polarization resistance and suppresses the electrochemical deposition.

In this investigation, the electrolyte package studied contained above additives except leveler. Leveler behaves very similarly to carrier in its characterization and mainly functions as surface leveling. To keep this research focused on the thiols and its degradation effect, leveler is not included in the electrolyte package.

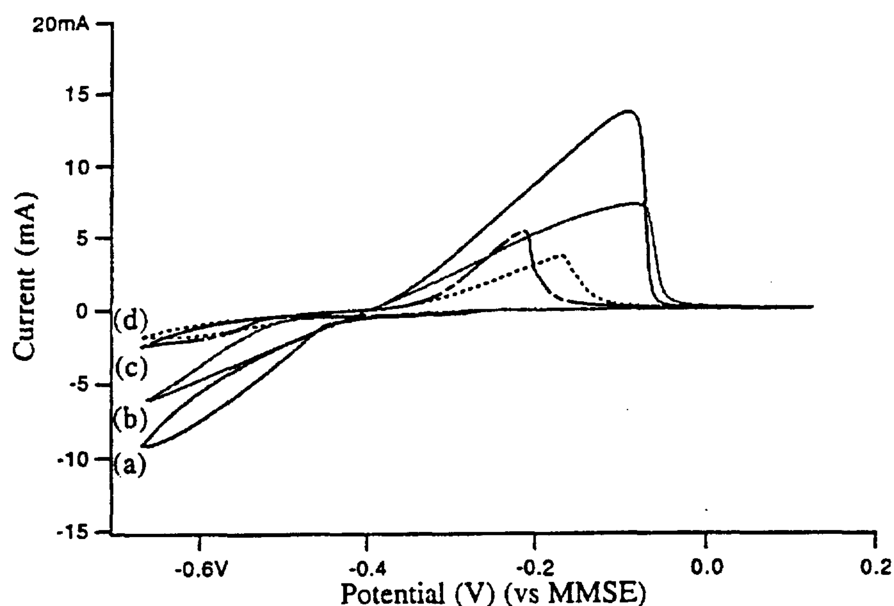

Fig. 3.5 Cyclic voltammograms of electrodeposition and dissolution of Cu at a Pt electrode in 2M H_2SO_4/0.7M $CuSO_4.5H_2O$ electrolyte. (a) no additive; (b) 10ppm Cl^-; (c) 100 ppm PEG; (d) 10 ppm PEG+10 ppm Cl^-.

3.2 Effect of Additives

3.2.1 Effect of Additives on Electrodeposition

Additives affect electrodeposition and crystal building processes as adsorbates at the surface of the cathode. There are two factors that determine adsorption: substrate and adsorbate. One classification of adsorption phenomena is based on the adsorption energy: the energy of the adsorbate-surface interaction. There are two basic types of adsorption in this classification: chemisorption (an abbreviation of chemical adsorption) and physisorption (an abbreviation of physical adsorption).

It is believed that additives are chemisorption bonded on the electrode surface [1]. Detail knowledge of this adsorption is lacking. A simple additive surface adsorption behavior is described in figure 3.6. This surface coverage theory has been used to

explain the superfilling property of electrolyte with organic additives [2]. This theory is discussed in next section.

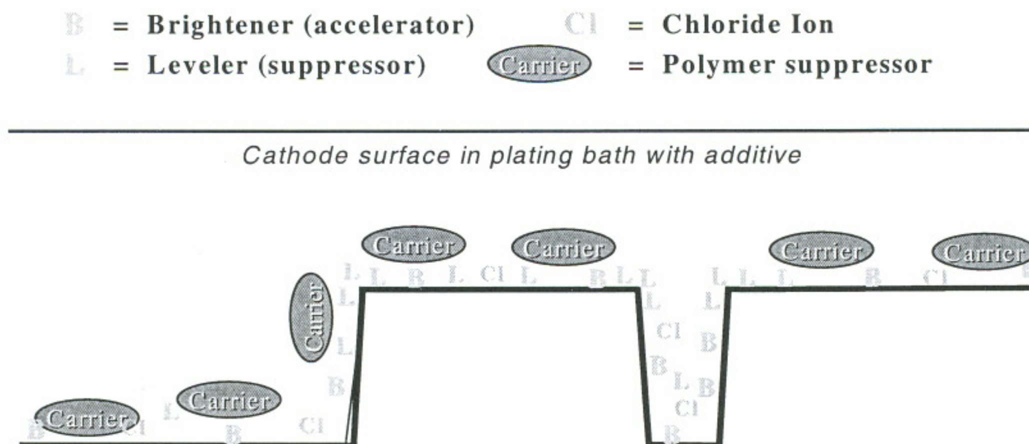

Figure 3.6 Additive Surface Adsorption Behavior

For electrodeposition process, the transfer of metal ion M^+ may proceed via one of two mechanisms from the solution into the ionic metal lattice: (1) direct mechanism in which ion transfer takes place on a kink site of step edge or on any site on the step edge (any growth site); or (2) terrace site ion mechanism. In the terrace site transfer mechanism a metal ion is transferred from the solution to the flat face of the terrace region. At this position the metal ion is in adion state and is weakly bound to the crystal lattice. From this position it diffuses on the surface seeking a position with lower potential energy. The final position is a kink site.

Adsorbed additives affect both of these mechanisms by changing the concentration of growth sites on the surface, concentration of adions on the surface, diffusion coefficient, and the activation energy of surface diffusion of adions. Nucleation process of electrodeposition can be affect by the change of these factors. In the presence of adsorbed additives the mean free path for lateral diffusion of adions is shortened, which is equivalent to a decrease in the diffusion coefficient D (diffusivity) of adions [1].

The thiol has been proposed to adsorb competitively with the inhibitor [2]. A wide accepted generic model of copper electrodeposition with multicomponent additives is proposed as following [13]. Copper deposition proceeds via two consecutive irreversible reaction steps:

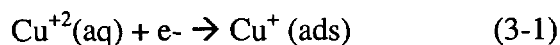

$$Cu^{+2}(aq) + e^- \rightarrow Cu^+ (ads) \qquad (3\text{-}1)$$

$$Cu^+ (ads) + e^- \rightarrow Cu \qquad (3\text{-}2)$$

One reported reaction mechanism of thiol involves SPS that showed a depolarizing effect (accelerating). The mechanisms accounting for this generally involve the formation of surface complexes, containing organic liqands which reduce more rapidly at more positive potentials than the corresponding aquo complexes, thus lowering the activation energy barrier [12]. Zukauskaite et al. Used potentiodynamic and UV spectroscopic techniques to show that over the range potentials used for copper deposition, Cu(I) organo complexes were present and that SPS was electroreduced to 3-mercapto-propanesulphonic acid (MPS), $HS(CH_2)_3SO_3H$ (see equation 4-7). MPS then reduces Cu^{2+} to produce a Cu(I) thiolate complex and SPS is regenerated. The SPS can again be reduced while the Cu(I) complex undergoes reduction to produce copper metal and MPS [12]. A possible reaction mechanism is as follows:

$$HO_3S(CH_2)_3SS(CH_2)_3SO_3H + 2H^+ + 2e^- \longleftrightarrow 2HS(CH_2)_3SO_3H \qquad (3\text{-}3)$$

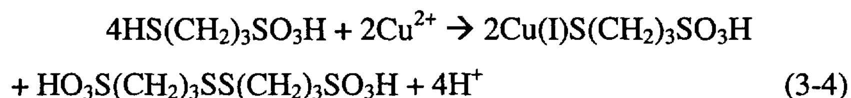

$$4HS(CH_2)_3SO_3H + 2Cu^{2+} \rightarrow 2Cu(I)S(CH_2)_3SO_3H + HO_3S(CH_2)_3SS(CH_2)_3SO_3H + 4H^+ \qquad (3\text{-}4)$$

SPS is therefore able to participate in repeated oxidation and reduction cycles and depolarization occurs because Cu^{2+} reduction to Cu^+ occurs chemically in reactions involving the additive in contrast to a purely electrochemical Cu^{2+} to Cu^+ electroreduction process.

Healy et al.[14] Suggested an alternative mechanism for the decomposition of SPS in electroplating baths. He showed that SPS acts as brightener by film formation at

sites where there is a high local flux of material from the solution. The film is a copper(I) complex, most likely $Cu(I)SCH_2CH_2CH_2SO_3H$, and its further reduction leads to copper metal. This again involved the formation of a stable Cu(I) complex $Cu(I)S(CH_2)_3SO_3H$, however, in this mechanism, he speculated that SPS reacts directly with Cu^+ ions to form the complex:

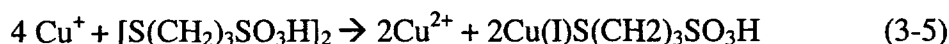

$$4\,Cu^{+} + [S(CH_2)_3SO_3H]_2 \rightarrow 2Cu^{2+} + 2Cu(I)S(CH2)_3SO_3H \qquad (3\text{-}5)$$

The observed reduciton of SPS is only possible because of the strong interaction of the thiolate ion with the Cu(I). In the absence of complex formation, neither Cu(I) nor Cu(o) are strong enough to reduce SPS.

i-E relationship is a reflection of electrodeposition kinetics. Additives have direct impact on electrodeposition *i-E* relationship as shown in Figure 3.7. It is seen that excess suppressor greatly suppressed electrodeposition reaction rate, whereas the excess accelerator in a suppressed bath makes electrodeposition close to additive-free electrolyte. For a normal bath with an appropriate accelerator/suppressor ratio for a good fill result, the electrodeposition reaction rate falls between two extremes.

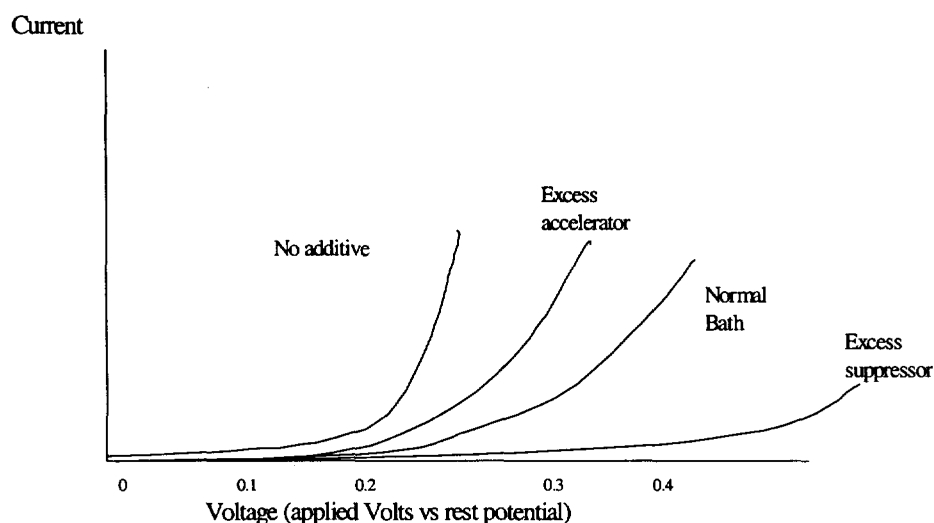

Fig. 3.7 Additive effect on *i-E* relationship

3.2.2 Effect of Additive on Electrodeposition Superfilling:

It has been reported in the literature [7,8] that small amount of organic additives added to the plating bath can provide bottom up fill or "super-fill", resulting in the complete gap fill of narrow trenches and vias. Two mechanisms by which these additives lead to bottom-up fill have been proposed.

The initial model focused on the location-dependent growth rate derived from diffusion-limited consumption of an inhibiting/suppressing species [9,10]. Explanation of bottom-up fill using the initial model is difficult when fill is observed in an electrolyte containing an accelerator additive and a single high concentration suppressor [2]. As a result, a second model proposed [11,3]. In this model, accelerated bottom-up deposition has been explained by a local relative coverage increase of accelerating species at the base of a feature. This coverage increase is thought to take place as the surface area within the feature decreases leading to increased surface concentration of strongly adsorbed species.

The first model hypothesized that the additives inhibit copper deposition by blocking the electrode surface. If this is true, the surface coverage of the additives can be estimated by the ratio of the current density in the presence of additives to current density measured without any additives [2]. This mode assumed additives not participate in faradic reaction. Their sole role is to alter copper nucleation process. Therefore, the copper deposition rate is inhibited by the adsorption of the suppressors, PEG. Based on cathodic copper deposition current-overpotential equation as discussed in Chapter 2, for a PEG-Thiol electrolyte package, the deposition rate in the presence of organic additive can be expressed as:

$$i = i_0 \frac{C_{Cu^{2+},0}}{C_{Cu^{2+},\infty}}(1-\theta_{eff})\exp\left(-\frac{\alpha_c nF}{RT}V\right) \qquad (3\text{-}6)$$

Where the effective surface coverage of additives:

$$\theta_{eff} = \theta_{PEG} + \theta_{thiol} \tag{3-7}$$

For the current density in the bath, which contains no organic additives, but does contain 50 ppm Cl-, $\theta_{eff} = 0$ and equation (3.1) becomes

$$i_{no} = i_0 \frac{C_{Cu^{2+},0}}{C_{Cu^{2+},\infty}} \exp\left(-\frac{\alpha_c nF}{RT} V\right) \tag{3-8}$$

i_0 is the exchange current density dependent on substrate surface. The Cu subscript o implies the condition of the electrode surface while ∞ represent bulk condition. n is the number of electron exchange in reaction, and F is Faraday's constant. α_c is an experimentally determined constant. Combining above equations, the effective surface coverage of the additive can be plotted against overpotential of the electrode.

3.2.3 Effect of Additive on Cu Film Microstructure

In addition to influencing the kinetics of metal reduction, electrolyte additives are also known to exert a dramatic effect on the metallurgical microstructure [3]. The microstructure of the electroplated Cu film has a direct effect on interconnect electromigration (EM) property, which is a major concern for interconnect reliability. Film texture and grain structure can also noticeably affect a variety of other film properties such as formability, corrosion resistance, wear resistance, etc [15]. Several reports have been published regarding the impact of barrier/seed layers on the morphology of electroplated copper [16]. However, only limited information is available on the impact of different conditions on the microstructure of electroplated Cu film [17]. This investigation started with the basic Cu electroplating bath study, without the organic additives as a control. Plating current density and Copper, chloride, and acid concentration were investigated for the impact on the film microstructure. Then the effect of thiols on Cu film microstructure in a Cl+PEG+thiol electrolyte was examined.

3.3 Multi-Component Bath Additive Characterization

The influence of additives on copper electrodeposition kinetics has been studied by various techniques.

To understand the working mechanisms of additives and surface coverage kinetics, certain electrode methods has been employed to extract the parameters for the kinetic study. These methods include linear sweep voltammetry(LSV), chronoamperometry(CA), and cyclic voltammetry (CV) on a rotating disk electrode. These measurement methods and their working mechanism have been discussed in Chapter 2. In this research, an EG&G potentiostat was used for this evaluation, coupled with a standard rotating disk Pt electrode.

Fill study was carried out to examine thiol's effect on superfilling property of the electrolyte. The fill result is correlated with the electrochemical characteristics of electrolyte package.

The successful implementation of copper electroplating technology in ULSI derives from the use of electrolyte additives to affect the local deposition rate, thereby allowing superfilling of trenches and vias in the damascene process. However, the understanding of additives working mechanism is limited and empirical. Organic additives participate in the charge transfer reaction during electrodeposition and make it hard to mathematically quantify or predict their influence on the charge transfer process. Electrochemical methods have been used extensively to characterize electrochemical reaction. In this investigation, six model thiols were studied in an electrolyte package with PGE and Cl^- for their potential role in Cu electrodeposition on ULSI. Their influences on electrodeposition reaction kinetics were investigated.

Reference

[1]. M. Paunovic, M. Schlesinger. Fundamentals of Electrochemical Deposition. Wiley & Sons, 1998, pp.1-5, pp.167-186.

[2] Y. Cao, P. Taephaisitphongse, R. Chalupa, and A. C. West. "Three-additive model of superfilling of copper," J. Electrochem. Soc., 148 (7), 2001, pp.466-472.

[3]. T.P. Moffat, J.E. Bonevich, W.H. Huber, et al. "Superconformal electrodeposition of copper in 500-90 nm features," J. Electrochem. Soc., 147 (12), 2000, pp.4524-4535.

[4] J. Kelly, C. West. "Copper deposition in the presence of polyethylene glycol, I. quartz crystal microbalance study," J. Electrochem. Soc., 145 (10), 1998, pp.3472–3476.

[5] J.P.Healy, D. Pletcher. "The chemistry of the additivves in an acid copper electroplating bath, Part I. Polyethylene glycol and chloride ion," J. Electroanal. Chem., 338, 1992, pp.155-165.

[6] J. Kelly, A. West. "Copper deposition in the presence of polyethylene glycol II. electrochemical impedance spectroscopy," J. Electrochem. Soc., 45 (10), 1998, pp.3477-3481.

[7] V.M. Dubin, C.H. Ting, R. Cheung. "Electro-chemical deposition of copper for ULSI metallization," International VLSI Multilevel Interconnect Conference, 1997, Santa Clara, CA, IMSIC-107, p.69.

[8] D. Edelstein, J. Heidenreich, R. Goldblatt, et al. "Full copper wiring in a sub-0.25 micro-m CMOS ULSI technology," Technical Digest, IEEE International Electron Devices Meeting, 1997, p.773.

[9] P.C. Andricacos, C. Uzoh, J.O. Dukovic, J. Horkans, H. Deligianni, "Damascene copper electroplating for chip interconnections," IBM Journal of Research and Development, V. 42, No. 5, 1998, p.567.

[10] A.C. West. "Theory of filling of high-aspect ratio trenches and vias in presence of additives," J. Electrochem. Soc., 147(1), 2000, pp.227-232.

[11] J. Reid, S. Mayer. "Factors influencing fill of IC features using electroplated copper," Advanced Metallization Conf., 1999, Proceedings, MRS, Warrendale, PA, pp. 53-62.

[12] E.E. Farndon, F.C. Walsh, S.A. Campbell. "Effect of thiourea, benzotriazole, and 4,5– dithiaoctane-1,8-disulphonic acid on the kinetics of copper deposition from dilute acid sulphate solutions," J. Appl. Electrochem., 25, 1995, pp.574-583.

[13] K. R. Hebert. "Analysis of current-potential hysteresis during electrodeposition of copper with additives," J. Electrochem. Soc., 148 (11), 2001, pp.726-732,

[14] J.P. Healy, D. Pletcher, M. Goodenouth. " The chemistry of the additives in an acid copper electroplating bath, Part III. The mechanism of brightening by 4,5-dithiaoctane-1,8-disulphonic acid," J. Electroanal. Chem., 338, 1992, pp.179-187.

[15] C. Ryu, K-W. Kwon, A.L. Loke, H. Lee, T. Nogami, V. Dubin, R.A. Kavari, G. W. Ray, S.S. Wong. "Microstructure and reliability of copper interconnects," IEEE Transactions on Electron Devices, 46 (6), June 1999, pp.1113-1120.

[16] S. S. Wong, C. Ryu, H. Lee, Alvin L.S. Loke, K-W. Kwon, "Effects of barrier/seed layer on copper microstructure," Advanced Metallization Conference, Tokyo, Japan, 1998, pp.53-54.

[17] V.M. Dubin, G. Morales, C. Ryu, S.S. Wong, "Microstructure and mechanical properties of electroplated Cu films for damascene ULSI metallization", MRS 1997 Fall Meeting, Boston, Massachusetts, Material Research Society Symposium Proceedings, 493, 1998, p.137.

CHAPTER 4

COPPER ELECTRODEPOSITION WITH DIFFERENT THIOLS

In this chapter, the copper electrodeposition on in high aspect ratio features is studied in the absence of and in the presence of different organic additives. Six model thiols: (sodium sulfopropyl)-disulfide(SPS), 3-Mercapto-1-propanesulfonic sodium salt (MPS), (O-Ethyldithiocarbonato)-s-(3-sulfoproplyl)-ester potassium salt(OPX), 3-S-Isothiuronium Propyl Sulfonate(UPS), N, N-Dimethyl-dithiocarbamylpropyl sulfonic sodium salt (DPS), and 3-(Benzothiazolyl-2-mercapto)-propyl-sulfonic sodium salt (ZPS), which all have a thiol and disulfide group on one side of their molecular structure, were characterized in a Cl-PEG-thiol electrolyte package. Each electrolyte package's electrodeposition kinetic and trench fill capability are examined. Film microstructure was studied to examine each thiol's influence on film microstructure.

4.1 Cu Electrodeposition without Organic Additives

This research started with the basic Cu electroplating bath called Virgin Metal Solution (VMS) or Make-Up Solution, without the organic additives, which are known to have significant influence on the electrolyte electrochemical properties and microstructure and mechanical properties of the films [1]. The Cu bath, in its very basic form consists of several variables, including concentration of copper cations, chloride ions, sulfate ions, and free acid. External parameter includes the current density that has known impact on Cu electrodeposition.

The study of VMS bath electrochemical property, its gapfill, and microstructure of electroplated Cu films have been used as a control for organic additives. A commercial standard copper sulfate solution was used as the base for electrochemical characterization and reaction kinetic study. It consists of 1.8 M (175 g/l) sulfuric acid, 0.24 M (17.5 g/l) $CuSO_4$, and 50 mg/l Chloride, which is called high acid electrolyte as explained in chapter 3.

Electrochemical methods used in this research have been reported in other research paper [2], and discussed in Section 2.3. By combining these measurement results, it gives a consistent electrochemical characterization of each electrolyte. The detailed information for each method used is listed as below:

Cyclic Voltammetrey (CV): CV can be used to check the hysteresis behavior of an electrolyte. For all the CV measurements, the scan rate was set to 2 mV/s, with a scan range between –0.025 V and –0.30 V vs Ag/AgCl reference electrode. Prior to each measurement, the working electrode was conditioned in a standard high acid VMS solution.

Linear Sweep Voltammetry(LSV): In all polarization experiments, the linear sweep voltammetry measurement was carried out at 2mV/sec from approximately -50 mV to the open circuit potential to –500 mV vs Ag/AgCl. After each polarization measurement, the copper was completely stripped in the same bath. The Pt RDE was taken out of the solution and immersed in concentrated HNO3 for 2 min followed by a DI rinse.

Chronoamperometry (CA): The pretreatment of the electrode was the same as that employed in the LSV experiments. A constant potential of –0.15 and –0.25 V vs. Ag/AgCl, was employed for all plating bathes. Rotation speed of 400 rpm was used in each experiment. The rotation speed was held constant until the measured current reached a plateau (1 to 1.5 minutes, depending on the both composition).

Copper electrodeposition was carried out in a modified Hull cell under a well-mixed condition. The wafer slice was placed inside a Hull cell. The substrates were 2” x 2” silicon wafer slices with a layer of SiO_2 followed by 15 nm thick sputtered Ta, 10nm TaN as a barrier and adhesion promotion layer, and finally a 150nm thick sputtered Cu

seed layer. The substrate roughness was around 0.5 to 2.0nm for all the substrates. DC plating conditions were used for this set of experiments. A thermometer was used to monitor bath temperature.

Fill was examined on a coupon wafer in a modified Hull cell. The coupon wafers were plated with a three steps constant current condition of $3mA/cm^2$, $9.5mA/cm^2$, and 23 mA/cm^2. The cross section of the copper films was examined by a JEOL 5600 scanning electron microscope (SEM).

The influence of additive chemistry on impurity incorporation and microstructureal evolution, e.g, recrystallization was evaluated by film resistivity on a 1um thick copper film deposited at room temperature. Immediately after rinsing, the freshly deposited samples were examined by a four-point resistance probe. Films were maintained at room temperature during the characterization period.

The microstructure of electroplated Cu films without organic additives have been studied as control for comparison. Current density, concentration of copper, sulfuric acid, and chloride were studied for their influence on grain size, film roughness and texture in the absence of electrolyte additives.

4.1.1. Electrochemical Characterization of VMS

Polarization Measurement

A commercial standard high acid copper sulfate solution was used for this study. The polarization curve was obtained by using Linear Sweep Voltammetry for VMS containing 1.8 M H_2SO_4, 0.24 M $CuSO_4$, and 50 ppm Chloride (Fig. 4.1). The linear region of this curve is used for calculating the Tafel slope. The diffusion coefficient of cupric ions in this copper sulfate bath by limiting-current, i_L, measurement is around 5 x 10^{-6} cm^2s^{-1} [2]. This value can be used in the Levich equation to estimate i_L as a function of rotation speed. At high overpotentials a diffusion-limited current, i_L, of ~ 100 mA/cm^2 is observed under rotation speed of 400 rpm.

Tafel plot, log i against electrode potential E, appears in Fig. 4.2. As reviewed in Chapter two, Tafel equation under large η for cathode can be expressed as $log\ i= log\ i_o - \alpha zF\eta/2.3RT$ with slope -αzF/2.3RT (V^{-1})=-αz/0.0591(V-1). In this case, the Tafel slope of this additive-free electrolyte at rotation of 400 rpm was found to –8.3 (V^{-1}), or equals to -121 mV/decade. The corresponding charge transfer coefficient was calculated from Tafel slope as 0.5 (25°C), and the exchange current density, i_o, as 1.822 mA/cm^2. These values compared well with other research results [3,4]. The charge transfer coefficient of 0.50 corresponded to a classical two-stage mechanism for the deposition of copper with the assumption of z =1. We have more discussion for deposition mechanism in next section.

This result will be used as a benchmark to quantify the influence of organic additives on the Tafel slope, which is a reflection of charge transfer reaction kinetics for Cu deposition.

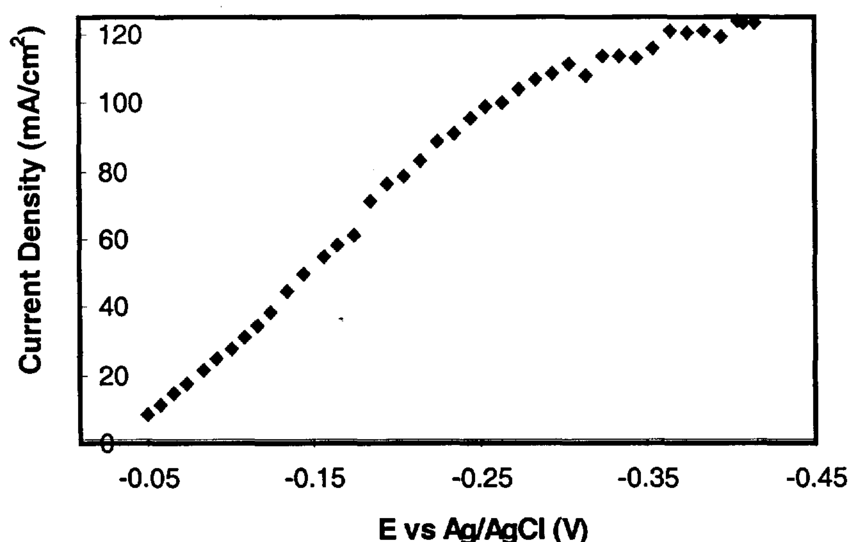

Fig. 4.1 Linear Sweep Voltammetry (LSV) curve obtained at a rotation speed of 400rpm on a platinum RDE in VMS electrolyte containing 1.8 M H_2SO_4, 0.24 M $CuSO_4$, and 50 mg/l Chloride

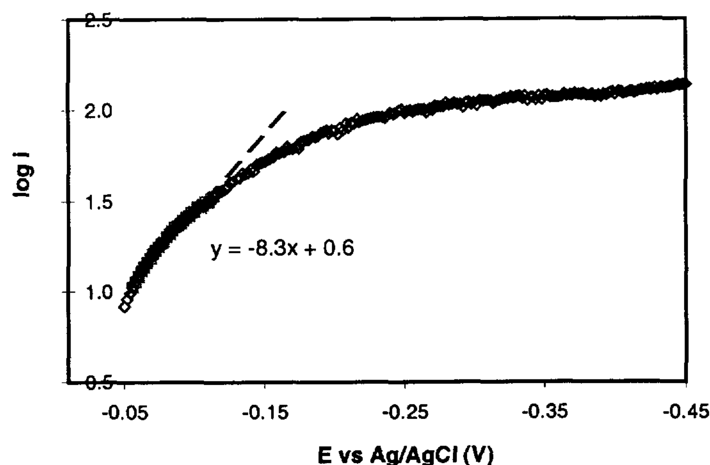

Fig. 4.2 Tafel plot of Cu electrodeposition without organic additives

Hysteresis Loop of VMS

Figure 4.3 shows a cyclic voltammetry curve of copper electrolyte without organic additives. The curve shows no sign of i-E hysteresis for the reverse plating. The lack of hysteresis of VMS indicates that no irreversible changes of the surface chemistry occur as the metal deposition proceeds. The lack of hysteresis from reverse plating normally result in a conformal trench fill growth, which causes center voids. The fill study results in next section have confirmed this characteristic

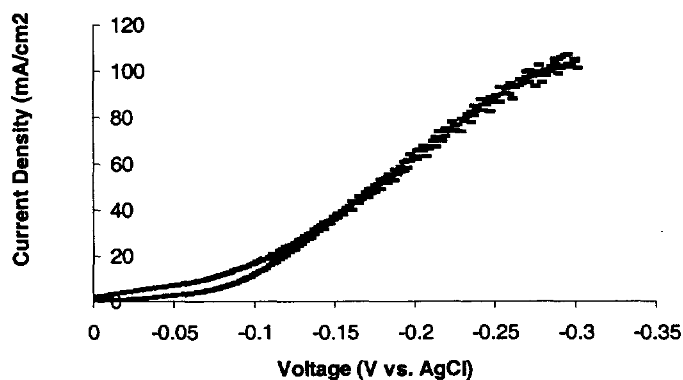

Figure 4.3. Cyclic Voltammetry curve of additive free copper electrolyte at rotation speed of 400 rpm containing 1.8 M H_2SO_4, 0.24 M $CuSO_4$ and 50 ppm Cl

Chronoamperometry Response of VMS

Figure 4.4 shows two current responses curves from two potential steps of –0.15 V and –0.20 V. For –0.15 V overpotential, it results in an initial current density of ~58 mA/cm^2 that decays within a few seconds to a steady-state value of ~50 mA/cm^2. This can be explained that the initial Cu deposition is charge transfer limited with fast deposition rate, but Cu diffusion cannot sustain this rate. It quickly becomes mass transfer control reaction, then reached the steady state. This result is also used as a benchmark to quantify organic additive influence on Cu deposition rate. For higher overpotential of –0.20 V vs AgCl, the deposition reaction started with mass transfer control and gradually reached steady state.

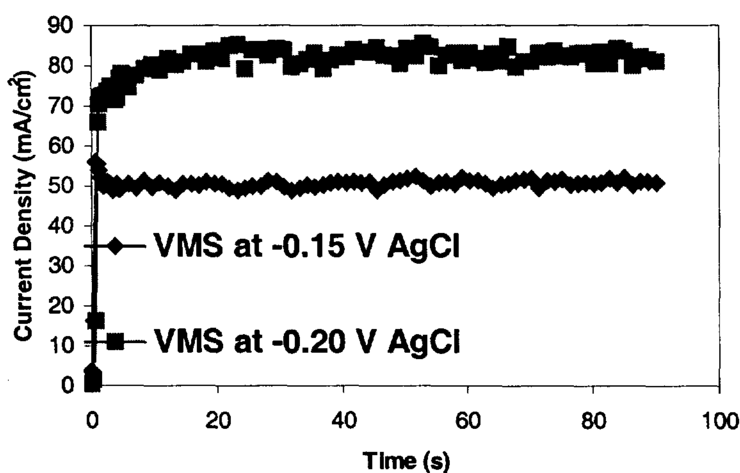

Fig.4.4 Two chronoamperometric transients for deposition at various potentials from the additive-free electrolyte.

4.1.2. Cu Electrochemical Deposition and Trench Fill

Before starting our investigation initial depositions were performed over a wide range of conditions to establish upper and lower limits of the various parameters for additive-free plating solution. For example, it was found that when Cu concentration was low (10 g/l) and plating current high (45 mA/cm^2), the Cu film was very rough and

porous due to hydrogen evolution. This film oxidized very quickly and film color changed to dark red within a couple of minutes. This defined the high current density limit as 45 mA/cm^2. When the Cu concentration was increased to 15 g/l, non-porous Cu film was produced. This marked the lower limit of the Cu concentration, which just met the acceptable level of film integrity.

Fill study was carried out with a Sematech standard via coupon wafer and plated in the modified Hull cell. Figure 4.5 shows the fill result from the standard high acid VMS electrolyte without any organic additives.

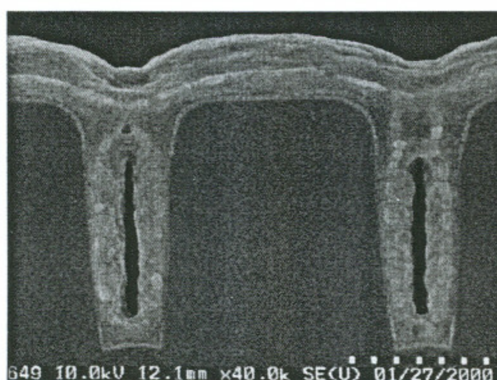

Figure 4.5 SEM cross section image of fill result from additive free copper electrolyte containing 1.8 M H_2SO_4, 0.24 M $CuSO_4$, and 50 ppm Cl.

The gapfill result shows a conformal growth of Cu in the via, which results in a center void. It is consistent with VMS electrolyte's electrochemical characteristics. This fill result is also used as the control for the organic additives.

4.1.3. Microstructure of Cu film Electrodeposited without Organic Additives

A very extensive study was carried out for Cu film microstructure plated without organic additives. The main purpose of this study is to find out the primary influencing

factor on film microstructure without organic additives. These results will help us to quantify the influence of thiols on the film microstructure in the later study.

The experiment was carried out with a series of different combinations of plating conditions to examine the effect of each plating parameter and its interaction with others on the microstructure. The range of plating conditions examined is listed in Table 4.1

A repeated 2^4 full factorial with 4 center points (total of 36 runs) were carried out to characterize the impact of these conditions on the film microstructure. Film thickness, texture, roughness, and grain size were measured for each plated sample.

Table 4.1 Plating variables for Cu film deposited without organic additives

	High	Middle	Low
Current Density (mA/cm^2)	45	25	5
Cu concentration (g/l)	30	20	15
Acid Concentration (g/l)	250	200	150
Cl concentration (mg/l)	90	60	30

Film thickness were 1um for all the conditions measured with a profilometer. Texture of electroplated Cu film was measured by using x-ray diffraction (XRD) utilizing Bragg-Bretano θ-2θ measurements using Siemens D5000. The roughness of the electroplated film was characterized with an atomic force microscope (AFM). The grain size distribution of copper film was obtained from plan-view transmission electron microscope (TEM) images and atomic force microscopy.

Copper sulfate solution was made with crystal of copper sulfate, 96% H_2SO_4, and HCl. Ten different electrolyte baths were used in this study based on Table 4.1.

The electroplating system for these blanket coupons consisted of a copper plating solution, an inert anode (Pt), where the substrate served as a cathode, all in a glass jar with a magnetic stirrer.

Film thickness, texture, roughness, resistivity, and grain size were measured for each plated sample after two days of electroplating on a blanket wafer fragment. This

allows for any self-annealing of plated copper film. Therefore, the study result presented here is the static film property and its microstructure.

Texture of electroplated Cu films

Regardless of the different plating conditions, all the Cu films had a predominant (111) XRD peak. It is known that the XRD peaks become broader as the grain size decreases [9]. Hence, the full width half maximum (FWHM) of this peak was used to examine the trend in the grain size with the process parameters. Our results showed that the FWHM was narrow for low current density films and wide for high current density films, independent of a wide range of other bath parameters. This is illustrated in Table 4.2 with a selected set of process conditions. Each sample was measured twice over a two week range to prove no or very little grain size change or film re-crystallization. Experimental result showed that grain size is highly dependent on the current density compared to other bath conditions.

Table 4.2 FWHMs of the Cu(111) x-ray diffraction peaks of samples plated under different conditions.

Sample ID	Plating Condition Cu(g/l)/ H+(g/l)/ Cl-(mg/l)/ I(mA/cm2)	Cu(111) FWHM	Intensity (arb. Units)
15	30/250/30/45	0.234	16,600
16	30/250/90/45	0.240	12,400
26	10/150/30/45	0.240	7,100
11	30/250/30/5	0.148	8,100

Microstructure of electroplated Cu films

The microstructure of the electroplated copper films was investigated initially using TEM and then with an AFM. Examination of the TEM micrographs showed a significant dependence of the grain size on the current density. Fig.4.6 shows a comparison of two TEM images, one sample produced with high current density and the

other with low current density. It consistently showed the trend that low current density generated large grain size and high current generated small grain size.

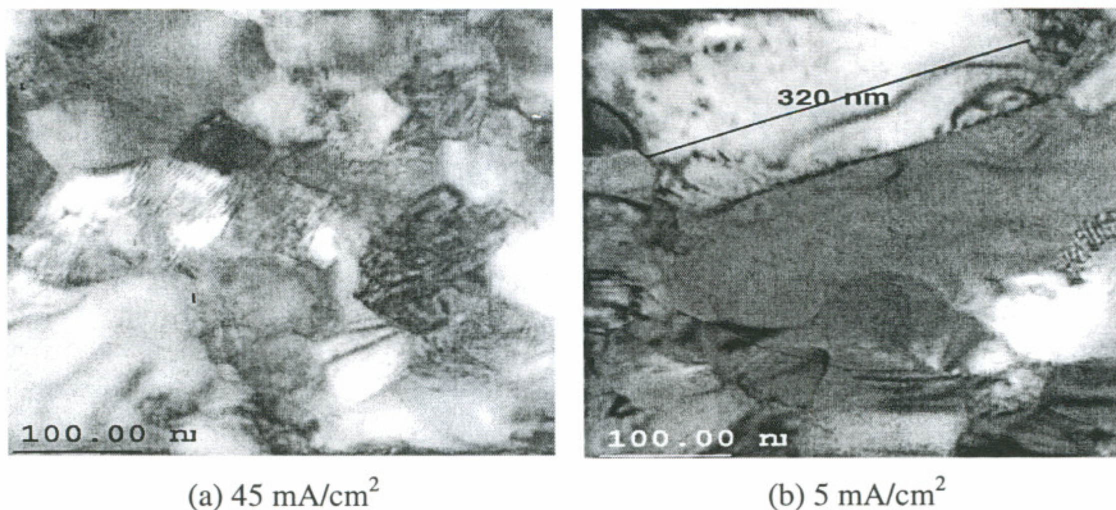

(a) 45 mA/cm^2 (b) 5 mA/cm^2

Figure 4.6 Transmission electron micrographs of the copper films electroplated at a current density of (a) 45 mA/cm^2 and (b) 5 mA/cm^2. In both cases the bath consisted of Cu(g/l)/H^+(g/l)/Cl(mg/l) : 30/250/30.

Three-dimensional AFM images of morphology and growth pattern of electroplated Cu under different electroplating conditions are shown in Figs. 4.7(a) - (d), showing a very different film topography, roughness, and grain size. The samples shown in Figures 4.7a and 4.7b had Cu(g/l), acid(g/l), and chloride (mg/l) concentrations of 15/150/30 and 30/250/90 respectively, hence different bath chemistries but the same current density of 45 mA/cm2. However, the texture and grain size of these samples are almost the same.

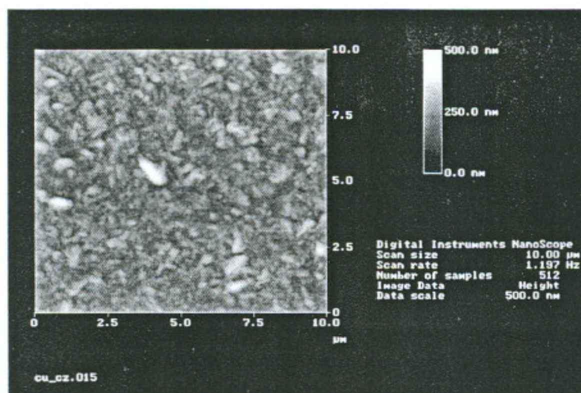

Fig. 4.7(a): 45mA/cm^2,
Cu(g/l)/H$^+$(g/l)/Cl(mg/l):15/150/30

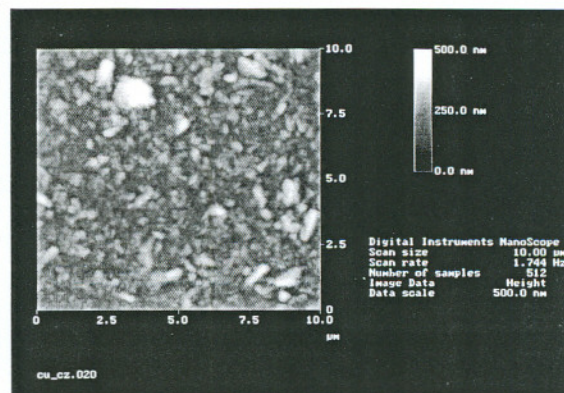

Fig. 4.7(b): 45mA/cm^2,
Cu(g/l)/H$^+$(g/l)/Cl(mg/l): 30/250/90

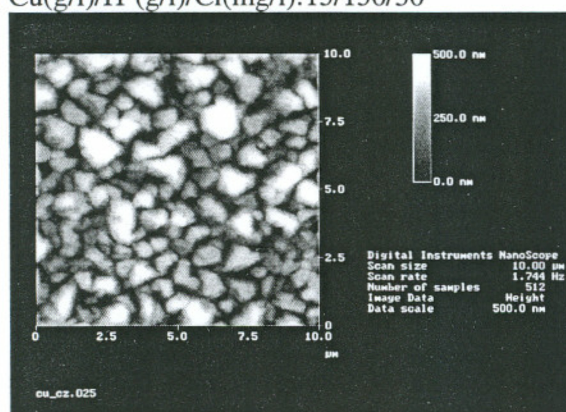

Fig. 4.7(c): 5 mA/cm^2,
Cu(g/l)/H$^+$(g/l)/Cl(mg/l): 30/250/30

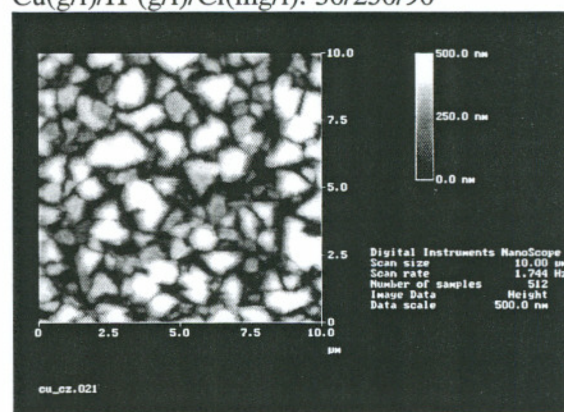

Fig. 4.7(d): 5 mA/cm^2,
Cu(g/l)/H$^+$(g/l)/Cl(mg/l): 30/150/30

Fig. 4.7 AFM views of Cu film surfaces deposited at (a),(b): 45 mA/cm^2 with different bath chemistry, and (c),(d): 5 mA/cm^2 with different bath chemistry, showing the film roughness and grain size difference at two current densities.

The grain size at a current density of 5 mA/cm2 is shown in Figures 4.7c and 4.7d, where the bath compositions had Cu, acid, and chloride concentrations of 30/250/30 and 30/150/30 respectively. These micrographs illustrate that regardless of the bath composition, the grain size is dependent only on the current density.

The grain size of electroplated Cu film first measured with TEM analysis was correlated to the AFM analysis. The AFM results of film roughness and film grain size are summarized in Table 4.3. The roughness and film grain size were measured and calculated with a 10 µm field of view. To compute the RMS roughness, a two dimensional plane is fit to the AFM height data. The resulting standard deviation of the fit is reported as the RMS surface roughness. The mean roughness (Ra), is also listed.

The grain size is calculated by AFM average grain size function with the same threshold height for each sample. A statistical analysis of AFM results was carried out to identify the impact of each bath parameter and their interaction on the film roughness and grain size.

Table 4.3 Roughness and Grain Size of Plated Cu Films

Sample ID	Plating condition Description				Roughness (nm)		Grain Size
	Cu Conc. g/l	I density mA/cm2	Acid Conc g/l	Cl conc. mg/L	RMS	Ra	Mean Diameter nm
1	15	5	150	90	66.39	53.11	346
2	30	5	150	90	95.15	75.40	352
3	15	45	250	30	25.90	20.09	151
4	30	45	150	30	22.06	16.49	168
5	30	45	150	90	27.44	20.13	130
6	30	5	150	30	60.45	49.08	405
7	15	45	250	90	41.77	30.56	133
8	15	5	250	90	92.09	73.28	473
9	30	5	250	30	97.50	78.90	512
10	15	5	250	30	82.30	66.04	676
11	30	45	250	30	26.15	18.68	161
12	30	45	250	90	34.12	24.61	219
13	30	5	150	90	130.95	105.90	708
14	15	5	150	30	48.60	39.30	385
15	15	45	150	30	29.27	21.5	190
16	15	45	150	90	30.16	21.77	154
17	17.5	25	200	60	27.67	20.93	267

Using statistical analysis, we found that the current density had the most significant impact on the film roughness, which is consistent with TEM and AFM analyses. Figure 4.8 shows the statistical analysis of Prediction Profile. From Prediction Profile, one can see that increase of copper concentration, acid concentration, and chloride concentration cause some increase in roughness. However, the current density showed a strong reverse impact on film roughness.

Pareto plot of estimates of different plating conditions, shown in Figure 4.9, indicate that next to current density, chloride concentration is the second most important

factor that influences the film roughness. The interaction of chloride concentration and current density also have an inverse impact on the film roughness and grain size following the interaction of chloride and current density. On the other hand, copper concentration and acid concentration have negligible impact on film roughness and grain size.

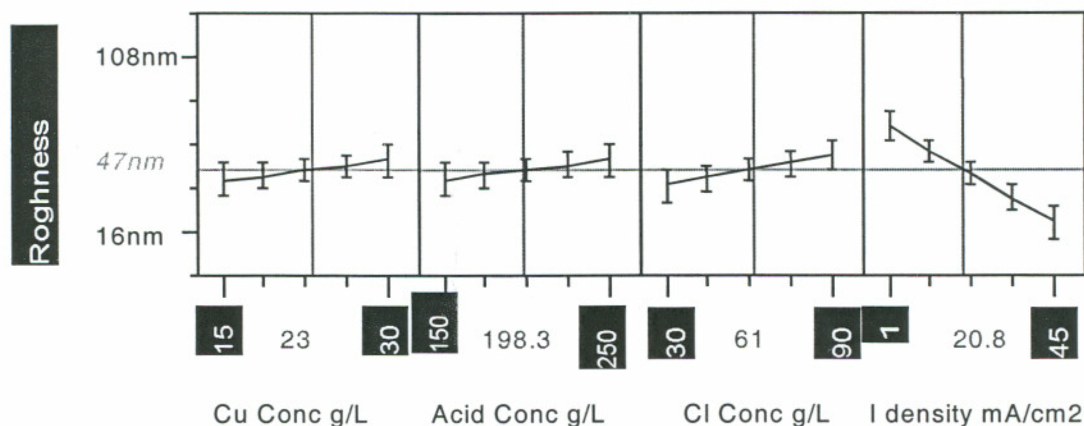

Figure 4.8 Prediction profile showing the surface roughness dependence on the Cu, acid and Cl concentrations, and the current density.

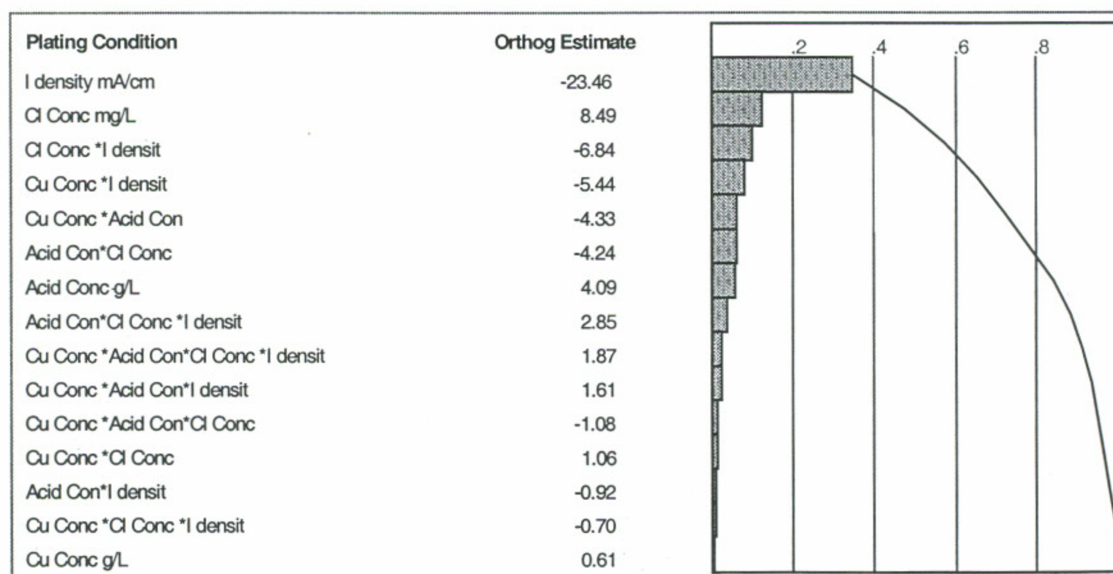

Plating Condition	Orthog Estimate
I density mA/cm	-23.46
Cl Conc mg/L	8.49
Cl Conc *I densit	-6.84
Cu Conc *I densit	-5.44
Cu Conc *Acid Con	-4.33
Acid Con*Cl Conc	-4.24
Acid Conc g/L	4.09
Acid Con*Cl Conc *I densit	2.85
Cu Conc *Acid Con*Cl Conc *I densit	1.87
Cu Conc *Acid Con*I densit	1.61
Cu Conc *Acid Con*Cl Conc	-1.08
Cu Conc *Cl Conc	1.06
Acid Con*I densit	-0.92
Cu Conc *Cl Conc *I densit	-0.70
Cu Conc g/L	0.61

Figure 4.9 Pareto plot shows the dependence of the surface roughness on the bath parameters and their interactions

All these parameters, to some degree, affect nucleation and subsequent growth rate of the Cu grains, hence the microstructure of the deposited film. In general, fine crystalline structures are produced under conditions favoring rapid nucleation and slow growth rate of the grain nuclei. Conversely, when the growth rate dominates the nucleation rate, large grains are produced. Based on this, it stands to reason that at low current density fewer nucleation sites are formed which then grow into larger grains, compared to high current density where large number of nucleation sites leads to more grains but of smaller size. Introduction of additives such as suppressors or accelerators to the bath will tend to lessen the dominance of the current density on the film morphology that we have observed. The effect of these additives on the microstructure of the Cu films and hence their EM reliability is the subject of discussion in the next section.

In summary, it was found that all electroplated Cu films had strong (111) orientation. Film roughness and grain size were dominated by plating current density in additive-free plating bath. XRD, AFM, and TEM data consistently showed large grain size and a rough film for low current density plating, and small grain size with a smooth film at high current density.

4.2 Cu Electrodeposition with Organic Additives

A commercial standard copper sulfate solution was used for copper sulfate bath with organic additives. It consisted of 1.8 M H_2SO_4, 0.24 M $CuSO_4$, and 50 mg/l Cl. PEG (MW 4600) which came as powder was weighed and dissolved in the standard copper sulfate solution. Six commonly used acid copper bath thiols, Bis-(sodium sulfopropyl)-disulfide(**SPS: $^-SO_3(CH_2)_3$-SS-$(CH_2)_3SO_3^-$**), 3-Mercapto-1-propanesulfonic acid(**MPS:HS-$(CH_2)_3SO_3^-$**),(O-Ethyldithiocarbonato)-s-(3-sulfoproplyl)-ester, potassium salt(**OPX:$^-$OSC-S-$(CH_2)_3SO_3^-$**), 3-S-Isothiuronium Propyl Sulfonate (**UPS:$^+NH_2NH_2$C-S-$(CH_2)_3SO_3^-$**), N,N-Dimethyl-dithiocarbamylpropyl sulfonic acid, sodium salt (**DPS: H_3C-N-H_3C-C=S-S-$(CH_2)_3$-SO_3Na),** and 3-(2-Benzthiazolylthio)-1-propanesulfonic acid, sodium salt (**ZPS: H_5C_5NSC-S-$(CH_2)_3$-SO_3Na**) were studied in this Cl-PEG-Thiol multi-component bath. SPS, OPX, DPS, UPS, MPS, ZPS (Raschig GmbH, Germany)

were first dissolved in deionized water to make a 600 ppm concentrated stock solution. These additives were well mixed 30 min. before experiments.

Levelers generally disrupt bottom-up filling resulting in center void formation at concentrations which level surface. From electrochemical characterization standpoint, leveler is behaving like a suppressor. Based on this conflicting role of leveler and its interference with Suppressor and Carrier, this additive is skipped from this research to get a clear signal of other additives.

The electrochemical characterization method used is same as the method for VMS solution. Fill study is carried out in the same manner as checking the VMS solution. For film Microstructure studies, all electrolyte concentrations are kept same except with different thiols.

4.2.1 Cu Electrodeposition with Cl-PEG-SPS Bath

In this section, one of the most commonly used thiols, SPS, in freshly made electrolyte package of Cl^-+PEG+SPS was studied. The bath was characterized by CVS, LSV, and CA on a rotating disk electrode. The influence of SPS on the trench filling capability and film microstructure was examined. The work was also focused on the effects of aging of acidic thiols solutions and finding criteria for detecting such effects, which is presented in next chapter. The characterization of this electrolyte package and its aging were used to provide explanation of trench-fill result and interpreted quantitatively to provide kinetic parameters. This information can be used for designing of new bath chemistries, developing process control strategies, and process modeling.

SPS is widely used as an accelerator for Cu electroplating bath. The Cl-PEG-SPS electrolyte bath is the most commonly used Cu electroplating bath for ULSI interconnects. The chemistry name of SPS is an abbreviation of Bis-(sodium sulfopropyl)-disulfide with a molecular structure shown in figure 4.10. It has a molecular weight of 354 g/M and is easy to dissolve in water. Allan West et al., have studied bath chemistry of (a) chloride, (b) chloride and polyethylene glycol (PEG) [5,6] together, and (c) chloride, PEG, thiol[(bits(3-sulfopropyl) disulfide(SPS)], and diethyl safranine azo

dimethyl aniline(Janus Green B) electrolyte package that stems from patent literature for printed circuit board (PCB)[2]. For this research, Cl-PEG-SPS bath was studied as a benchmark organic electrolyte package to provide a comparison for the characterization of other thiols.

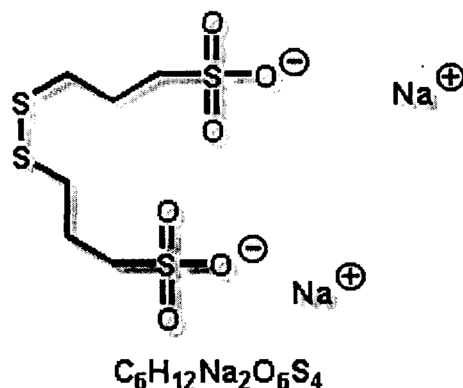

Fig. 4.10 SPS: Bis-(sodium sulfopropyl)-disulfide(SPS).

4.2.1.1 Electrochemical Characterization of Cl-PEG-SPS Electrolyte

Polarization Measurement of Cl, PEG, and SPS bath:

The polarization measurements for copper deposition from electrolytes containing various combinations of Cl-PEG-SPS are shown in Fig. 4.11. In agreement with previous reports [5,6,7], the addition of Cl-PEG provides significant inhibition of the deposition reaction compared to the polarization characteristics for copper deposition from the bath containing only chloride ions. It has also been verified by a CVS study that chloride or PEG individually does not suppress copper deposition [5,6].

When chloride, PEG, and SPS are all present, the combined action of all three additives yields net inhibition relative to a Cl^- only electrolyte, although an acceleration of the rate relative to Cl-PEG electrolyte is apparent, which reflects the competition

between the effects of PEG and SPS. However, it has to be noted that, without PEG in the electrolyte, SPS has an insignificant influence on current density.

The agreement of this research result with previous reports validates the electrochemical characterization method. Fig. 4.11 is also used as a benchmark for comparison with other thiols.

Tafel kinetics for copper deposition from solutions containing organic additives showed marked changes compared to those with additive-free electrolytes. Figure 4.12 shows cathodic Tafel slopes for Cl^- (additive-free), Cl^-+PEG, and Cl^-+PEG+SPS electrolytes. An increase in the Tafel slope from its original value of –121 mV for additive –free electrolyte to –7.4 (V^{-1}) or -135 mV for electrolyte containing 300 ppm PEG (MW 4600), and to –8.5 (V^{-1}) or –122 mV for electrolyte containing 300 ppm PEG and 6 ppm SPS. The corresponding charge transfer coefficient, assuming a one electron change, was found to be 0.44 for PEG and 0.51 for PEG+SPS. The observed changes in the cathodic Tafel slope and the corresponding decrease in α in the presence of Cl+PEG suggests that the process taking place on the electrode surface no longer be a simple one electron transfer. This may be attributed to formation of complex between organic additives and cuprous ions at the electrode surface as part of charge transfer reaction. Further more, the presence of PEG results in lower charge transfer coefficient, i.e., makes charge transfer reaction more difficult than the additive-free electrolyte. On the other hand, the addition of SPS increases the charge transfer coefficient compared to Cl-PEG electrolyte. Hence, Cl^-+PEG+SPS electrolyte stays between these two limits.

The exchange current density was 0.079 mA/cm^2 for Cl-PEG electrolyte, and was 0.501 mA/cm2 for Cl-PEG-SPS electrolyte based on Tafel plot. The exchange current can be viewed as the equilibrium charge exchange speed across the interface. The observed decreases in the exchange current density in the presence of Cl-PEG confirmed that they act together inhibiting the copper deposition reaction. It requires very high overpotential to activate the electrodeposition reaction for Cl-PEG electrolyte. In sharp contrast, the addition of SPS increased the exchange current density compared to Cl-PEG electrolyte, which confirmed the accelerating characteristic of SPS.

More discussion of organic additive working mechanism is presented in next section.

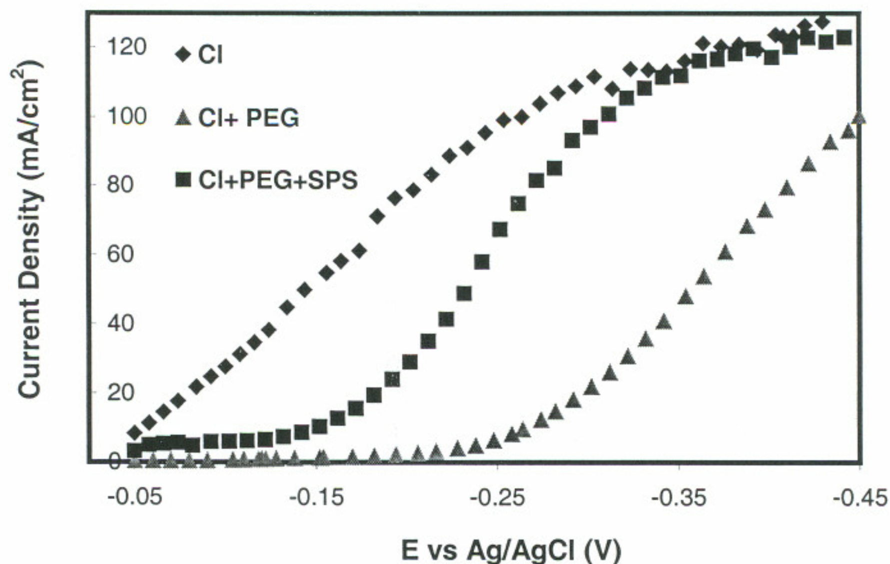

Figure 4.11 LVS curves obtained at a rotation speed of 400 rpm on a platinum RDE in the baths with various combinations of additives. All electrolytes contain 1.8 M H_2SO_4, 0.24 M $CuSO_4$. In addition, the curve labeled Cl^- has 50 ppm Cl^-. PEG: has 300 ppm PEG (M.W.4600); SPS has 6 ppm SPS.

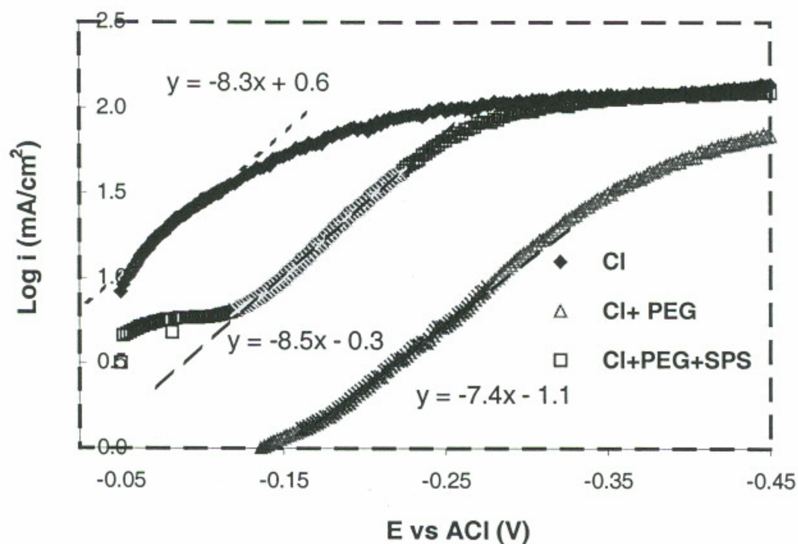

Fig. 4.12 Tafel plot of Cu electrodeposition with various organic additives.

Hysteresis Loop of Cl-PEG-SPS Bath;

One important consequence of the competition between inhibition and acceleration process is the possibility of hysteresis in the cyclic voltammetric behavior [1,8]. As shown in Fig. 4.13, significant hysteresis is apparent in the case of Cl-PEG-SPS electrolyte, although little or no hysteresis is observed for the binary combination of Cl-PEG, or the additive-free electrolyte. The lack of hysteresis of the Cl-PEG and additive-free electrolyte indicates that no irreversible changes of the surface chemistry occur as the metal deposition process is reversed. In contrast, the hysteresis associated with the full combination of additives indicates that the competition between inhibition provided by the Cl-PEG Cu^{2+}/Cu interaction and the catalytic effects of $Cl^{-}SPS/Cu^{2+}/Cu$ interaction leads to an irreversible change in the reaction dynamics. This characteristic correlates with superfilling capability of the electrolyte package and is critical for a strong bottom up trench fill. Fill study result presented in next section is consistent with this characterization.

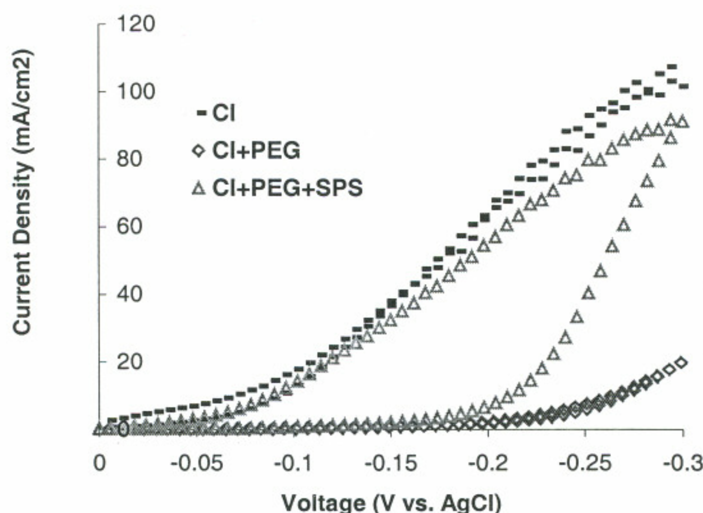

Figure 4.13 Cyclic Voltammetry curve of Cl+PEG+SPS electrolyte. The base electrolyte contains 1.8 M H_2SO_4, 0.24 M $CuSO_4$ and 50 ppm. of Cl.

Chronoamperometry Response of Cl, PEG, and SPS

Fig. 4.14 shows the chronoamperometry response of VMS and electrolytes with Cl+PEG and Cl+PEG+SPS under overpotential of –0.15 V vs. Ag/AgCl. It clearly demonstrated that the presence of Cl+PEG greatly suppressed deposition rate, and SPS increased the current compared to Cl+PEG electrolyte. This result is consistent with all other characterization results.

Fig 4.15 presents chronoamperometry curve of VMS and electrolytes with Cl+PEG and Cl+PEG+SPS under overpotential of –0.20 V and –0.25 V vs. Ag/AgCl. The Cl+PEG+SPS curve showed although charge transfer controls the initial phase of the deposition rate, diffusion of copper becomes the rate control factor in about 30s, which makes the CA curve almost equivalent to VMS. However, Cl+PEG electrolyte is still completely suppressed under this higher overpotential.

These results will be used as the benchmark for other thiols in the later sections.

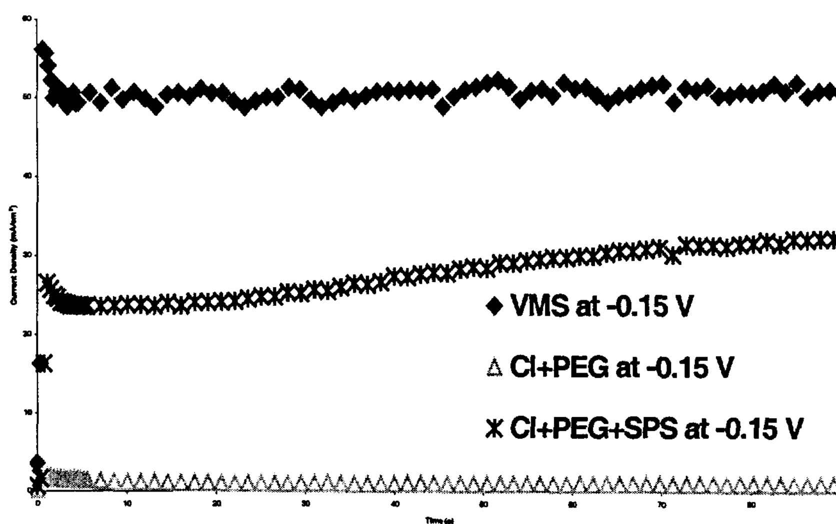

Fig. 4.14 A series of chronoamperometry curves for various electrolytes under overpotential of –0.15 V vs. Ag/AgCl.

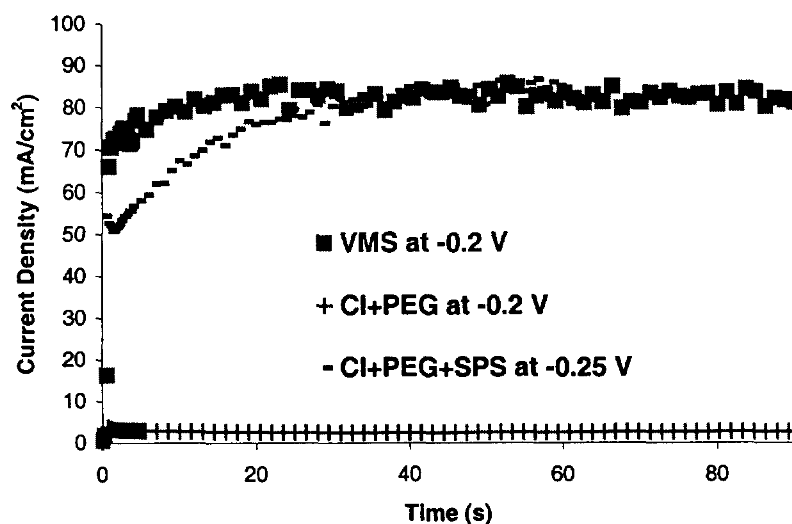

Fig. 4.15 A series of chronoamperometry curves for various electrolytes under overpotential of –0.20 and –0.25 V vs. Ag/AgCl.

4.2.1.2 Result of Fill Studies of Cl-PEG-SPS Bath

Effect of Cl and PEG

The substrates used for this phase investigation contained an array of trench sizes. The aspect ratio of trenches, as measured by SEM cross-sections was around 1:6.

Fig. 4.16 shows the fill result of bath with PEG only and PEG/Cl only. In both cases, a conformal Cu growth was produced in trenches and generated no bottom-up fill. This result is consistent with the electrolyte electrochemical characterization results discussed in the above section.

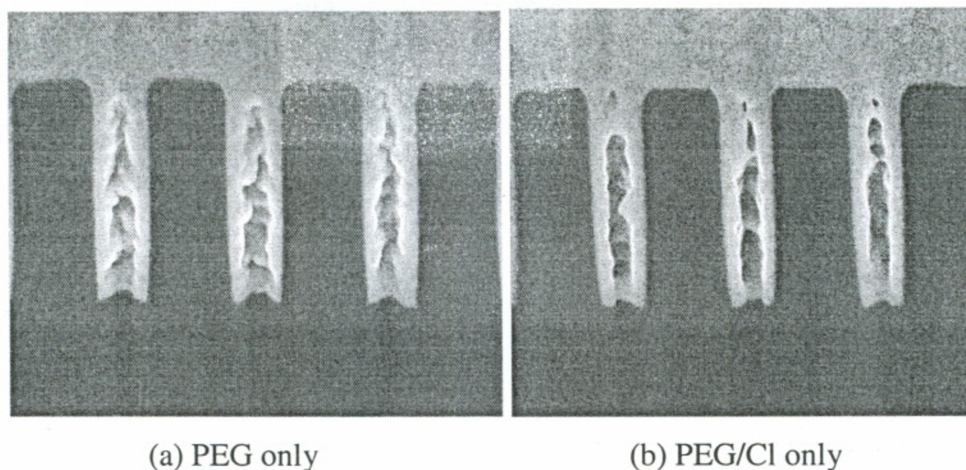

(a) PEG only (b) PEG/Cl only

Fig. 4.16 SEM cross sections of vias deposited with (a) PEG only, and (b) PEG/Cl only. The base electrolyte composition is 1.8 M H_2SO_4, 0.24 M $CuSO_4$, 50 ppm Cl, and 300 ppm PEG (MW 4600).

Effect of SPS

The concentration of SPS in the electrolyte also has an important influence on the process. When SPS concentration was 2 ppm, voids were observed. However, at Concentration of 12 ppm, void-free deposits resulted as shown in Fig. 4.17. The fill result can be influenced by many factors such as seed condition, mass transfer condition, and current density. In this research, all the factors were fixed for the fill study. The current density is a three step ramp plating that is normally used by IC industry.

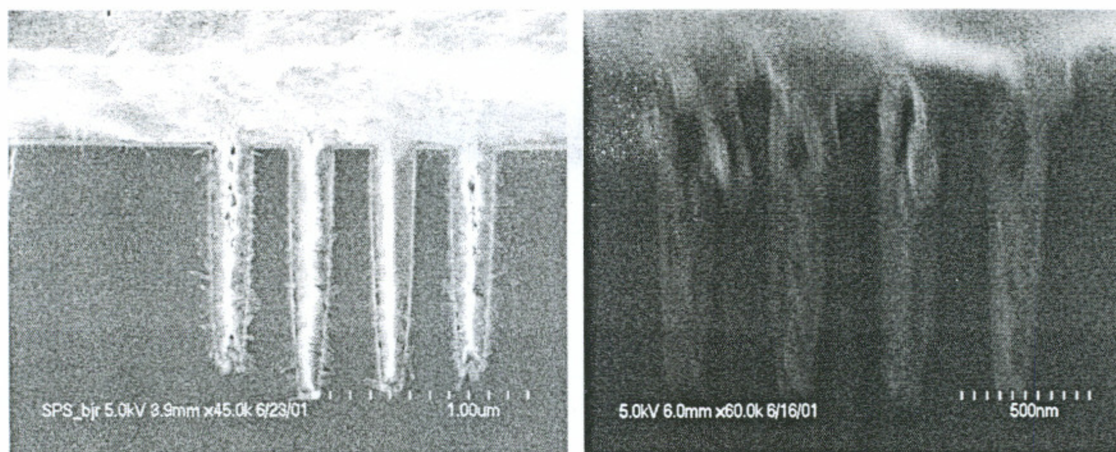

(a) 12 ppm SPS (b) 2 ppm SPS

Figure 4.17. Fill result of SPS at 12ppm. The base electrolyte composition is 1.8 M H_2SO_4, 0.24 M $CuSO_4$, 50 ppm Cl, 300 ppm PEG (MW: 4600) and (a) 12 ppm SPS; (b) 2 ppm SPS.

4.2.1.3 Microstructure of Cu Film Electroplated with Cl-PEG-SPS

Resistivity of Cu Film

Electroplated copper films typically have much higher electrical resistivity than bulk copper. The excess resistivity is associated with the defect structure in the electrodeposited films and is the result of scattering from grain boundaries, dislocations, vacancies, impurity atoms in solution, as well as second-phase particles [1]. The electrical resistance of thin blanket films was used to probe the influence of additive chemistry on impurity incorporation and its effect on microstructure evolution. The temporal evolution of the sheet resistance of 1 μm thick copper films, electrodeposited from the copper electrolyte containing various additives, is summarized in Fig. 4.18. Copper film electrodeposited from electrolytes containing no additives (VMS) showed nearly identical resistance-time behavior during the first 72 hrs after deposition while copper film from Cl-PEG bath had higher initial resistance but with little decreases. In sharp contrast, copper films electrodeposited from electrolyte containing Cl+PEG+SPS

had an initial resistance that was 12-15% higher than the other films but decreased by 25% within 24 hrs. This finding is in agreement with results reported for films deposited from proprietary electrolytes [1].

Examination of the initial film resistance shown in Fig 4.18 provided some insight into the extent of additive incorporation and the effectiveness of the various additives with regards to grain refinement. The minor change of the resistance over time induced by Cl-PEG reflects minimal perturbations of the microstructure that are in sharp contrast to the effects induced by the combination Cl-PEG-SPS. The change in the latter case was a direct indication of additive incorporation and grain refinement. Thus, resistivity data provide another measure of the synergism that exists between the constituents of the Cl-PEG-SPS electrolyte. This observation also supports the attribution of the hysteresis in the i-E curves to additive incorporation and the coincident alternation of the surface structure and reaction dynamics.

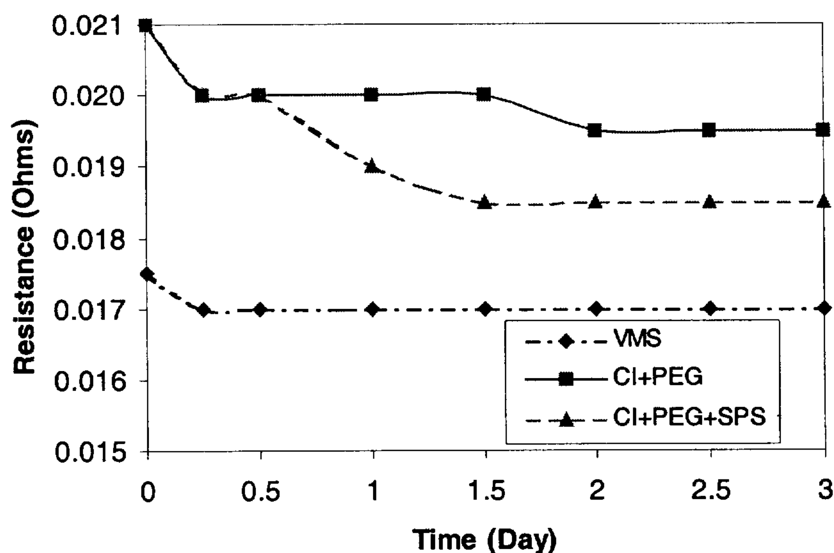

Fig. 4.18 Resistance transients during aging of 1 um thick Cu films at room temperature.

Texture of electroplated Cu films

Additives have known impact on the properties and structure of deposits. Other XRD study found that the hardness, structure, and texture of copper films obtained in deposition with additives change with time, and the evolution depended on the type of additives used [1]. For this investigation, XRD measurement was carried after two days of Cu film deposition. Therefore the XRD measurement result is based stabilized Cu film structure. The texture of electroplated Cu films from VMS and electrolytes containing Cl+PEG and Cl+PEG+SPS all showed dominated (111) oriented crystal structure (Fig. 4.19). However, Cu film from Cl-PEG-SPS bath has stronger diffraction density than Cu film from Cl-PEG bath, which has a stronger diffraction density than Cu film deposited from VMS (all measured at same time). This can be attributed to grain refinement by organic additive and inclusion of the additive in the deposit.

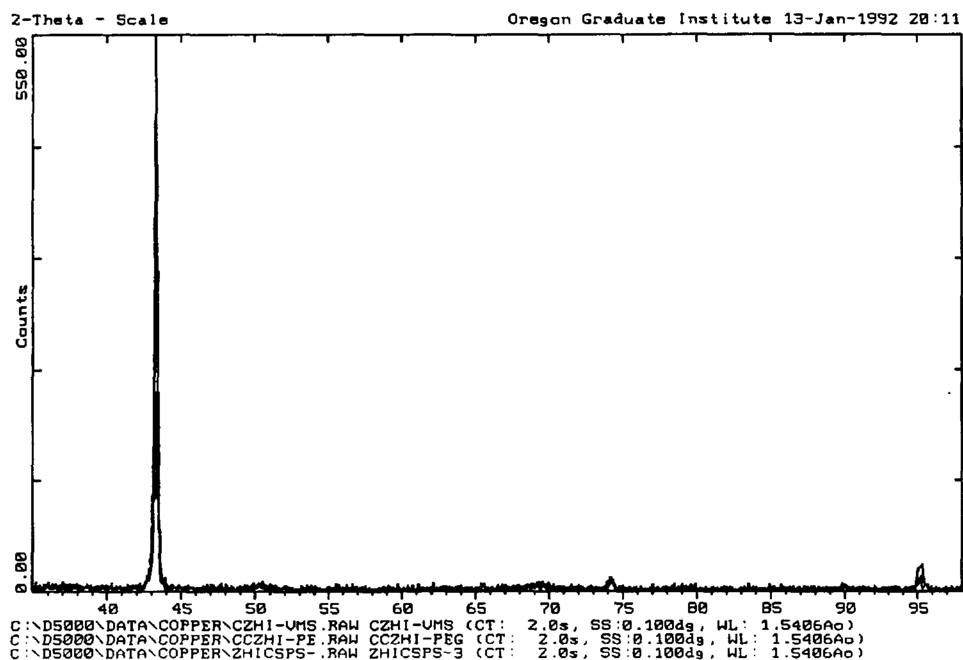

Fig. 4.19 X-ray diffraction pattern of Cu films electrodeposited from VMS, Cl-PEG, and Cl-PEG-SPS bath.

Morphology of electroplated Cu films

The AFM results of Cu films electrodeposited from VMS, Cl-PEG, and Cl-PEG-SPS bath were shown in Fig. 4.20, Fig. 4.21, and Fig. 4.22. Cu film from VMS has a RMS roughness of 105 nm while Cu film from Cl-PEG bath has a RMS roughness of 79nm. In contrast, Cu film from Cl-PEG-SPS has a RMS roughness of 55 nm. From roughness data and the AFM images, it is clearly seen that organic additives have a dramatic influence on Cu film microstructure. The addition of PEG refined grain size compared to Cu film from VMS. However, the presence of SPS significantly changed Cu film grain size and film microstructure. This is in good agreement with other research reports [9].

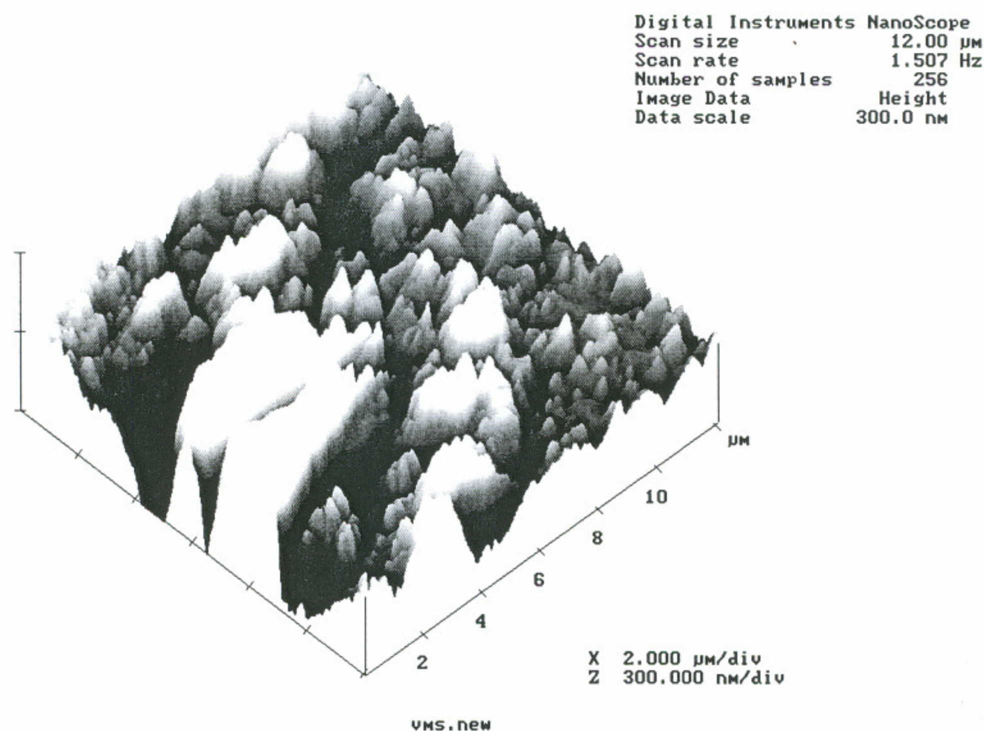

Fig. 4.20. AFM image of Cu film electrodeposited from VMS.

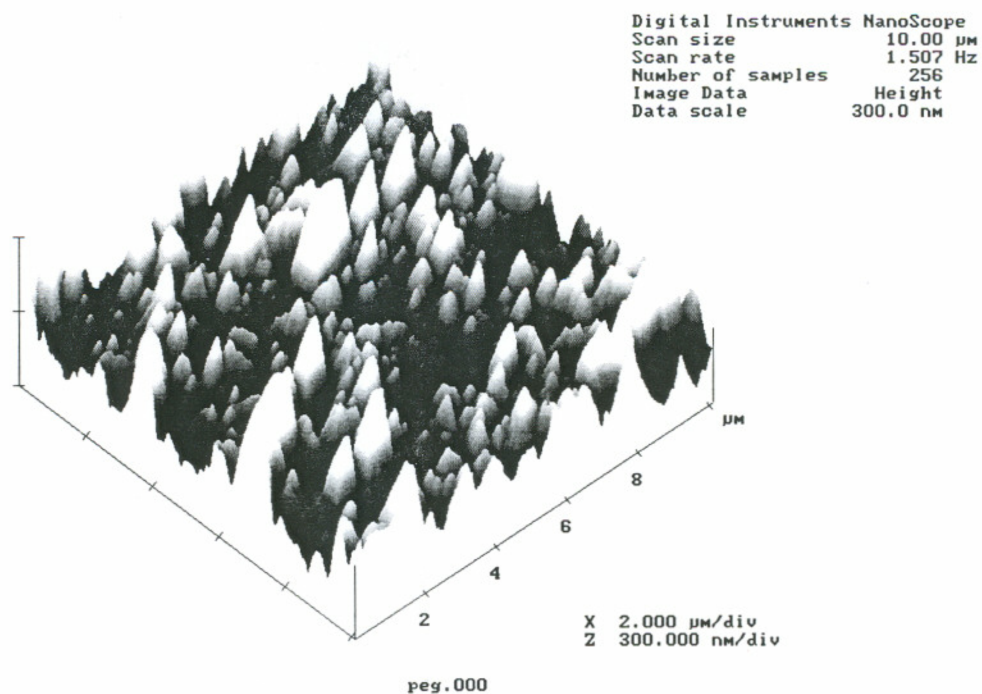

Fig. 4.21. AFM image of Cu film electrodeposited from Cl-PEG bath.

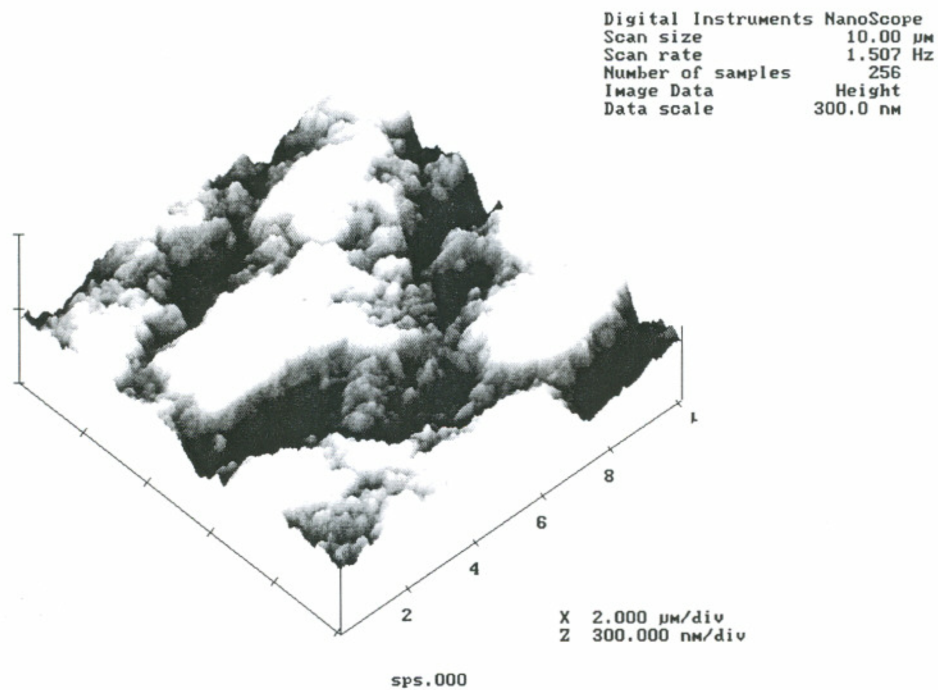

Fig. 4.22. AFM image of Cu film electrodeposited from Cl-PEG-SPS bath.

4.2.2 Cu Electrodeposition with Cl+PEG+UPS

UPS is the abbreviation of 3-[(Amino-iminomethyl)-thio]-1-propanesulfonic acid (**UPS:$^{+}NH_2NH_2C$-S-$(CH_2)_3SO_3^{-}$**), as shown in figure 4.23. It is a reactive sulfonate, additive for electroplating baths. It is also used as an anti-fog agent and stabilizer in the photographic industry. Compared with SPS, half of SPS structure is replaced with Amino-iminomethyl-thio. From knowledge of general electrochemistry, the nitrogen compound normally gives the organic additive more leveler-like characteristic, which suppresses the deposition rate.

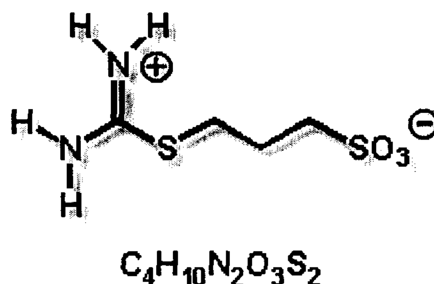

Fig. 4.23 UPS: 3-[(Amino-iminomethyl)-thio]-1-propanesulfonic acid.

4.2.2.1 Electrochemical Characterization of Chloride+PEG+UPS Bath

Polarization Measurement

The polarization measurement for copper deposition from electrolytes containing Cl-PEG-UPS is shown in Fig. 4.24. The polarization curve from Cl-PEG-UPS bath is very close to Cl-PEG bath with the deposition current totally suppressed. The lack of accelerating capability of this electrolyte package would normally result in a conformal growth for the trench fill. This conclusion is confirmed by the fill study result presented in next section.

The Tafel plot of Cl-PEG-UPS electrolyte package with other benchmark electrolytes is shown in Fig. 4.25. UPS bath has a Tafel slop of –7.3 (V-1) or –137 mV. The corresponding charge transfer coefficient is 0.43, which is equivalent to Cl-PEG

electrolyte. This indicates UPS retarding copper elecctrodeposition and acting more like a PEG to suppress electroplating current flow. The exchange current density of Cl-PEG-UPS electrolyte is 0.126 mA/cm^2, which is higher than that of Cl+PEG bath of 0.079 mA/cm^2, but much lower than benchmark SPS bath of 0.501 mA/cm^2. This again suggested the suppressing characteristic of UPS. Comparing the molecular structure of UPS with SPS, it indicates that the other end of group is apparently very important even though they both have thiol and disufide group on one side. We have more discussion in next section for UPS working mechanism in Cu electroplating bath.

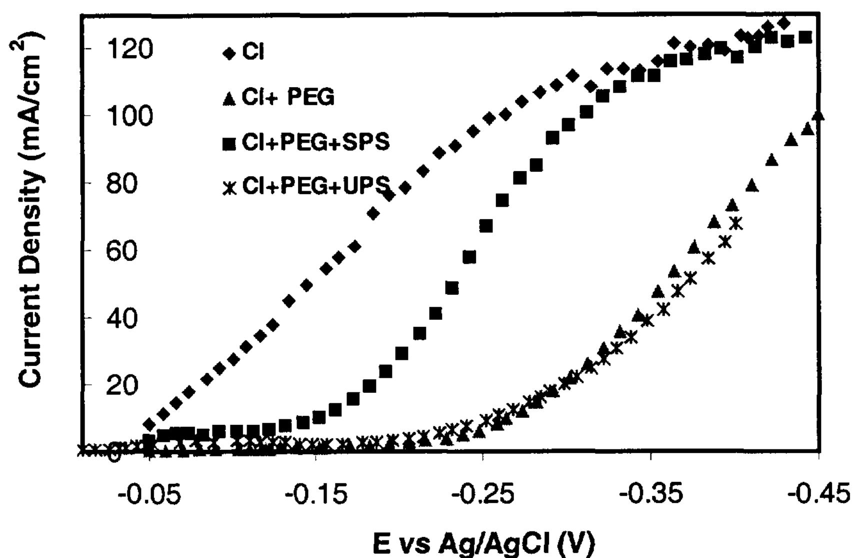

Figure 4.24 LVS curves obtained at a rotation speed of 400 rpm on a Pt. RDE in the baths with various combination of additives. All electrolytes contain 1.8 M H_2SO_4, 0.24 M $CuSO_4$. In addition, the curve labeled Cl^- has 50 ppm Cl^-. PEG: 300 ppm PEG (MW.4600); SPS: 6 ppm SPS; UPS: 6ppm UPS

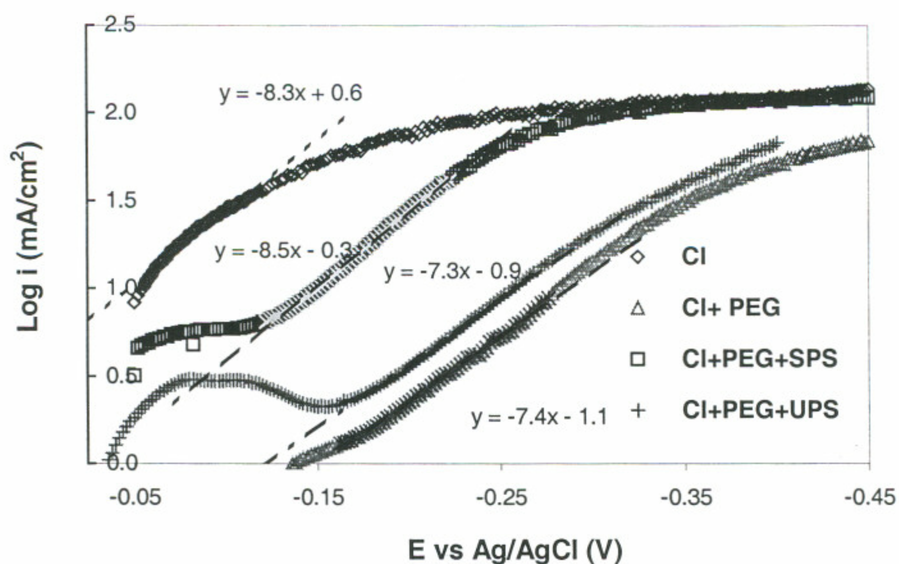

Fig. 4.25 Tafel plot for Cu electrodeposition in electrolytes with various organic additives.

Hysteresis Loop of Cl-PEG-UPS Bath;

The hysteresis loop of Cl-PEG-UPS is shown in Fig. 4.26 with other curves. Comparing with SPS hysteresis curve, UPS bath showed totally suppressed current with no i-E hysterisis. This characteristic is very similar to a carrier's behavior, which normally result in a conformal trench growth. This result is consistent with other characterization results and confirmed by fill result in next section.

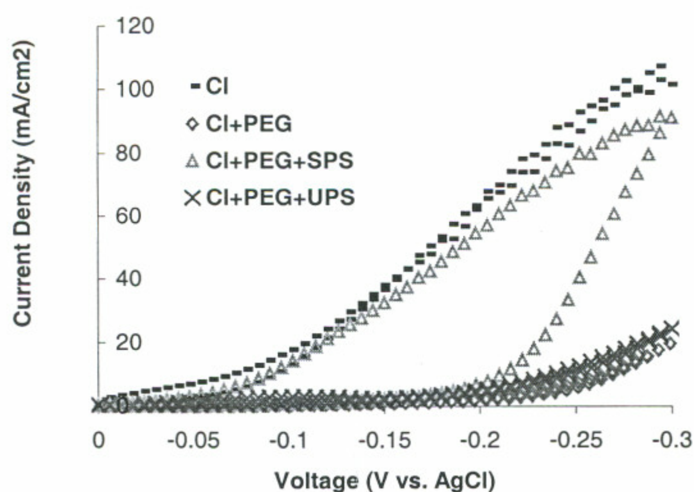

Figure 4.26. CV curves obtained at a rotation speed of 400 rpm on a platinum RDE in the baths with various combination of additives. All electrolyte contain 1.8 M H_2SO_4, 0.24 M $CuSO_4$. In addition, the curve labeled Cl- has 50 ppm Cl^-; PEG: 300 ppm PEG (MW.4600); SPS: 6 ppm; UPS: 6 ppm.

Chronoamperometry Response of Cl-PEG- UPS Bath

Fig. 4.27 showed the chronoamperometry response of VMS and electrolytes with Cl-PEG, Cl-PEG-SPS, and Cl-PEG-UPS under overpotential of –0.15 V vs. Ag/AgCl. It indicated very little accelerating capability of UPS in Cl-PEG-UPS electrolyte package. This confirmed the suppressing characteristic of UPS from another angle, and showed that UPS is acting as a suppressor and suppresses the copper deposition reaction.

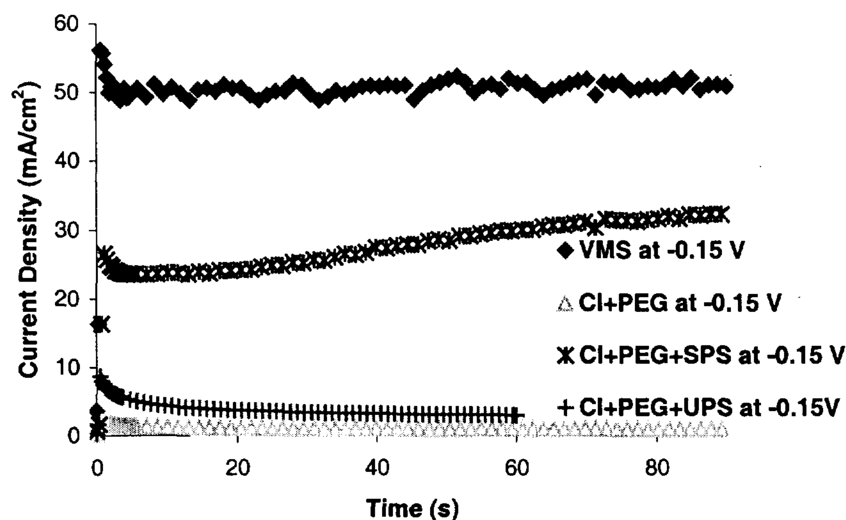

Fig. 4.27 A series of chronoamperometry cuves for various of electrolyte under overpotential of –0.15 V vs. Ag/AgCl

4.2.2.2 Result of Fill Study of Cl-PEG-UPS Electrolyte Bath

The fill results of different concentration of UPS in a standard Cl-PEG base are shown in figure 4.28 for (a) C_{UPS} = 6 ppm and (b) C_{UPS} = 12 ppm. Both results showed a center void resulting from conformal growth of Cu in the trench. Compared to the fill result from VMS and Cl+PEG bath, it showed a similar growth behavior. This result indicates that Cl-PEG-UPS electrolyte lacks superfilling capability. It is consistent with electrochemical characteristics of UPS discussed above. Based on electrochemical characterization and fill result, UPS should be categorized as suppressor. This result indicated that it would not warrantee the accelerating characteristic for an organic additive with a thiol and disufide structure. The other end of molecular group plays an important role for the electrochemical characteristics of a thiol.

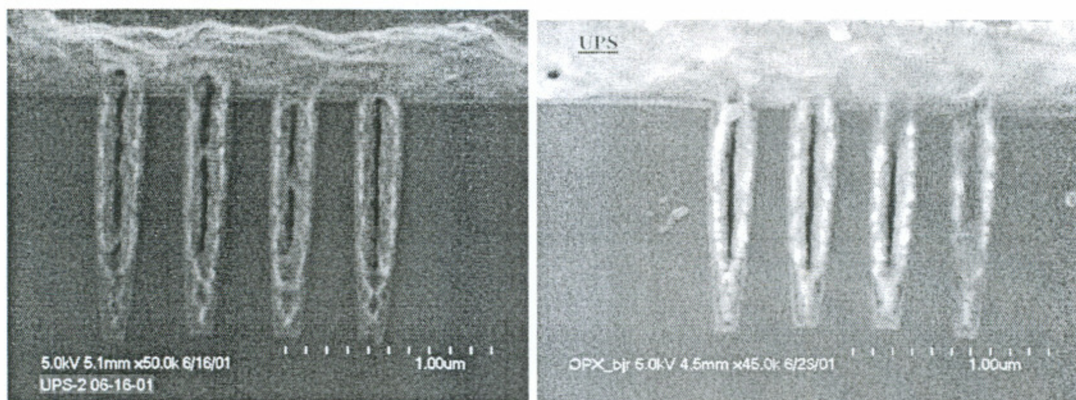

(a) 6ppm UPS (b) 12 ppm UPS

Figure 4.28. Fill result of UPS. The base electrolyte contains 1.8 M H_2SO_4, 0.24 M $CuSO_4$, 50 ppm Cl, 300 ppm PEG (MW = 4600), (a) 6 ppm UPS; (b) 12 ppm UPS.

4.2.2.3 Microstructure of Cu Film Electroplated with Cl-PEG-UPS

Resistivity of Cu film plated with Cl-PEG-UPS electrolyte

The temporal evolution of the sheet resistance of 1 μm thick copper films, electrodeposited from the copper electrolyte containing various additives, is shown in Fig. 4.29. Compared to benchmark electrolyte of Cl-PEG-SPS, copper film electrodeposited from electrolyte containing Cl-PEG-UPS had similar initial high resistance and the decrease within 72 hrs after electrodeposition. However, Cu film from UPS bath showed higher initial resistance and more decrease of resistance over time than Cu film from SPS bath. This is an indication for the difference of impurity incorporation and grain refinement between Cu film from SPS bath and Cu film from UPS bath. This difference provides another support for the difference of UPS functionality in copper electroplating bath compared to SPS. This observation also supports the attribution of the hysteresis in the i-E curves to additive incorporation and reaction dynamics.

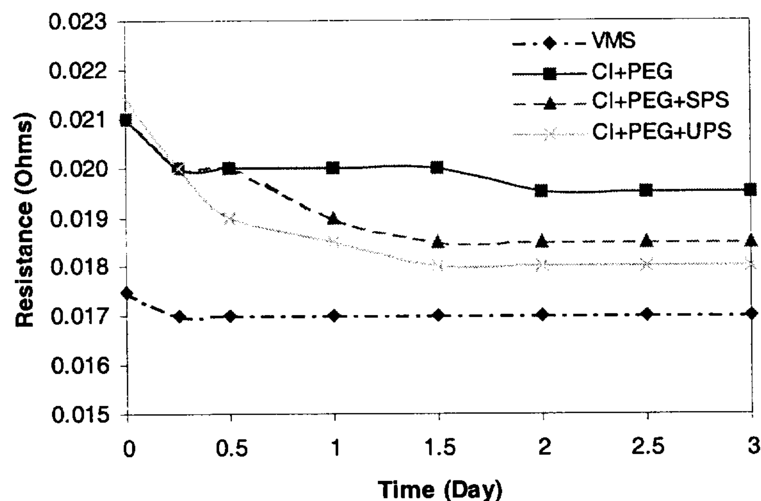

Fig. 4.29. Resistance transients during aging of 1 um thick Cu films at room temperature.

Texture of electroplated Cu films

The texture of Cu film electrodeposited from Cl-PEG-UPS electrolyte is shown in Fig. 4.30. Compared to benchmark Cu film deposited from Cl-PEG-SPS bath, it also showed a strong (111) oriented crystal structure. However, several small peaks were observed in the texture of Cu film from UPS bath, which was not in the Cu film from SPS bath. This is another indication of the film structure difference between two films.

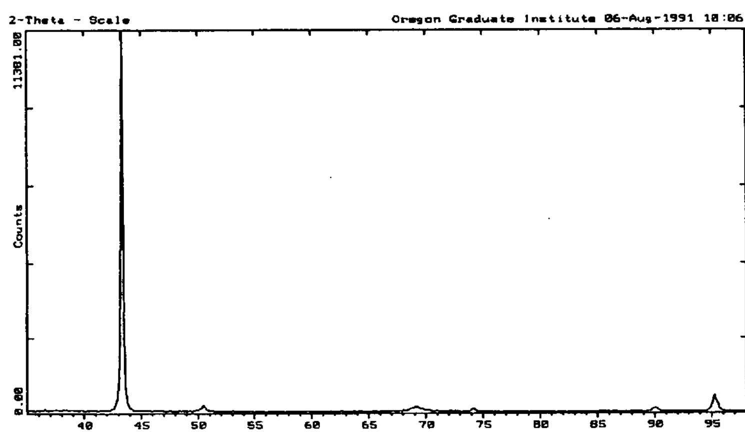

Fig. 4.30 X-ray diffraction pattern of Cu films deposited from Cl-PEG-UPS bath.

Morphology of electroplated Cu films

The AFM image of Cu films electrodeposited from Cl-PEG-UPS bath is shown in Fig. 4.31. It showed a film RMS roughness of 83 nm, the highest among Cu films electroplated with organic additives. Cu film electroplated from UPS bath was not shiny and showed a dull reddish color. The grain size and structure observed from AFM image showed a similarity with Cu film electrodeposited from Cl-PEG electrolyte.

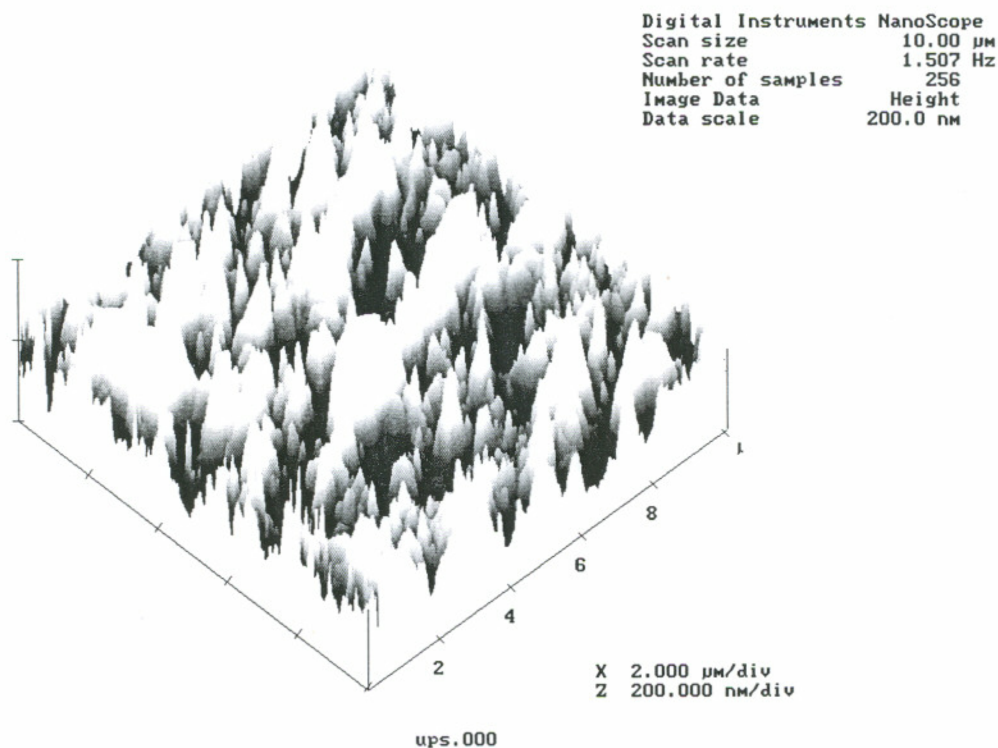

Fig. 4.31. AFM image of Cu film electrodeposited from Cl-PEG-UPS bath.

4.2.3 Cu Electrodeposition with Cl+PEG+OPX

OPX is the abbreviation of (O-Ethyldithiocarbonato)-S-(3-sulfopropyl)-ester, potassium salt **($CH2$-O-SC-S-$(CH2)_3$-SO_3K)** as shown in figure 4.32 for its molecular structure. It is a reactive sulfonate and an additive for electroplating baths.

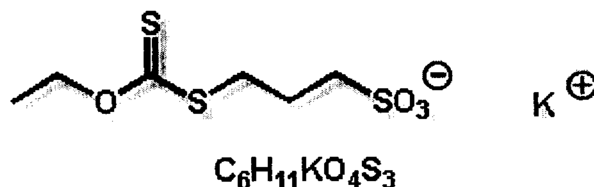

Fig. 4.32 OPX: (O-Ethyldithiocarbonato)-S-(3-sulfopropyl)-ester, potassium salt

4.2.3.1 Electrochemical Characterization of Cl-PEG-OPX Bath

Polarization Measurement

The polarization curve of Cl+PEG+OPX bath is shown in figure. 4.33. Compared with benchmark I-E curve of Cl-PEG-SPS bath, OPX bath showed a moderately suppressed current, but more accelerated than Cl-PEG bath. This characteristic gives OPX bath a moderate superfilling capability, but may not be enough for a good trench fill.

The Tafel plot of Cl+PEG+OPX bath shows a slope of –12.9 (V^{-1}) or -78 mV, as presented in figure. 4.34. The corresponding charge transfer coefficient is 0.76. The observed changes in the cathodic Tafel slope and corresponding increase of charge transfer coefficient suggest that the process taking place on the electrode surface is very different from the reaction mechanism in Cl-PEG-SPS electrolyte. Further more, the exchange current density of Cl-PEG-OPX is calculated as 0.032 mV/cm^2, which is much lower than Cl-PEG-SPS electrolyte, even lower than Cl-PEG bath. The exchange current can be viewed as kind of “idle speed” for charge exhange across the interface. It is a

measure of any system's ability to deliver a net current without a significant energy loss due to activation. Exchange current density in real systems reflect that wide range in k^o, the equilibrium reaction rate. Therefore, for Cl-PEG-OPX electrolyte system, the "idle speed" of charge exchange is slow, and a high overpotential is required to activate this electrodeposition reaction.

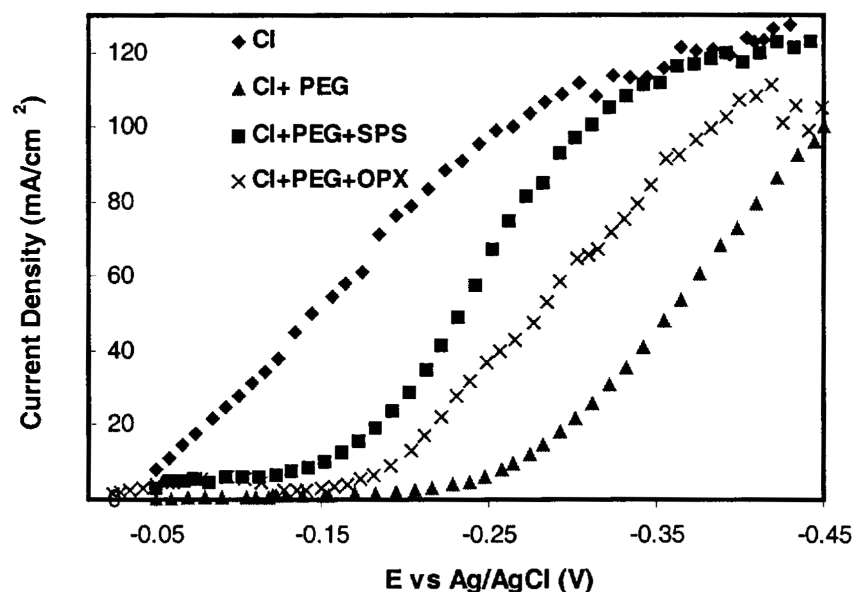

Figure 4.33 LVS curves obtained at a rotation speed of 400 rpm on a Pt. RDE in the baths with various combinations of additives. All electrolytes contain 1.8 M H_2SO_4, 0.24 M $CuSO_4$. In addition, the curve labeled Cl^- has 50 ppm; PEG: 300 ppm PEG (MW.4600); OPX: 6 ppm OPX;

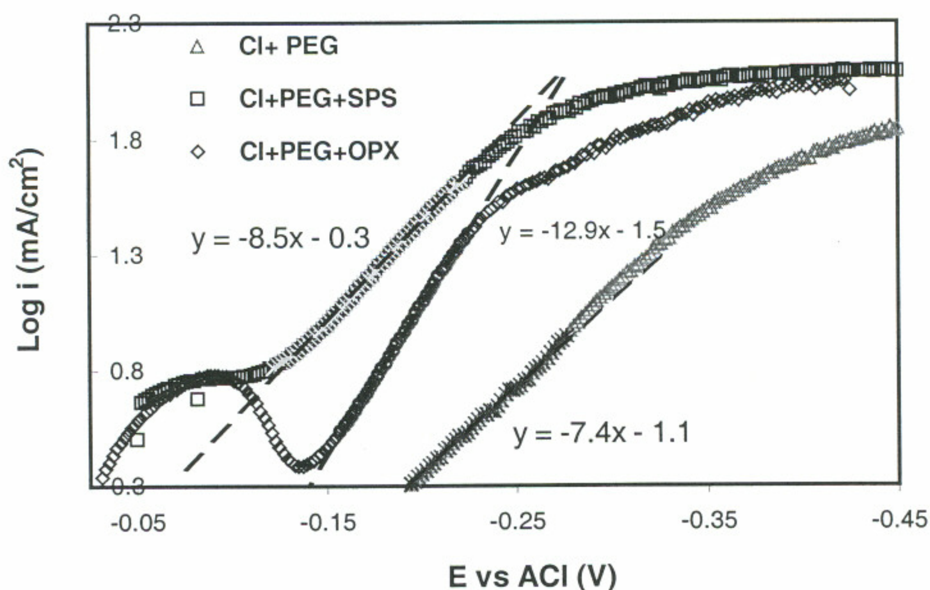

Figure 4.34 Tafel plot of Cu electrodeposition with various electrolytes including OPX.

Hysteresis Loop of Cl+PEG+OPX Bath

The CV hysteresis curve of Cl+PEG+OPX is shown in figure 4.35. Compared with benchmark SPS bath hysteresis curve, OPX bath does show a moderate i-E hysteresis. However, the i-E hysteresis started much later than SPS bath (-100 mV vs. – 25 mV), which indicated that a higher overpotential is required to activate the electrodeposition reaction. The moderate i-E hysteresis indicates that there is an irreversible change of surface chemistry when overpotential sweep back. The Tafel kinetic study result and the hysteresis characteristic of Cl-PEG-OPX electrolyte suggested that the reaction mechanism of OPX bath is very different with SPS bath. OPX bath needs a higher overpotential to overcome the reaction barrier. However, as soon as this barrier is overcome, it does generate a moderate i-E hysteresis, which could be an indication for the acceleration of OPX. By comparing OPX melocular structure with SPS, the O-Ethyldithiocarbonato group causes OPX inhibiting characteristic in the

initial reaction phase, but this inhibition can be overcomed with higher overpotential. As soon as electrodeposition reaction started, OPX does show some accelerating capability. This is a very unique characteristic for OPX and will discuss more in following section.

The unique characteristic of OPX also indicated the need to use bath polarization and hysteresis measurement to fully characterize an organic additive in a copper bath.

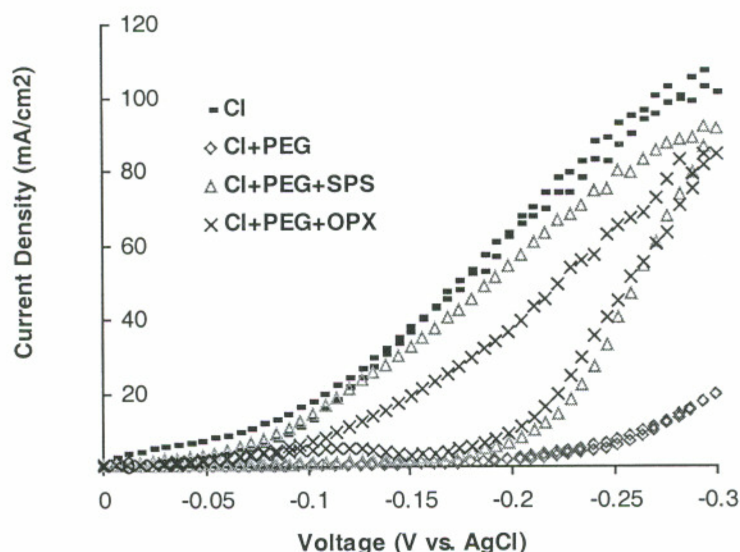

Fig. 4.35 Hysteresis curves obtained at a rotation speed of 400 rpm on a Pt. RDE in the baths with various combination of additives. All electrolytes contain 1.8 M H_2SO_4, 0.24 M $CuSO_4$. In addition, the curve labeled Cl^- has 50 ppm Cl^-. PEG: 300 ppm (MW.4600); SPS: 6 ppm SPS; OPX: 6 ppm OPX.

Chronoamperometry Response of Cl+PEG+OPX Bath

Figure 4.36 shows the chronoamperometry response of VMS, Cl+PEG, Cl+PEG+SPS, and Cl+PEG+OPX under overpotential of –0.15 V vs. Ag/AgCl. It confirmed that OPX inhibited the electrodeposition reaction in the beginning of the reaction. After 60 seconds of reaction, the acceleration of OPX increased almost to the same level as SPS bath under –0.15 V overpotential. For the reaction under –0.25 V

overpotential in Fig. 4.37, it required 30 seconds to overcome the reaction barrier to reach the plateau of full accelerated current.

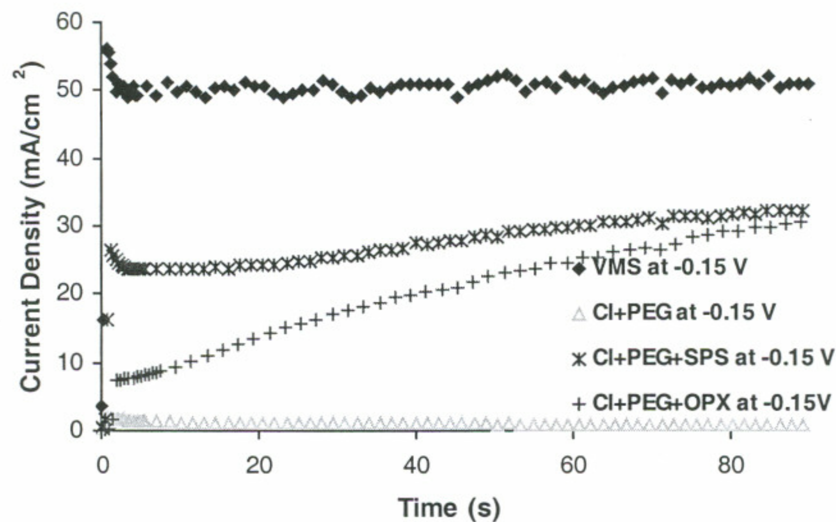

Fig. 4.36 Chronoamperometric curves of electrolytes with various combinations of additives under –0.15 V overpotential vs. Ag/AgCl.

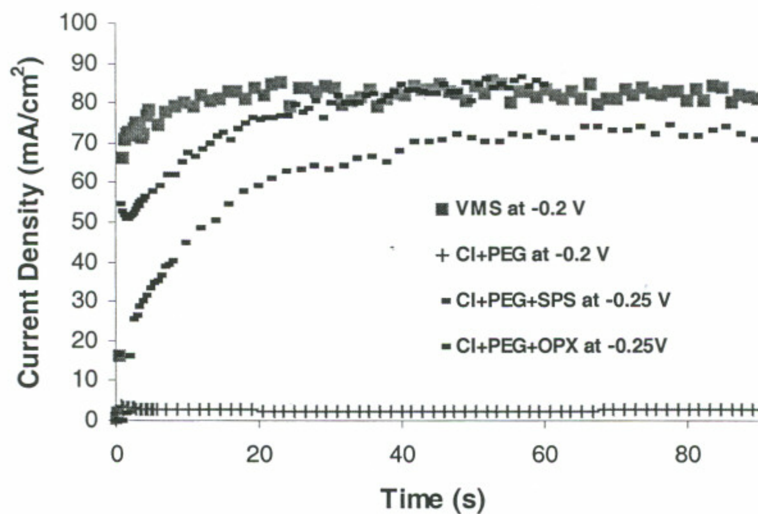

Fig. 4.37 Chronoamperometric curves of electrolytes with various combinations of additives under –0.25 V overpotential vs. Ag/AgCl.

4.2.3.2. Result of Fill Study of Cl-PEG-OPX Bath

The trench fill result of Cl-PEG-OPX bath is shown in Fig. 4.38. Center voids are observed for electrolytes with 6 ppm OPX and 12 ppm OPX. This indicates that OPX bath is lacking of strong superfilling capability even with higher concentration of OPX. This result could also be caused by the slow reaction in the beginning of the electrodeposition. More study is needed for fill study of this electrolyte.

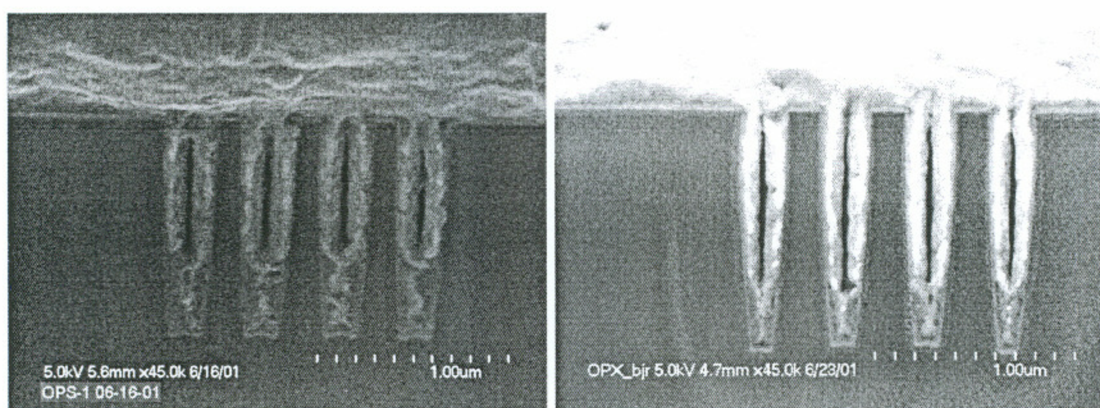

(a) 6 ppm OPX (b) 12 ppm OPX

Fig. 4.38 Trench fill result of Cl+PEG+OPX electrolyte with (a) 6 ppm OPX and (b) 12 ppm OPX.

4.2.3.3 Microstructure of Cu Film Electroplated with Cl-PEG-OPX

Resistivity Measurements

The temporal evolution of the sheet resistance of 1 μm thick copper film, electrodeposited from the electrolyte containing various additives including OPX, is summarized in Fig. 4. 39. Compared with the benchmark curve of Cl+PEG+SPS bath, OPX bath showed a little higher initial sheet resistance than Cu film deposited from SPS bath. This indicated either higher impurity incorporation or different grain refinement by

OPX. However, the resistance decrease over time of Cu films from OPX bath is similar to that deposited from SPS bath, which indicated similar microstructure evolution after electrodeposition.

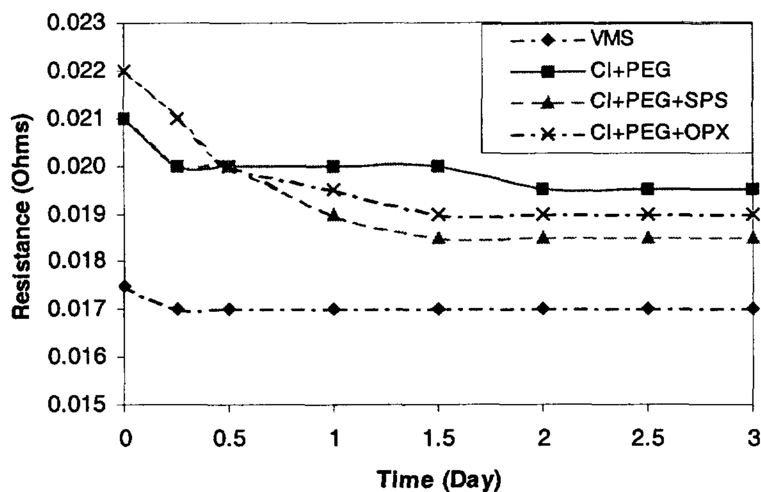

Fig. 4.39. Resistance transients during aging of 1 um thick Cu films at room temperature.

Texture of electroplated Cu films

The texture of electroplated Cu film from Cl-PEG-OPX electrolyte shows a crystal orientation similar to other electrodeposited Cu films with a strong (111) texture. A smaller (222) texture is also observed.

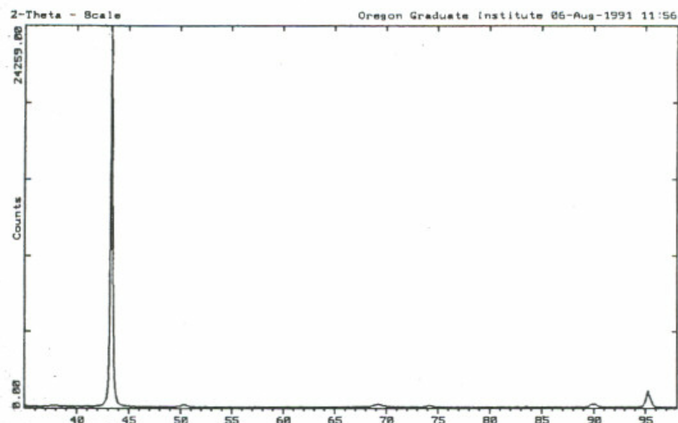

Fig. 4.40 X-ray diffraction pattern of Cu film electrodeposited from Cl-PEG-OPX bath.

Microstructure of Cu film electrodeposited from Cl-PEG-OPX bath:

The AFM image of Cu film electrodeposited from Cl-PEG-OPX bath is shown in Fig. 4.41. It has a RMS roughness of 46 nm. Compared with benchmark film from Cl-PEG-SPS bath, it has similar roughness and shiny surface. This indicated the similarity of the microstructure of Cu film from Cl-PEG-OPX bath and Cu film electrodeposited form SPS bath.

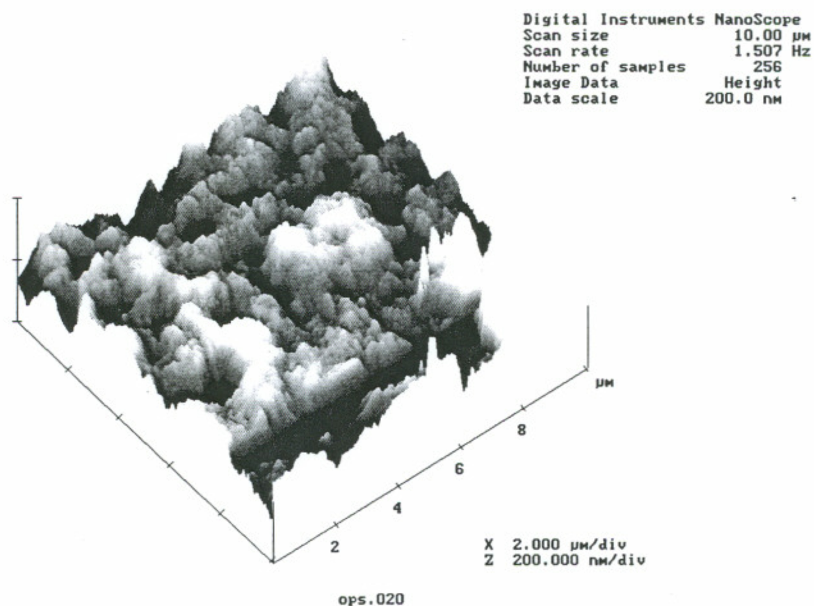

Fig. 4.41. AFM image of Cu film electrodeposited from Cl-PEG-OPX bath.

4.2.4 Cu Electrodeposition with Cl-PEG-DPS

DPS is the abbreviation of N,N-Dimethyldithiocarbamic acid (3-sulfopropyl) ester, sodium salt as shown in figure 4.42. It has a same thiol and disulfide group on one end of its structure as SPS, but a different functional group on other end.

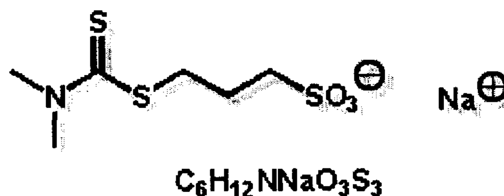

Fig. 4.42 DPS: N,N-Dimethyldithiocarbamic acid (3-sulfopropyl) ester, sodium salt

4.2.4.1 Electrochemical Characterization of Cl+PEG+DPS Bath

Polarization Measurement:

The polarization measurement of various combinations of organic additives including DPS is shown in Fig. 4.43. Compared with SPS bath, DPS bath shows a shift to higher overpotential for electrodeposition rate to increase. This is similar to OPX bath, which requires higher overpotential compared with SPS bath to activate the electrodeposition reaction.

The Tafel plot of DPS curve, shown in Fig. 4.44, gives a Tafel slope of – 13.6 (V-1) or -74 mV and a corresponding charge transfer coefficient of 0.80. The exchange current density is calculated as 0.025 (mA/cm^2), which is even lower than OPX bath (0.032 mA/cm^2). This indicated a strong inhibiting characteristic of DPS in the equilibrium stage. It requires high overpotential to overcome this inhibiting barrier to start this electrodeposition reaction. The charge transfer cofficient of 0.80 indicated the complex formation between DPS and cuprous ions at the electrode surface and resulted in

many complicated reaction steps to complete the reaction. More discussion of reaction mechanism of DPS is followed in next section.

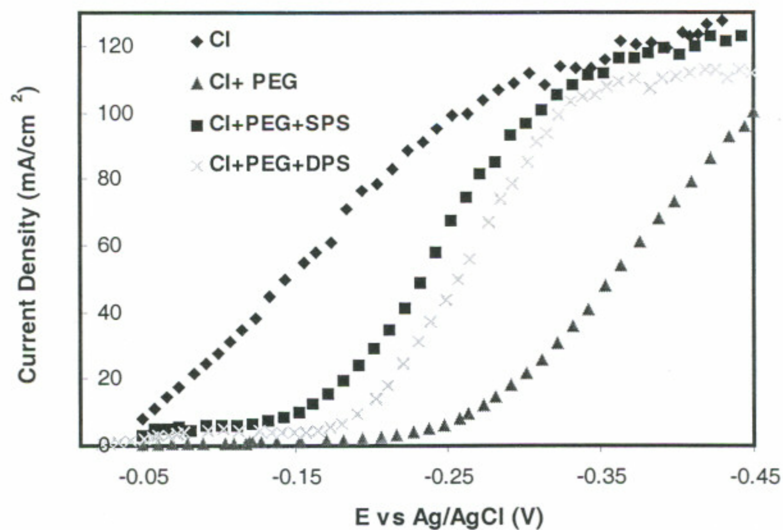

Fig. 4.43 Polarization curves of electrolytes with various combinations of additives including DPS.

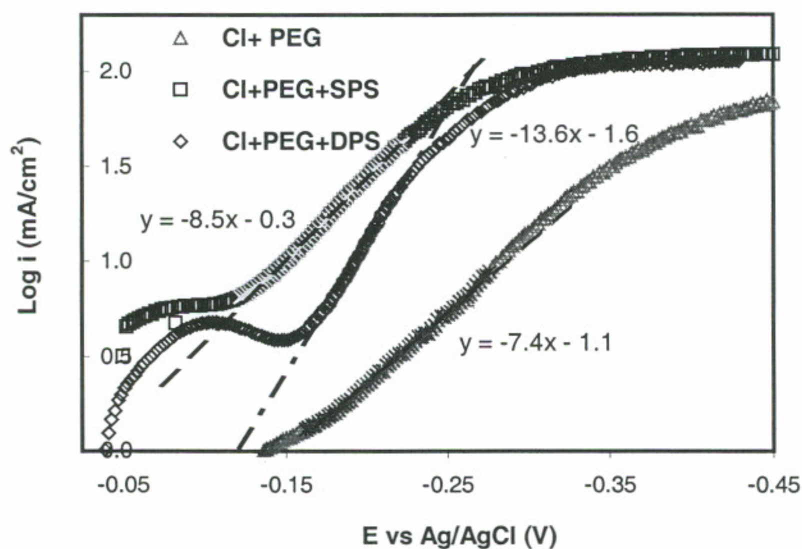

Fig. 4.44 Tafel plot of Cu electrodeposition with various additives including DPS.

Hysteresis Loop of Cl-PEG-DPS Bath

The Hysteresis CV curve of Cl-PEG-DPS bath is shown in Fig. 4.45. Compared with benchmark bath of Cl-PEG-SPS, DPS bath showed a close hysteresis loop with SPS bath, but with a shift towards higher potential to start the electrodeposition reaction. This observation supported the Tafel kinetic study result presented above. DPS has a very similar electrochemical characteristic to OPX. By Comparing their molecular structure below, we can see the only difference between them is that the oxygen compound on other end of OPX is replaced with a nitrogen compound for DPS. The similarity of the molecular structure of these two thiols could be the cause for their close electrochemical characteristics.

DPS:

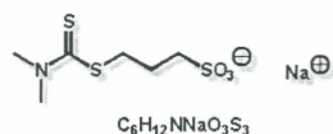

OPX:

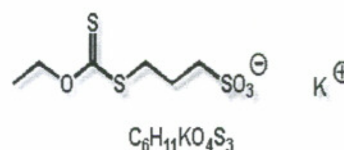

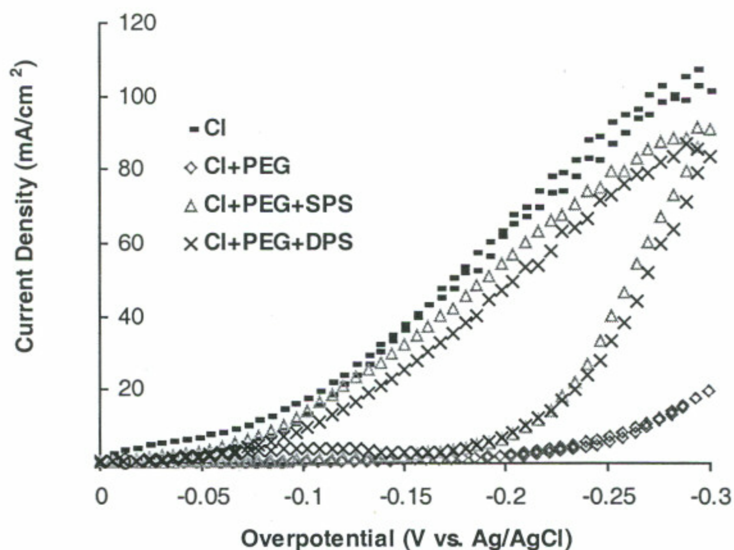

Fig. 4.45 Hysteresis curves of electrolytes with various combinations of organic additives including DPS

Chronoamperometry Response of Cl+PEG+DPS Bath

Figure 4.46 shows the chronoamperometry response of VMS, Cl+PEG, Cl+PEG+SPS, and Cl+PEG+DPX under overpotential of –0.15 V vs. Ag/AgCl. It confirmed the inhibition behavior of DPS in the equilibrium stage. It showed a 20 seconds time lap for electrodeposition rate to reach a plateau, which is close to SPS bath. At higher overpotential of –0.25 V vs. Ag/AgCl shown in Fig. 4.37, the reaction barrier was easily overcome for DPS bath. The reaction rate reached the plateau in much shorter time compared with –0.15 V overpotential. The difference between DPS and SPS current response curves was very small. This observation supported the Tafel kinetic study result and proved the similarity between DPS and OPX. They both require a higher overpotential to activate the electrodeposition reaction than SPS bath.

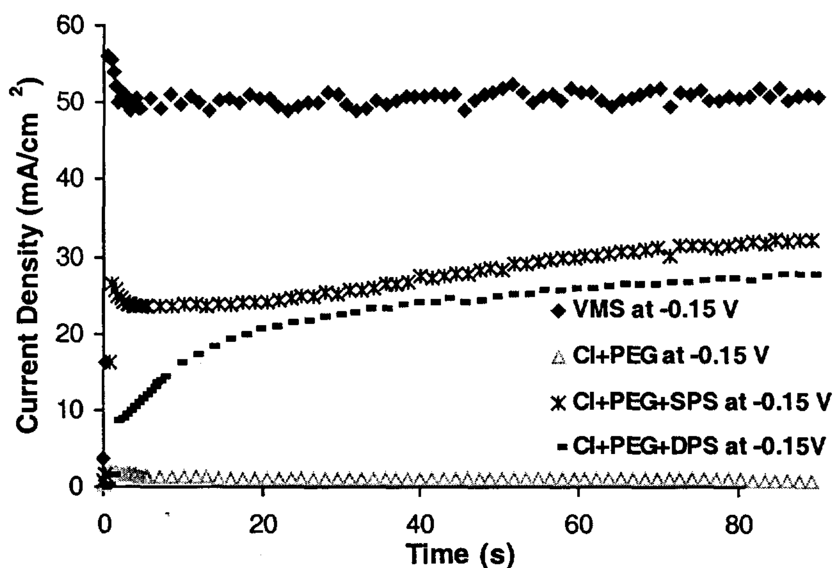

Fig. 4.46 Chronoamperometric curves of electrolytes with various combinations of organic additives under –0.15 V overpotential vs. Ag/AgCl.

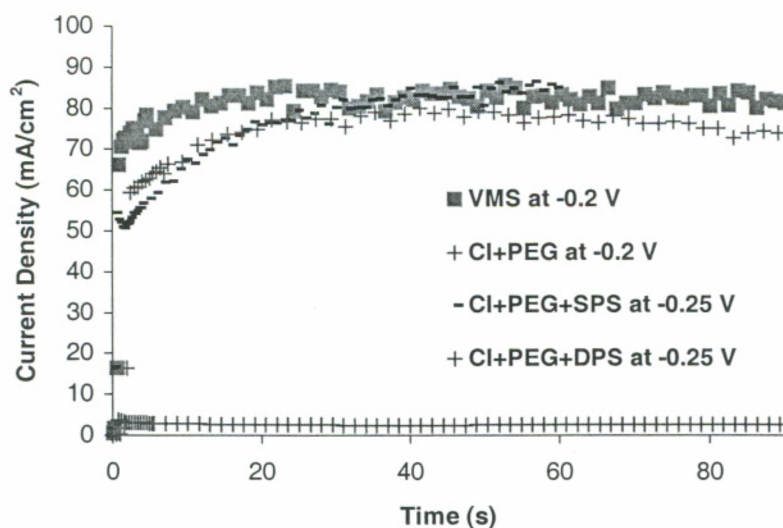

Fig. 4.47 Chronoamperometric curves of electrolytes with various combinations of additives under –0.25 V overpotential vs. Ag/AgCl.

4.2.4.2. Result of Fill Study of Cl-PEG-DPS Bath

The fill result of Cl-PEG-DPS bath is shown in Fig. 4.48. A fill structure of 6:1 ratio via was used for this study. It is seen a conformal growth pattern in the via, which resulted in center voids. This fill result is similar to OPX bath fill study result although different fill structure was used for this investigation. This indicated that OPX and DPS are very similar in electrochemical characteristics and give the similar fill result. It also proved that other end of the thiol molecular structure is very important for the superfilling property of electrolytes.

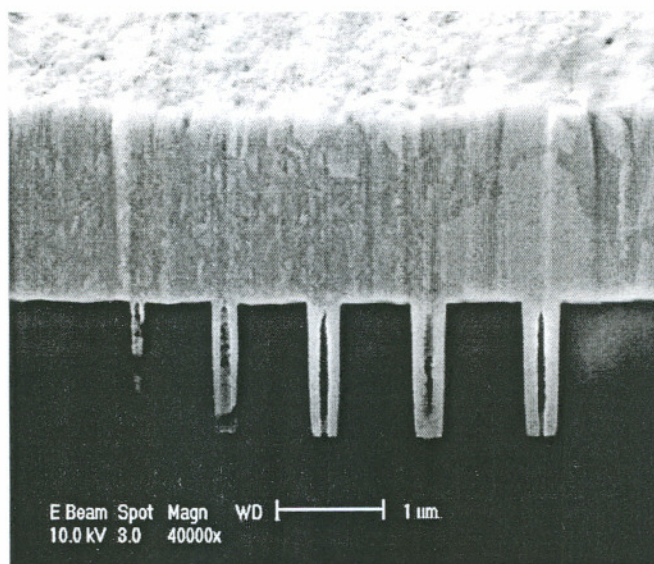

Fig. 4.48 Via fill result of Cl-PEG-DPS electrolyte with 6ppm DPS

4.2.4.3 Microstructure of Cu Film Electroplated with Cl-PEG-DPS Bath

Resistivity Measurements

The temporal evolution of the sheet resistance of 1 μm thick copper film, electrodeposited from the electrolyte containing various additives including DPS, is summarized in Fig. 4.49. Compared with resistance curve of Cu film from Cl+PEG+OPX bath, Cu film electroplated from DPS bath showed same resistance decrease over time curve. This indicated the similarity of impurity incorporation and film grain refinement between OPX and DPS, and is consistent with above study results.

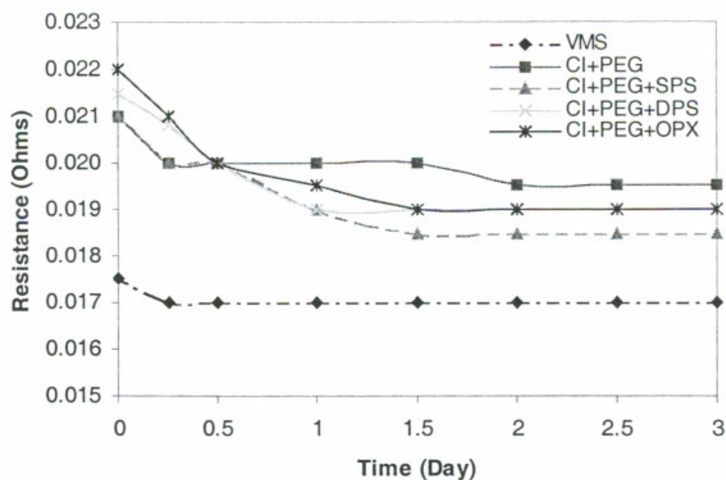

Fig. 4.49. Resistance transients during aging of 1 um thick Cu films at room temperature.

Texture of electroplated Cu film from Cl-PEG-DPS bath

The Cu film texture electrodeposited from Cl-PEG-DPS bath is shown in Fig. 4.50. The film is highly (111) oriented and is similar to other electrodeposited Cu film texture.

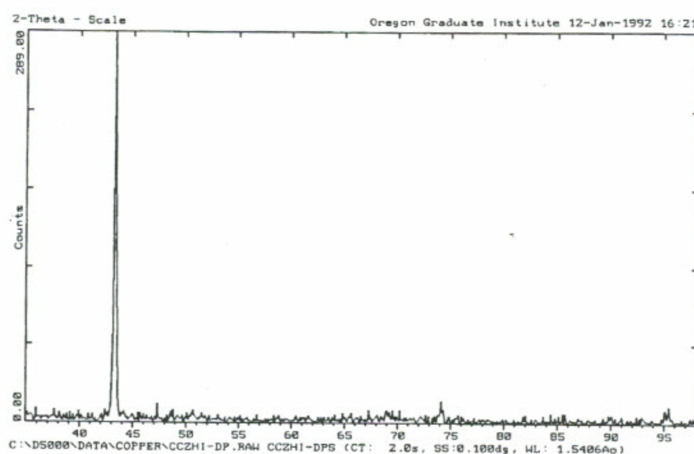

Fig. 4.50 X-ray diffraction pattern of Cu film deposited from Cl-PEG-DPS bath.

Microstructure of electroplated Cu film from Cl-PEG-DPS bath

The AFM image of Cu film electrodeposited from Cl-PEG-DPS bath is shown in Fig. 4.51. The RMS roughness of the film is 53 nm, very similar to Cu film from OPX bath (46 nm). It has a very shiny surface. The film morphology that observed from AFM image showed similar grain structure and size to Cu film from OPX bath. It indicated the similar impurity incorporation and grain refinement. This provided another support for the electrochemical characterization results.

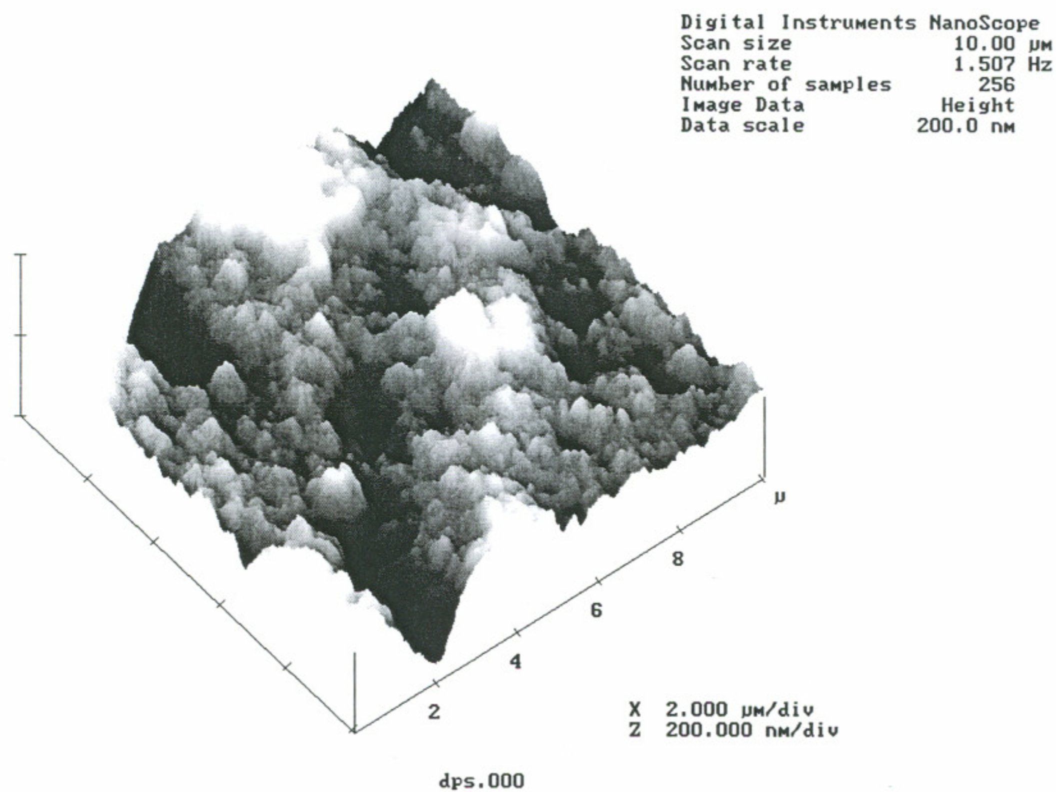

Fig. 4.51. AFM image of Cu film electrodeposited from Cl-PEG-DPS bath.

4.2.5 Cu Electrodeposition with Cl-PEG-ZPS

ZPS is the abbreviation of 3-(2-Benzthiazolylthio)-1-propanesulfonic acid, sodium salt as shown in figure 4.52 for its molecular structure. It showed that ZPS is formed by replacing other end of SPS function group with 3- (2-Benzthiazolylthio).

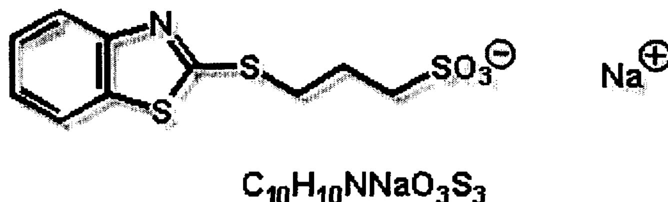

$C_{10}H_{10}NNaO_3S_3$

Figure 4.52 ZPS: 3-(2-Benzthiazolylthio)-1-propanesulfonic acid, sodium salt

4.2.5.1 Electrochemical Characterization of Cl-PEG-ZPS Bath

Polarization Measurement

The polarization measurement for copper deposition from electrolytes containing Cl-PEG-ZPS is shown in Fig. 4.53. The i-E relationship curve from Cl+PEG+ZPS bath is very similar to the relationship of Cl+PEG and Cl+PEG+UPS electrolytes with electrodeposition reaction current suppressed. It showed more suppressing than Cl-PEG electrolyte when overpotential is high.

The Tafel plot of Cl-PEG-ZPS electrolyte package is shown in Fig. 4.54. It showed a Tafel slop of –8.0 (V^{-1}) or –125 mV and the corresponding charge transfer coefficient is 0.47. More important, it has an exchange current density of 0.079 mA/cm^2 that is exactly same as Cl+PEG electrolyte. This indicated ZPS that inhibits copper elecctrodeposition in the equilibrium stage. A very high overpotential is required to activate this reaction. More discussion of ZPS working mechanism is followed in next section.

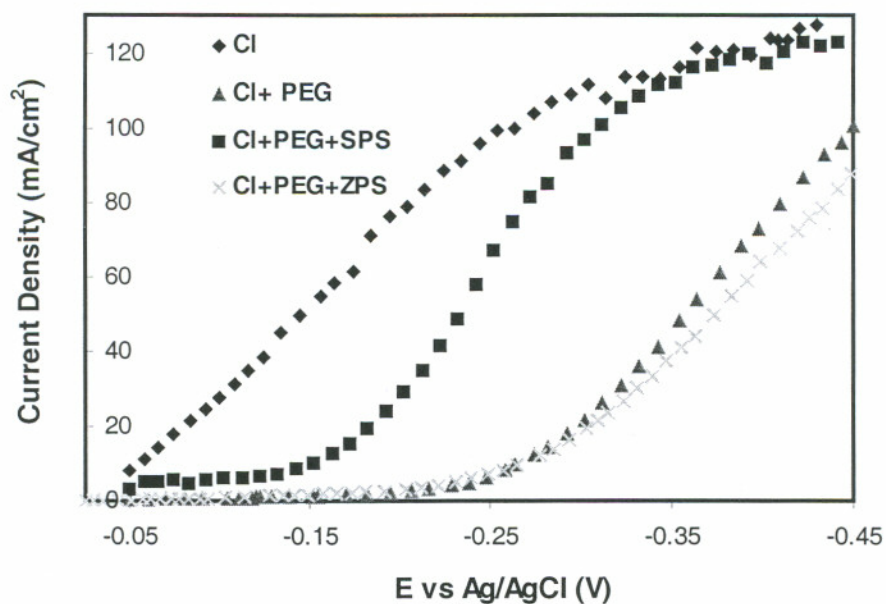

Fig. 4.53 LSV curves of electrolytes with various combinations of additives including ZPS.

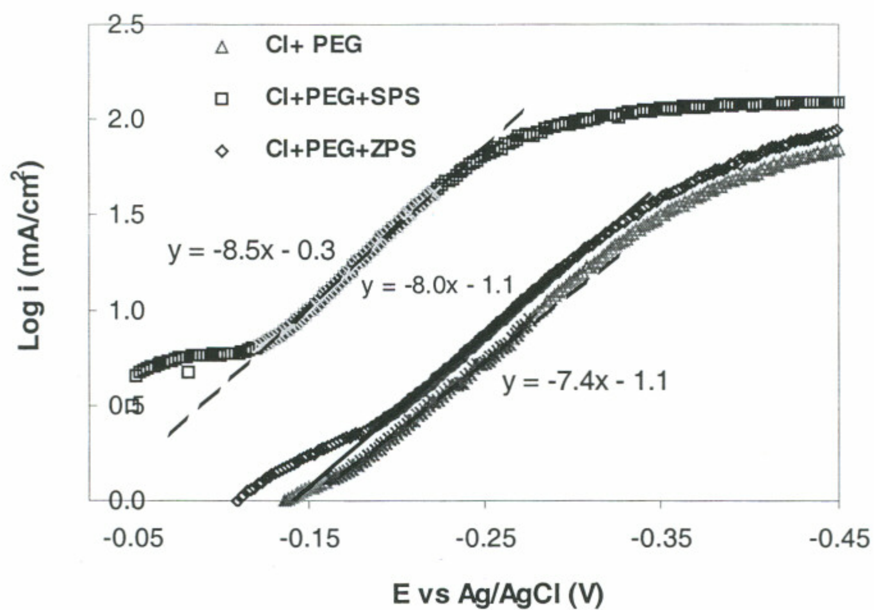

Fig. 4.54 Tafel plot of Cu elctrodeposition with various combinations of organic additives including ZPS.

Hysteresis Loop of Cl-PEG-ZPS Bath

The i-E hysteresis of Cl-PEG-ZPS is shown in Fig. 4.55 with other curves. ZPS bath showed totally suppressed current with no i-E hysterisis. It suppressed even more than Cl-PEG electrolyte when overpotential is high. It indicated that there are no irreversible surface chemistry changes when overpotential sweep back, similar to Cl-PEG and Cl-PEG-UPS electrolytes. ZPS could act just like PEG to block the charge transfer process, but not participate in the charge transfer reaction.

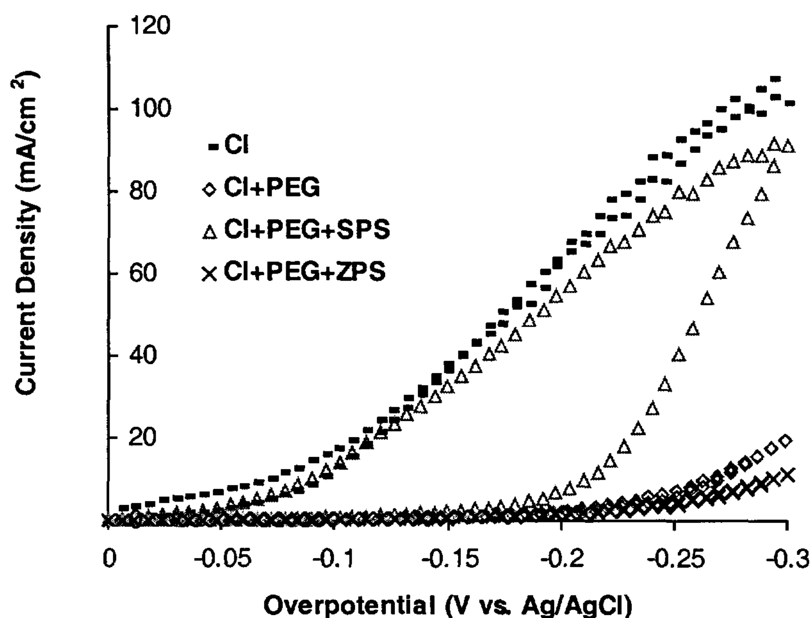

Fig. 4.55 Hysteresis curves of electrolytes with various combinations of organic additives including ZPS

Chronoamperometry Response of Cl+PEG+ZPS Bath

Figure 4.56 shows the chronoamperometry response of VMS, Cl+PEG, Cl+PEG+SPS, and Cl+PEG+ZPS under overpotential of –0.15 V vs. Ag/AgCl. It demonstrated that electrodeposition reaction was totally suppressed and showed no response over time. This is similar to Cl+PEG electrolyte response curve. The CA

curve under –0.25 V overpotential vs Ag/AgCl, shown in Fig. 4.57, demonstrated a similar suppressing characteristic with very small increase of electrodeposition rate under higher overpotential.

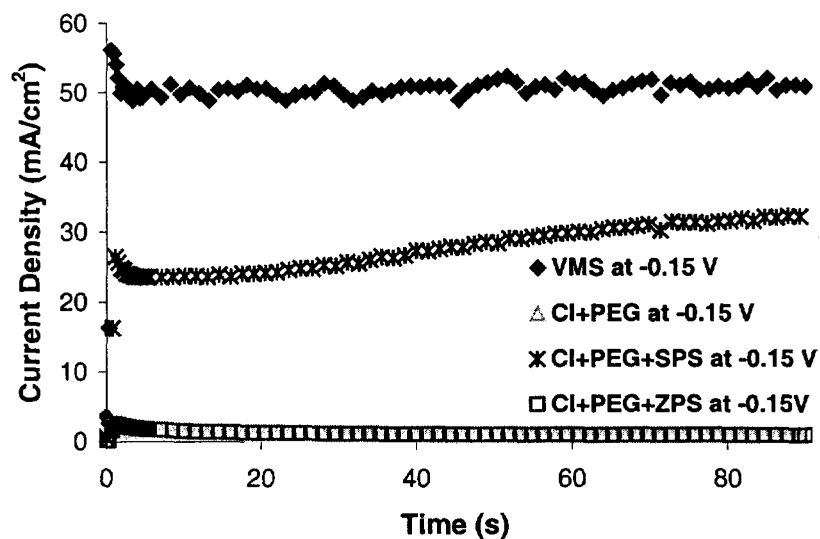

Fig. 4.56 Chronoamperometric curves of electrolytes with various combinations of additives under –0.15 V overpotential vs. Ag/AgCl.

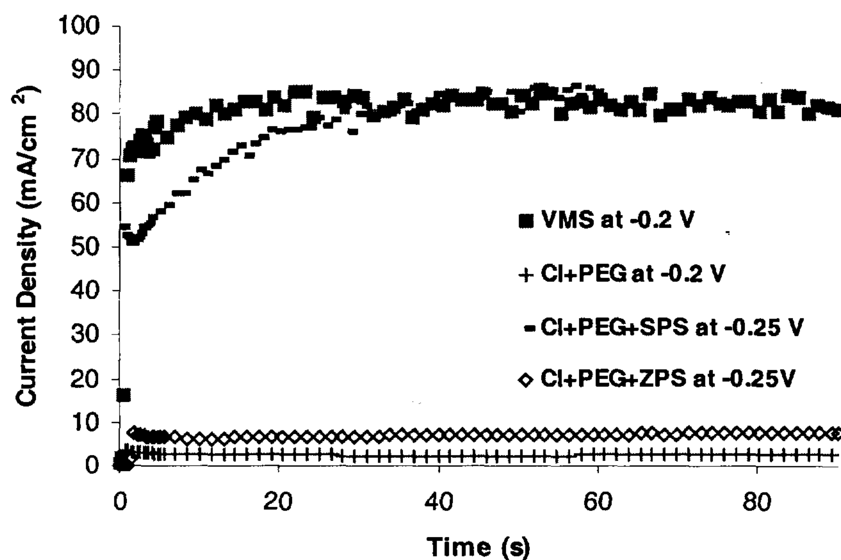

Fig. 4.57 Chronoamperometric curves of electrolytes with various combinations of additives under –0.25 V overpotential vs. Ag/AgCl.

4.2.5.2. Result of Fill Study of Cl-PEG-ZPS Bath

The fill study result is shown in Fig. 4.58 for Cl-PEG-ZPS electrolyte package. It showed a conformal growth in the via, which resulted in a center void for the fill. This result is consistent with electrochemical characterization result for this electrolyte, and is similar to Cl-PEG electrolyte fill result.

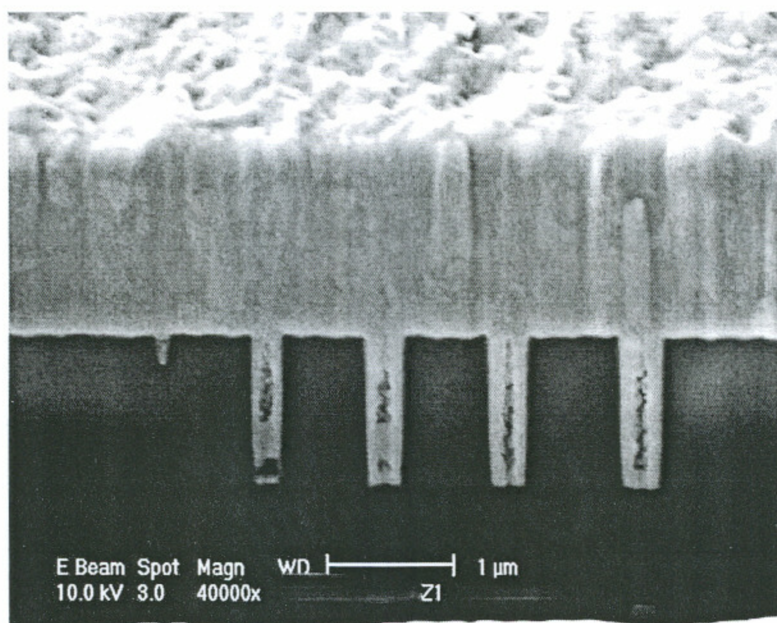

Fig. 4.58 Via fill result of Cl-PEG-ZPS electrolyte with 6ppm ZPS.

4.2.5.3 Microstructure of Cu Film Electroplated with Cl-PEG-ZPS Bath

Resistivity Measurements

The temporal evolution of the sheet resistance of 1 um thick copper film, electrodeposited from the electrolyte containing various additives including ZPS, is shown in Fig. 4. 59. Compared with the benchmark curve of Cl+PEG+SPS bath, Cu film electrodeposited from ZPS bath showed higher initial resistance and very little decrease over time. This characteristic is very similar to Cu film electrodeposited from Cl-PEG

bath, but with higher resistance. This observation provided the another support for the i-E characterization result of ZPS bath, which concluded that ZPS acts like PEG and retards Cu electrodeposition reaction.

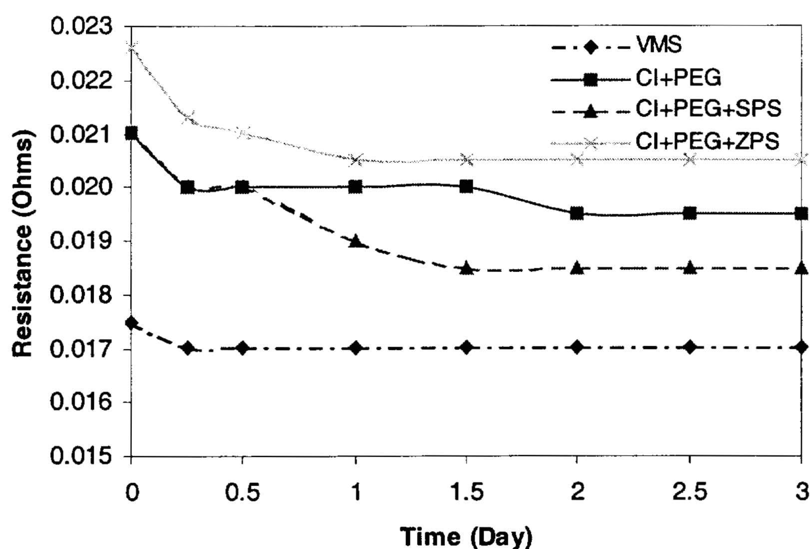

Fig. 4.59. Resistance transients during aging of 1 um Cu films at room temperature.

Texture of electroplated Cu films

The texture of electroplated Cu film from Cl-PEG-ZPS electrolyte is shown in Fig. 4.60. It demonstrated a similar texture orientation as other electrodeposited Cu film with a predominately (111) oriented film. A smaller (222) texture is also observed. The diffraction density of this Cu film is very similar to the Cu film electrodeposited from Cl-PEG bath.

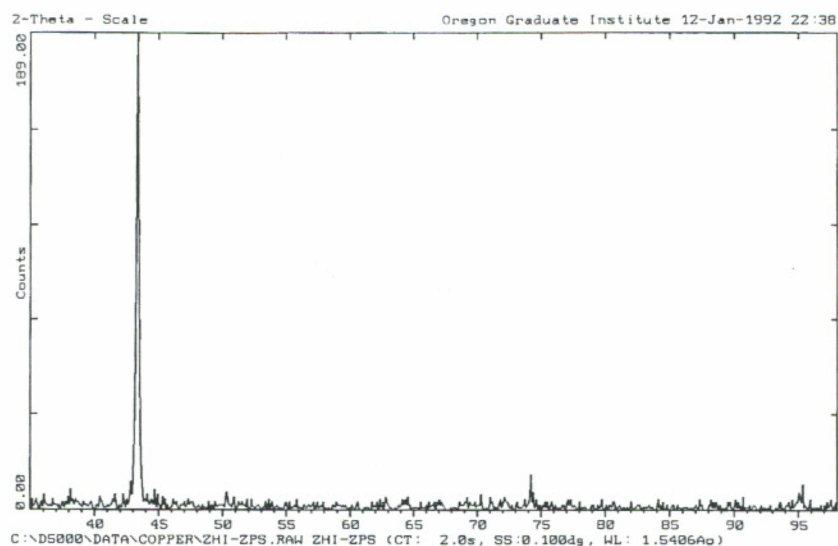

Fig. 4.60 X-ray diffraction pattern of Cu film electrodeposited from Cl-PEG-ZPS bath.

Morphology of electroplated Cu film from Cl-PEG-ZPS bath

The AFM image of Cu film electrodeposited from Cl-PEG-ZPS bath is shown in Fig. 4.61. It has a film roughness of 49 nm (RMS), which is lower than Cu film from Cl-PEG and Cl-PEG-UPS electrolyte. It has a shiny surface and is significantly different from Cu film electroplated from Cl-PEG and Cl-PEG-UPS electrolytes, which have a reddish and dull film surface color. Compared to benchmark film from Cl-PEG-SPS bath, it has similar film morphology.

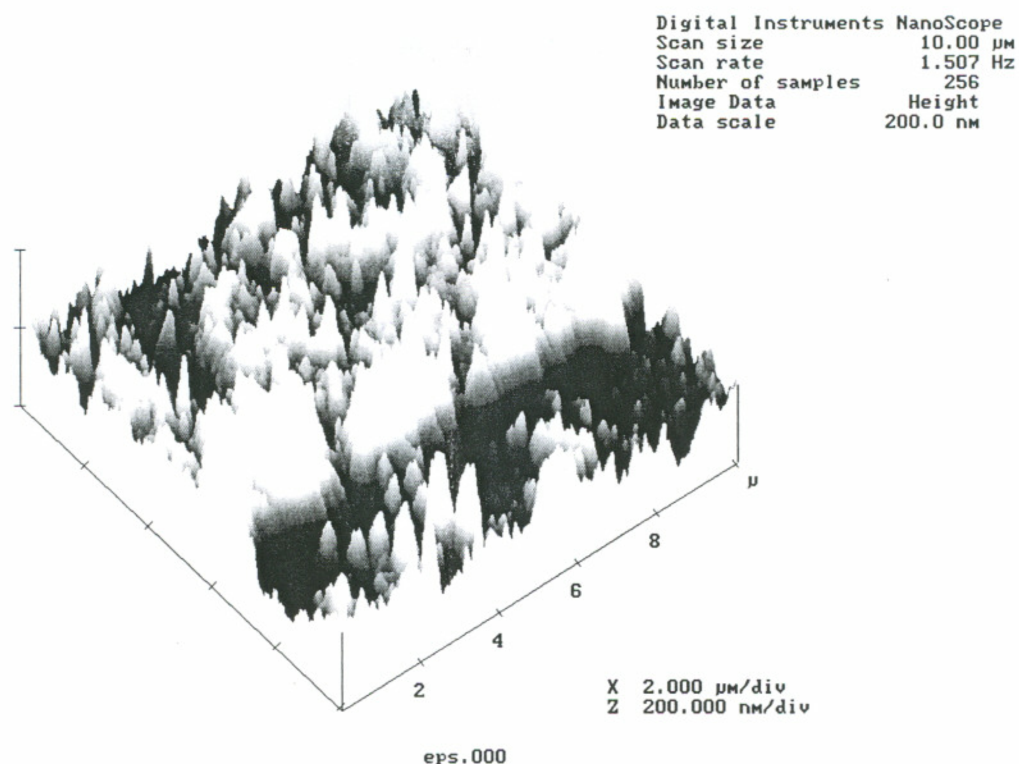

Fig. 4.61. AFM image of Cu film electrodeposited from Cl-PEG-ZPS bath.

4.2.6 Cu Electrodeposition with Cl-PEG-MPS

MPS is the abbreviation of 3-Mercaptopropane sulfonic acid, sodium salt as shown in fighure 4.62 for its molecular structure. It is a thiol and an additive for electroplating baths and for the photographic industry. It is seen that MPS is exact half of SPS molecular structure.

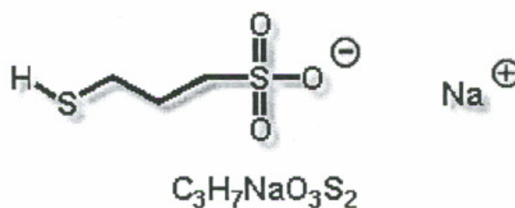

Figure 4.62 MPS: 3-Mercaptopropane sulfonic acid, sodium salt.

4.2.6.1 Electrochemical Characterization of Cl-PEG-MPS Bath

Polarization Measurement

The polarization measurement of various combinations of organic additives including MPS is shown in Fig. 4.63. Compared with SPS bath, MPS bath shows a similar I-E relationship, but a shift towards higher potential for current response.

The Tafel plot of MPS curve, shown in Fig. 4.64, gives a Tafel slope of – 10.4 (V^{-1}) or -96 (mV) and a corresponding charge transfer coefficient of 0.62. However, the exchange current density of MPS bath is 0.126 mA/cm^2, which is much lower than SPS bath (0.501 mA/cm^2). The low exchange current density indicated that MPS inhibits current exchange in the equilibrium stage and requires high overpotential to activate the electrodeposition reaction.

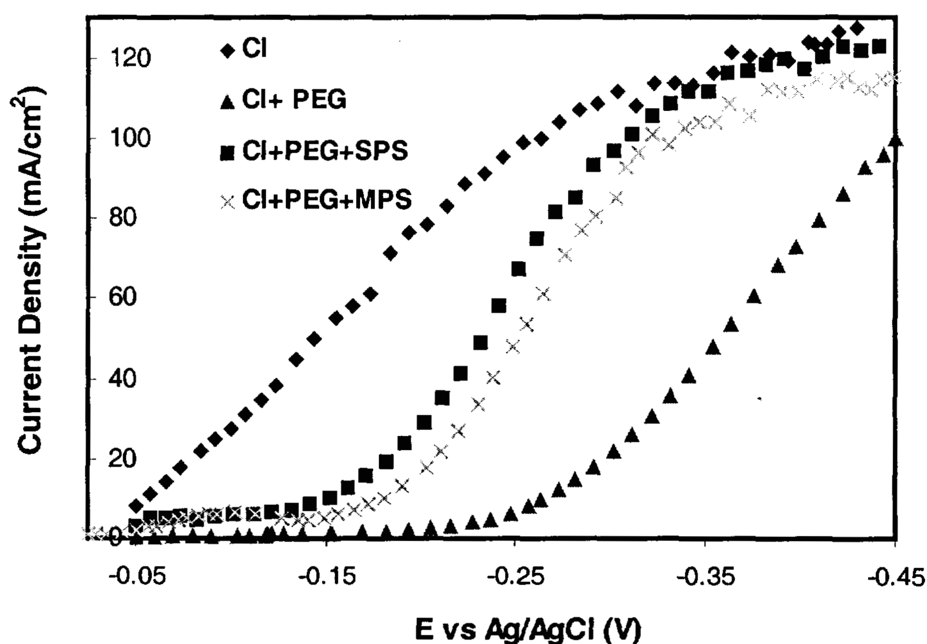

Fig. 4.63 Polarization curves of electrolytes with various combinations of organic additives including MPS.

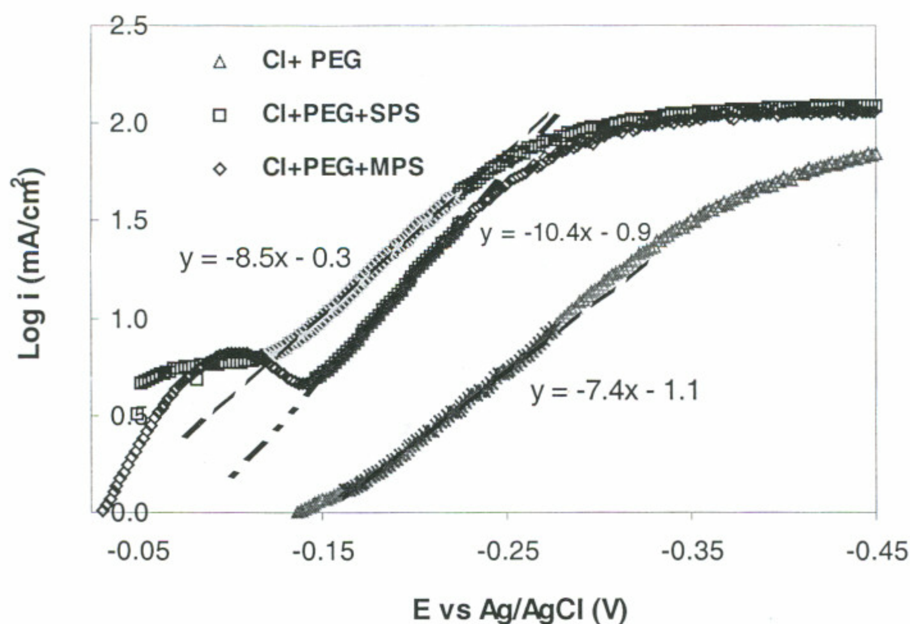

Fig. 4.64 Tafel plot of Cu electrodeposition with various combinations of organic additives including MPS.

Hysteresis Loop of Cl-PEG-MPS Bath

The i-E hysteresis curve of Cl-PEG-MPS electrolyte is shown in figure 4.65. Compared to benchmark SPS bath, MPS bath showed a clear shift towards higher overpotential for the hysteresis curve, which is consistent with its low exchange current density characteristic. The hysteresis curve of Cl-PEG-MPS demonstrated a moderate i-E hysteresis, which reflects the irreversible surface chemistry change when overpotential sweeps back. This indicated that MPS participated the electrodeposition reaction with complex formation between MPS and cuprous ions at electrode surface. More discussion of MPS working mechanism is followed in next section.

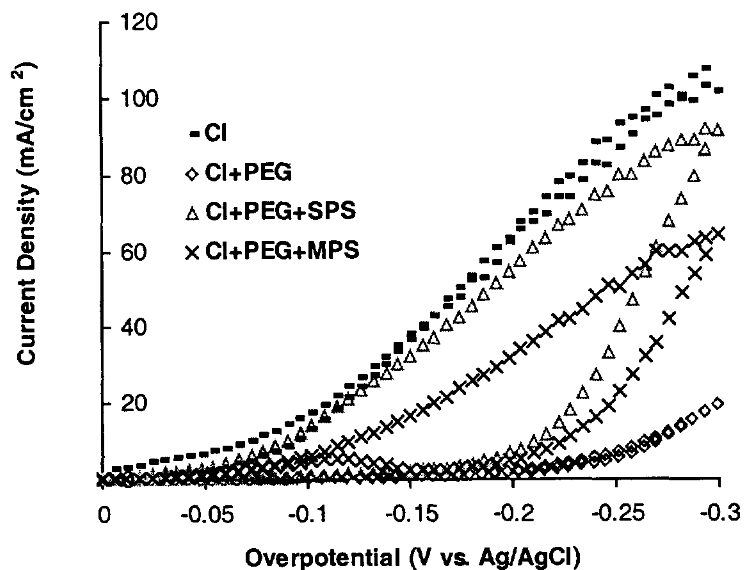

Fig. 4.65 Hysteresis curves of electrolytes with various combinations of organic additives including MPS.

Chronoamperometry Response of Cl+PEG+MPS Bath

Figure 4.66 shows the chronoamperometry response of VMS, Cl+PEG, Cl+PEG+SPS, and Cl+PEG+MPS under overpotential of –0.15 V vs. Ag/AgCl. It showed less acceleration compared to SPS bath. The initial current response is also lower than SPS bath, which is consistent with its kinetic study result. The CA curve under –0.25 V overpotential vs Ag/AgCl, shown in Fig. 4.67, damenstrated a similar trend as Fig. 4.66.

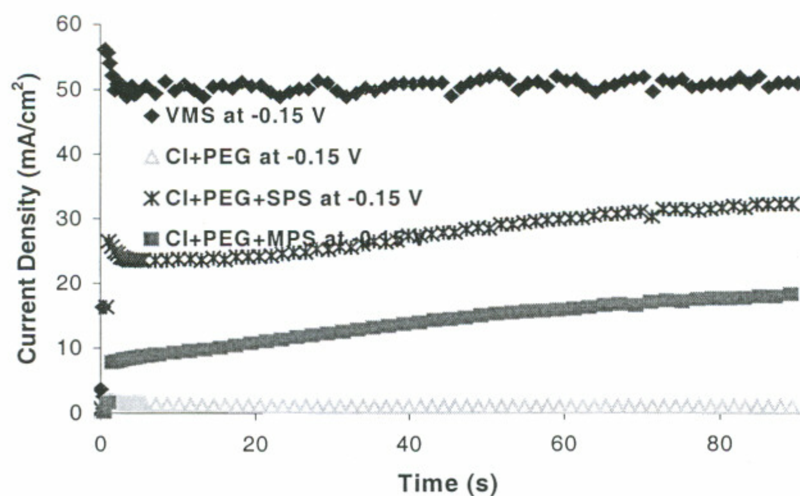

Fig. 4.66 Chronoamperometric curves of electrolytes with various combinations of additives including MPS under –0.15 V overpotential vs. Ag/AgCl.

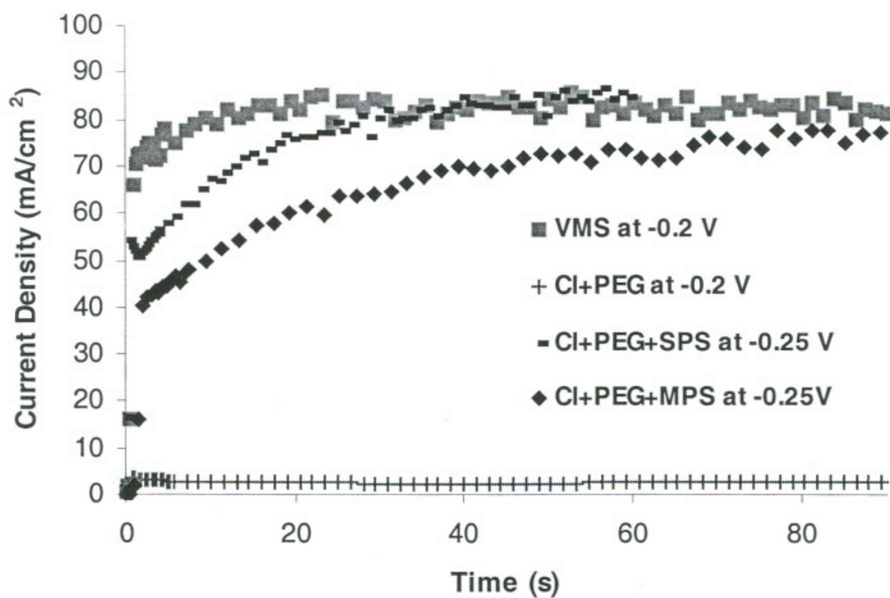

Fig. 4.67 Chronoamperometric curves of electrolytes with various combination of additives including MPS under –0.25 V overpotential vs. Ag/AgCl.

4.2.6.2 Result of Fill Study of Cl-PEG-MPS Bath

The fill study result is shown in Fig. 4.68 for Cl-PEG-MPS electrolyte package. It showed a conformal growth pattern and center voids. This could be attributed to the low exchange current density of MPS. However, fill result can be influenced by many factors and further study is needed to make a conclusion.

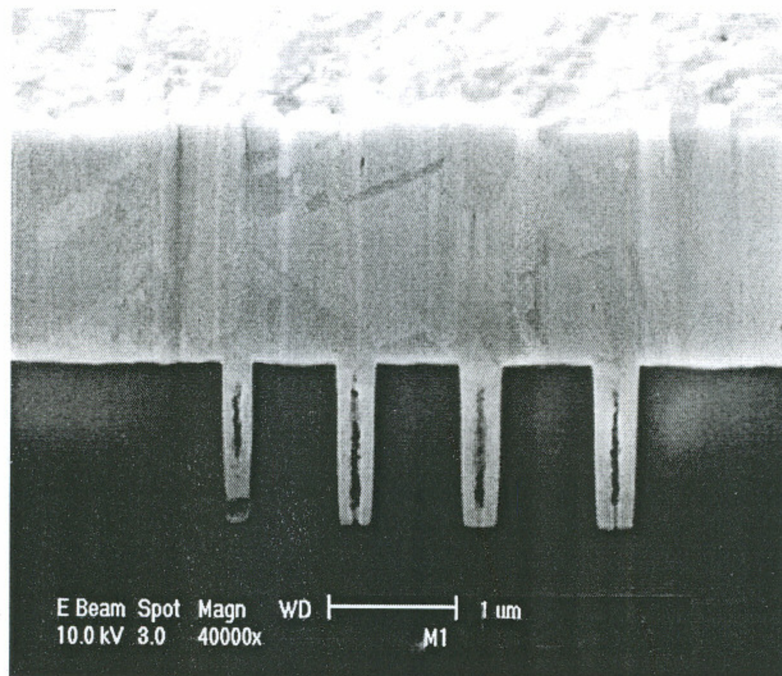

Fig. 4.68 Via fill result of Cl-PEG-MPS electrolyte with 6ppm MPS.

4.2.6.3 Microstructure of Cu Film Electroplated with Cl-PEG-MPS

Resistivity Measurements

The temporal evolution of the sheet resistance of 1 um thick copper film, electrodeposited from the electrolyte containing various additives including MPS, is summarized in Fig. 4.69. Cu film electrodeposited from MPS bath showed similar initial

sheet resistance and resistance over time evolution to Cu film electroplated from Cl+PEG electrolyte. This is a very unique characteristic of Cu film from MPS bath. It indicated the difference impurity incorporation and grain refinement between Cu films from MPS bath and SPS bath. This demonstrated the complex interactions of organic additives even though MPS is exact half of SPS structure.

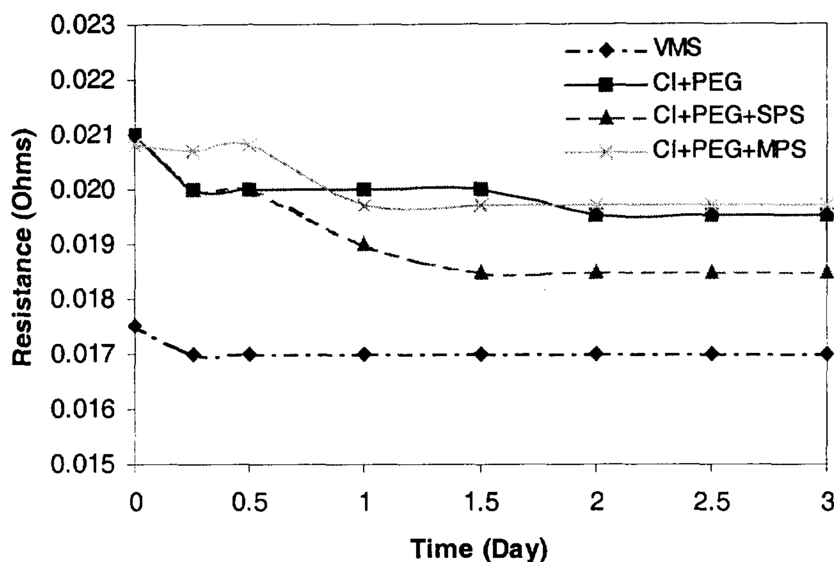

Fig. 4.69 Resistance transients during aging of 1 um Cu films at room temperature.

Texture of electroplated Cu films

The texture of electroplated Cu film from Cl-PEG-MPS electrolyte, as shown in Fig. 4.70, demonstrated a similar texture orientation as other electrodeposited Cu film with a strong (111) orientation. A smaller (222) texture is also observed.

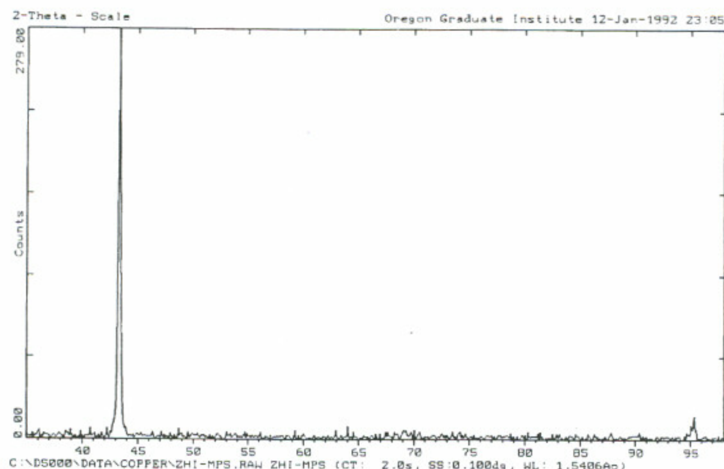

Fig. 4.70 X-ray diffraction pattern of Cu film deposited from Cl-PEG-MPS bath.

Morphology of electroplated Cu film from Cl-PEG-MPS bath

The AFM image of Cu film electrodeposited from Cl-PEG-MPS bath is shown in Fig. 4.71. The film roughness is 46 nm (RMS). It has a shiny surface. The observation of AFM image showed similar film grain size and morphology to Cu film electrodeposited from SPS bath.

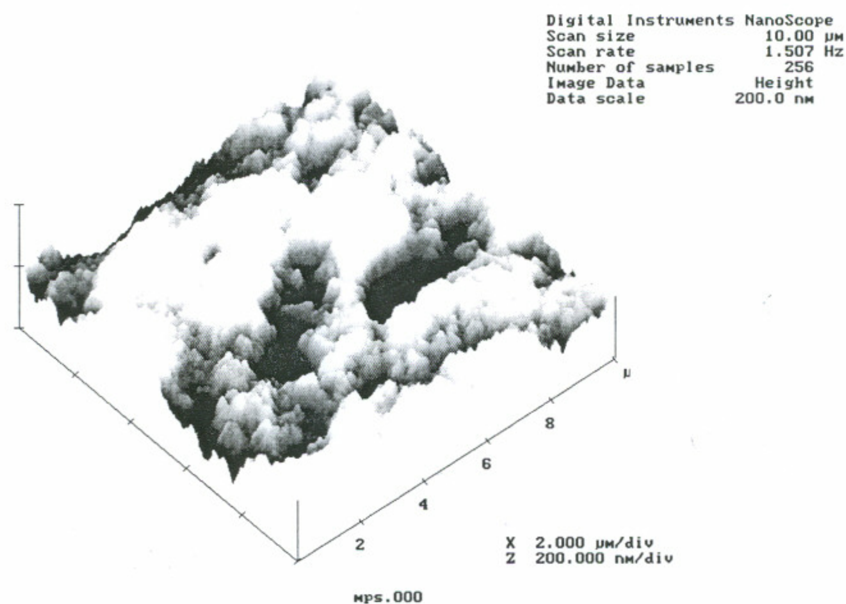

Fig. 4.71 AFM image of Cu film electrodeposited from Cl-PEG-MPS bath.

4.3 Mechanism of Action of Thiols

4.3.1 Effecs of thiols on the kinetics of Cu electrodeposition reaction

Charge transfer data can be used in the characterization of the kinetics of the copper deposition reaction. The exchange current density i_0 and charge transfer coefficient α can be determined from a plot of i against overpoential, η, using Tafel equation (see chapter 2):

$$i = -i_o \exp(\frac{-\alpha z F \eta}{RT}) \qquad (4\text{-}1)$$

Consider its inverse form, $\eta = f(i)$, we get the **Tafel Equation** for the cathodic process (high mass transfer rate):

$$\eta = a - b \log |i| \qquad (4\text{-}2)$$

Where $a = \frac{2.303RT}{\alpha z F} \log i_o, b = \frac{2.303RT}{\alpha z F}$.

And we can get $\alpha = 2.303RT/bzF$; $i_o = a\alpha zF/2.303RT$.

Based on Tafel plots and above equations, the Tafel slope, charge transfer coefficient, and exchange current density of all six thiols are calculated and summarized in Table 4.4.

Table 4.4 Cu electrodeposition reaction kinetic parameters with different thiols

Thiols	Tafel slope (mV/decade)	Charge transfer coefficient	Exchange current density (mA/cm^2)
Additive-free	-121	0.50	1.822
Cl-PEG	-135	0.44	0.079
Cl-PEG-SPS	-122	0.51	0.501
Cl-PEG-UPS	-137	0.43	0.126
Cl-PEG-OPX	-78	0.76	0.032
Cl-PEG-DPS	-74	0.80	0.025
Cl-PEG-ZPS	-125	0.47	0.079
Cl-PEG-MPS	-96	0.62	0.126

The exchange current density:

When an electrode is at the equilibrium, $\Delta\phi$ has its equilibrium value $\Delta\phi eq$ and the net current is zero. Even though the net current is zero at equilibrium, we still envision balanced faradaic activity that can be expressed in terms of the exchange current density, i_o, which is equal in magnitude to either component current i_c or i_a. This partial current at anode or cathode on an atomic scale means that a constant exchange of charge carriers (electrons or ions) takes place across the metal-solution interface.

The exchange current density is one of the most important parameters of electrochemical kinetics. It defines the kinetic properties of the particular electrochemical reaction and the electrode material. Exchange current density in real systems reflect the wide range of k^o, the standard heterogeneous reaction rate constant [13]. The exchange current can be viewed as a kind of “idle speed” for charge exchange across the interface. It is also a measurement of any system’s ability to deliver a net current without a significant energy loss due to activation.

The exchange current density of six model six thiols in a Cl+PEG+Thiol electrolyte is summarized in Table 4.4. From this summary, we can clearly see that additive-free electrolyte is the easiest electrolyte to be activated for electrodeposition reaction, followed by Cl+PEG+SPS bath. OPX, DPS, and ZPS have an exchange current density even smaller than Cl+PEG bath, which indicated a strong inhibition by these additives in the beginning of the reaction. They require a large overpotentail to activate the reaction. UPS and MPS have higher exchange current density than OPX, DPS, and ZPS, but still much lower than SPS electrolyte. SPS electrolyte has highest exchange current density among six thiols, which indicates more favorable kinetics for the copper deposition reaction. This could be the cause that SPS electrolyte has the best superfilling capability among six thiols.

Tafel slope and charge transfer coefficient

If the electrode kinetics are fairly facile, we will approach the mass transfer limited current by the time such an extreme overpotential is established. Tafel relationship cannot be observed for such systems, because they require the absence of mass transfer effects on the current. When the electrode kinetics are sluggish and significant activation overpotential are required, good Tafel relationships can be seen. This point underscores the fact that Tafel behavior is an indicator of totally irreversible kinetics. Systems in that category allow no significant current flow except at high overpotentials, where the faradaic process is effectively unidirectional and, therefore, chemically irreversible.

The charge transfer coefficient, α, is a measure of the symmetry of the energy barrier to reaction. In most systems α turns out to lie between 0.3 and 0.7 [13]. It is an indicator for the severity of irreversible reaction, which is contributed by reaction surface. Careful evaluation of kinetic parameters shows that none of them permits a determination of α without knowledge of z, the number of limiting step electron. That is, one can only determine αz. In complex electrode processes involving more than one charge transfer step, the z value of the kinetically limiting step may not be readily apparent.

From Table 4.4 of electrodeposition kinetic parameters, we can see that additive-free electrolyte has a charge transfer coefficient of 0.5, which corresponded to a classical two-stage reversible reaction mechanism for the deposition of copper accepted by many researchers [3]. This mechanism is reviewed in following section. SPS electrolyte has a Tafel slope of –122 mV and charge transfer coefficient of 0.51, which indicated a very similar two-stage mechanism as additive-free electrolyte. For rest of thiols, there is a significant cathodic Tafel slope and corresponding charge transfer coefficient change compared with additive-free copper electrolyte. It suggested a more complex electrode process than the simple one electron transfer for additive-free copper electrolyte. More discussion of reaction mechanism is discussed in following section.

4.3.2 Mechanisms for the action of thiols

Experimental investigations of the chemical mechanism of Cu deposition with additives are complicated by the multicomponent additive mixtures necessary to obtain superfilling. Among these studies available in the open literature, a minimum of three components of Cl+PEG+thiol is necessary to achieve the superfilling in submicrometer cavities.

From Cu electrodeposition without any organic additives, a Tafel slope of –121 mV and the corresponding charge transfer of 0.50 was obtained by this investigation, which is in good agreement with other research results [3]. They showed that a charge transfer coefficient of 0.50 corresponded to a classical two-stage mechanism for the deposition of copper.

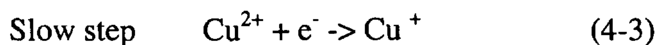

Slow step $Cu^{2+} + e^- \rightarrow Cu^+$ (4-3)

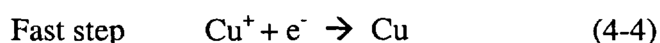

Fast step $Cu^+ + e^- \rightarrow Cu$ (4-4)

It was proposed that the first step in this process occurred slowly and was rate controlling with Cu^+ existing in equilibrium with copper at the electrode surface.

The effect of PEG has been elucidated by a kinetic study of deposition in chloride-only and PEG-chloride baths, and a quartz crystal microbalance (QCM) investigation of PEG adsorption [5,7]. The results showed that in the presence of chloride, PEG functions as an inhibitor for deposition, adsorbing at high coverage and blocking sites for cupric ion adsorption.

The thiol has been proposed to adsorb competitively with the inhibitor [12]. A widely accepted generic model of copper electrodeposition with multicomponent additives is reviewed in chapter 3. Copper deposition proceeds via two consecutive irreversible reaction steps:

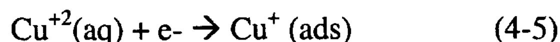

$$Cu^{+2}(aq) + e- \rightarrow Cu^{+} (ads) \qquad (4\text{-}5)$$

$$Cu^{+} (ads) + e- \rightarrow Cu \qquad (4\text{-}6)$$

However, for each individual thiol, this process could be very complex and hard to prove.

SPS showed a depolarizing effect (accelerating). The mechanisms accounting for this effect generally involve the formation of surface complexes, containing organic liqands which reduce more rapidly at more positive potentials than the corresponding aqueous complexes, thus lowering the activation energy barrier [3]. Zukauskaite et al.[3] Used potentiodynamic and UV spectroscopic techniques to show that over the potential range used for copper deposition, Cu(I) organo complexes were present and that SPS was electroreduced to 3-mercapto-propanesulphonic acid (MPS), $HS(CH_2)_3SO_3H$ (see equation 4-7). MPS then reduces Cu^{2+} to produce a Cu(I) thiolate complex and SPS is regenerated. The SPS can again be reduced while the Cu(I) complex undergoes reduction to produce copper metal and MPS. A possible reaction mechanism is as follows:

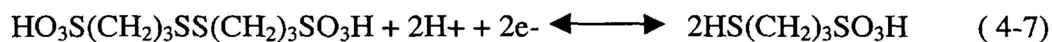

$$HO_3S(CH_2)_3SS(CH_2)_3SO_3H + 2H+ + 2e- \longleftrightarrow 2HS(CH_2)_3SO_3H \qquad (4\text{-}7)$$

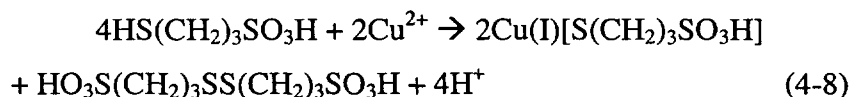

$$4HS(CH_2)_3SO_3H + 2Cu^{2+} \rightarrow 2Cu(I)[S(CH_2)_3SO_3H] + HO_3S(CH_2)_3SS(CH_2)_3SO_3H + 4H^{+} \qquad (4\text{-}8)$$

SPS is therefore able to participate in repeated oxidation and reduction cycles and depolarization occurs because Cu^{2+} reduction to Cu^{+} occurs chemically in reactions involving the additive in contrast to a purely electrochemical Cu^{2+} to Cu^{+} electroreduction process.

Healy et al.[10,11] Suggested an alternative mechanism for the decomposition of SPS in electroplating baths. He showed that SPS acts as brightener by film formation at sites where there is a high local flux of material from the solution. The film is a copper(I) complex, most likely $Cu(I)SCH_2CH_2CH_2SO_3H$, and its further reduction leads to copper metal. This again involved the formation of a stable Cu(I) complex $Cu(I)S(CH_2)_3SO_3H$, however, in this mechanism, he speculated that SPS reacts directly with Cu^{+} ions to form the complex:

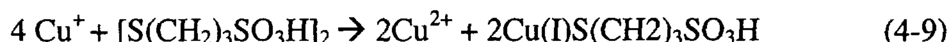

$$4\,Cu^{+} + [S(CH_2)_3SO_3H]_2 \rightarrow 2Cu^{2+} + 2Cu(I)S(CH2)_3SO_3H \qquad (4\text{-}9)$$

The observed reduction of SPS is only possible because of the strong interaction of the thiolate ion with the Cu(I). In the absence of complex formation, neither Cu(I) nor Cu(o) are strong enough to reduce SPS.

MPS is half the structure of SPS and has a close electrochemical characteristic with SPS. Healy et al. suggested again the reaction mechanism of thiols with copper(II) leading to copper(I) dithiolate complexes for MPS. With MPS as the reactant in an acid copper plating bath, the corresponding reaction would be

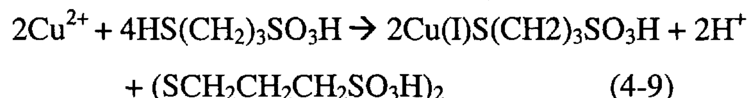

$$2Cu^{2+} + 4HS(CH_2)_3SO_3H \rightarrow 2Cu(I)S(CH2)_3SO_3H + 2H^{+} + (SCH_2CH_2CH_2SO_3H)_2 \qquad (4\text{-}9)$$

From chemical transformation (4-9), it is believe that MPS will be oxidized immediately and most of the material will be converted to SPS. Therefore, the only possible brightening agents in the bath are SPS and the product from the air oxidation of the Cu(I)-thiolate complex. Both will be present whether the added thiol is SPS or MPS.

For UPS, OPX, DPS, and ZPS, other end of thiol and disulfide function group is replaced with different compounds. The electrochemical characterization results indicated that these different compounds have caused a significant difference for their electrochemical behavior. Based on Healy et al. proposed thiol working mechanism, these compounds have changed the reduction of thiols and the formation of stable Cu(I)-thiolate complex, which has a direct impact on the accelerating capability of thiols. The detailed working mechanism for any above four thiols has never been speculated and need further investigation.

Reference

[1]. T.P. Moffat, J.E. Bonevich, W.H. Huber, et al. "Superconformal electrodeposition of copper in 500-90 nm features," J. Electrochem. Soc., 147 (12), 2000, pp.4524-4535.

[2] P. Taephaisitphongse, Y. Cao, and A.C.West. "Electrochemical and fill study of a multicomponent additive package for copper deposition," J. Electrochem. Soc., 148(7), 2001, pp.492-497.

[3] E.E. Farndon, F.C. Walsh, S.A. Campbell. "Effect of thiourea, benzotriazole, and 4,5–dithiaoctane-1,8-disulphonic acid on the kinetics of copper deposition from dilute acid sulphate solutions" J. Appl. Electrochem., 25, 1995, pp.574-583.

[4] G.-S. Tzeng, "Effect of additive agents on the kinetics of Tin electrodeposition from an acidic solution of Tin(II) sulfate," Plating & Surface Finishing, November, 1995, pp.67-71

[5] J. Kelly, C. West. "Copper deposition in the presence of polyethylene glycol, I. quartz crystal microbalance study" J. Electrochem. Soc., 145(10), 1998, pp.3472 – 3476

[6] J. Kelly, A. West. "Copper deposition in the presence of polyethylene glycol II. electrochemical impedance spectroscopy," J. Electrochem. Soc., 45 (10), 1998, pp.3477-3481.

[7] J.P.Healy, D. Pletcher. "The chemistry of the additives in an acid copper electroplating bath, Part I. Polyethylene glycol and chloride ion," J. Electroanal. Chem., 338, 1992, pp.155-165.

[8] K. R. Hebert. "Analysis of current-potential hysteresis during electrodeposition of copper with additives," J. Electrochem. Soc., 148 (11), 2001, pp.726-732.

[9] J. Kelly, C. Tian, and A.C. West. "Leveling and microstructural effects of additives for copper electrodeposition," J. Electrochem. Soc., 146 (7), 1999, pp. 2540-2545.

[10] J.P. Healy, D. Pletcher, M. Goodenouth. " The chemistry of the additives in an acid copper electroplating bath, Part II. The instability of 4,5-dithiaoctane-1,8-disuphoneic acid in the bath on open circuit," J. Electroanal. Chem., 338, 1992, pp.167-177.

[11] J.P. Healy, D. Pletcher, M. Goodenouth. " The chemistry of the additives in an acid copper electroplating bath, Part III. The mechanism of brightening by 4,5-dithiaoctane-1,8-disulphonic acid," J. Electroanal. Chem., 338, 1992, pp.179-187.

[12] Y. Cao, P. Taephaisitphongse, R. Chalupa, and A. C. West. "Three-additive model of superfilling of copper," J. Electrochem. Soc., 148 (7), 2001, pp.466-472.

[13]. A.J. Bard and L.R. Faulkner. Electrochemical Methods. John Wiley & Sons, 1980, pp.105-121.

Chapter 5

Influence of Aging of Thiols on Cu Electrodeposition

Thiols are the least stable additive components. They are subject to hydrolysis in acidic solution, oxidation by air (oxygen), electrochemical oxidation at anode, and catalytic decomposition at Cu surface. The by-products of thiols are often detrimental to properties of films deposited and trench filling capability. It was the purpose of this research to study the effects of thiols on the electrode surface deposition using rotating disc technique, to especially focus on the effects of aging of acidic thiol solutions and to find criteria for detecting such effects.

5.1. SPS Degradation Evaluation in Cl-PEG-SPS Bath

The acidic Cl-PEG-Thiol solutions were allowed to age at room temperature without contact with metallic copper (anode). Thus hydrolysis of thiols and complex formation in solution could take place but no reactions between thiols and metallic copper were possible during storage. Cyclic Voltammetry and Chronoamperometry were then utilized in 3, 7, and 16 day old solutions to characterize the influence of thiol degradation on Cu electrodeposition on a Pt electrode surface.

Cyclic voltammetry experiments during deposition of Cu films revealed current-potential (I-E) hysteresis. The hysteresis is unusual, in that the cathodic deposition current is smaller in the initial cathodic scan than in the return anodic scan. Hysteresis evidently results from transient changes of the surface coverage of PEG, reflecting a transition between "active" and "inhibited" states for deposition. This activated

deposition may correspond to the acceleration of plating rate observed during bottom-up filling of cavities. Therefore, the thiols degradation can be indirectly measured by their degradation of acceleration capability. This investigation has proved I-E hysteresis measurement is a sensitive tool to detect the aging of thiols [1]. Chronoamperometry measurement is a supplement measurement for cyclic voltammetry result to confirm the accelerating degradation of thiols by checking the deposition current over time. It is especially important for thiols such as UPS and ZPS that are lacking of clear hysteresis from beginning.

Cyclic Voltammetry

Fig. 5.1 shows the influence of 12 ppm SPS decay in the standard Cl+PEG+SPS electrolyte. It is clearly seen that the i-E hysteresis degrades a little for first three days, but aging of SPS is obvious after seven days. According to the literature [2], the decay would be even faster if the solutions were aging in contact with metallic copper. Additive can be consumed at the cathode by incorporation into the deposit and/or by the electrochemical reaction at the cathode or anode. Thiols are in particular vulnerable for electrochemical oxidation at anode. After 16 days, the hysteresis characteristic of CV curve totally disappeared. This indicated that SPS was totally degraded in an acidic solution after two weeks.

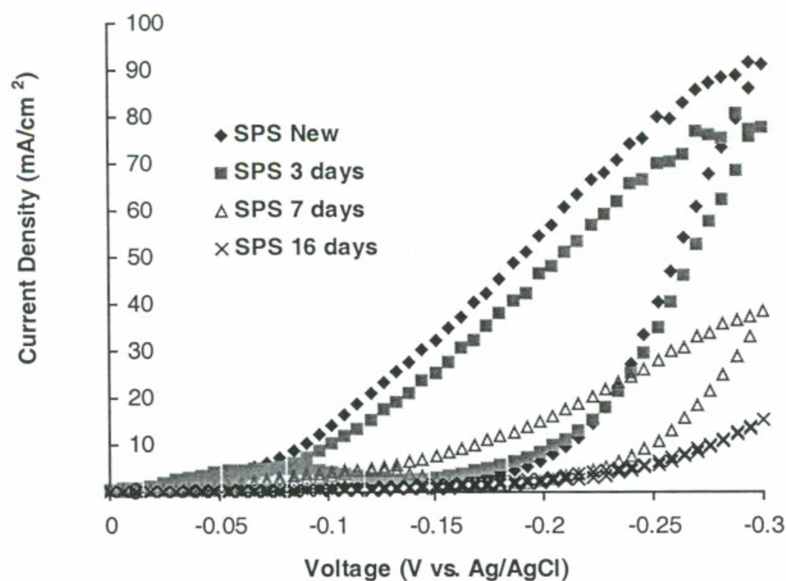

Fig. 5.1 Influence of aging of 12 ppm SPS on the current-potential curves at Pt RDE. The base solution contained 1.8 M H_2SO_4, 0.24 M $CuSO_4$, 50 ppm Cl, and 300ppm PEG (MW 4600).

Chronoamperometry Responses

The chronoamperometry curves of aging Cl+PEG+SPS bath is shown in Fig. 5.2. It is seen that a dramatic degradation of accelerating capability of SPS bath occurred in the first three days. SPS bath showed very small response with overpotential of –0.15 V, especially the first 15 seconds. By the end of seven days, little SPS accelerating capability is left. After 16 days of aging, it becomes almost equivalent to a Cl+PEG only bath with no accelerating. This observation provided another support the cyclic voltammetry measurement result.

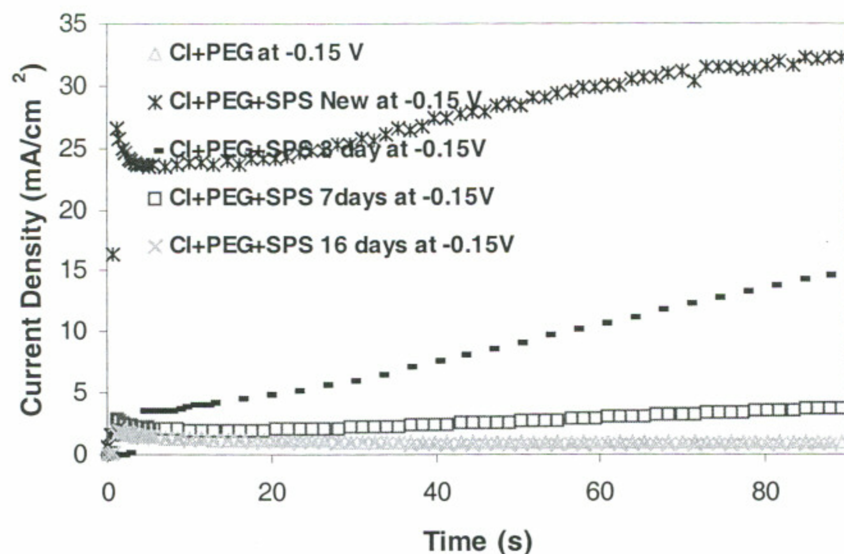

Fig. 5.2 Influence of aging of 12 ppm SPS on the chronoamperometry curves at Pt RDE. The base solution contained 1.8 M H_2SO_4, 0.24 M $CuSO_4$, 50 ppm Cl, and 300ppm PEG (MW 4600)

5.2. UPS Degradation Evaluation in Cl-PEG-UPS Bath

Cyclic Voltammetry

As discussed in chapter 4, UPS is acting more like a suppressor than an accelerator. It retards electrodeposition reaction. The hysteresis CV curves, in Fig. 5.3, show the aging of UPS bath in 16 days. Although it is lacking of i-E hysteresis, UPS does show degradation over time, mainly after three days. By the end of seven days, it showed no signs of any acceleration.

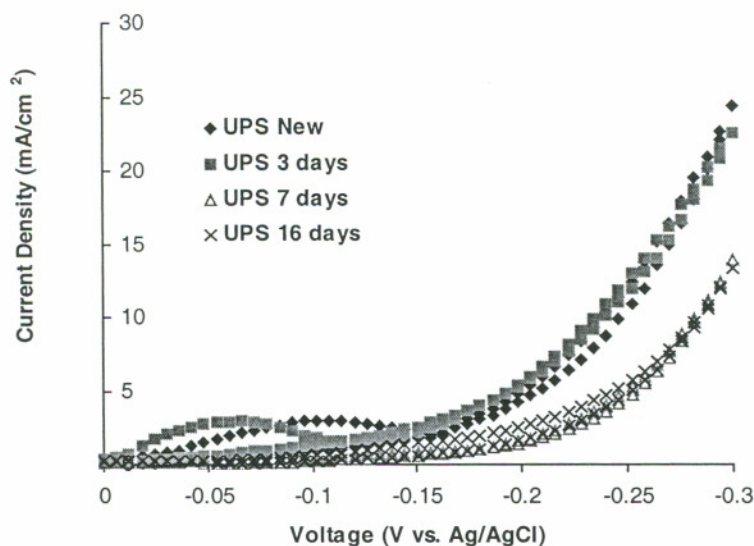

Fig. 5.3 Influence of aging of 12 ppm UPS on the current-potential curves at Pt RDE. The base solution contained 1.8 M H_2SO_4, 0.24 M $CuSO_4$, 50 ppm Cl, and 300ppm PEG (MW 4600)

Chronoamperometry Responses

The CA response curves of UPS bath, as shown in Fig. 5.4, are consistent with CV characterization result of UPS bath aging. It indicates that a major degradation happened in the first three days. By the end of seven days, UPS bath became equivalent to a Cl+PEG bath.

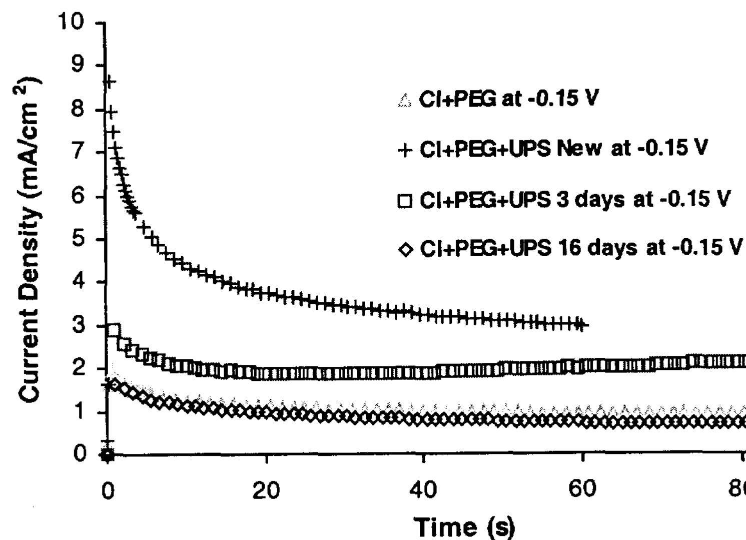

Fig. 5.4 Influence of aging of 12 ppm UPS on the chronoamperometry curves at Pt RDE. The base solution contained 1.8 M H_2SO_4, 0.24 M $CuSO_4$, 50 ppm Cl, and 300ppm PEG (MW 4600)

5.3. OPX Degradation Evaluation in Cl-PEG-OPX Bath

Cyclic Voltammetry

The CV hysteresis of aging OPX bath is shown in Fig. 5.5. It has similar degradation behavior compared to benchmark electrolyte of SPS bath, but with a moderate hysteresis loop as discussed in Chapter 4. It shows a major degradation in first seven days. After 16 days, the hysteresis characteristic of Cl+PEG+OPX bath totally disappeared. It became equivalent to a Cl+PEG bath.

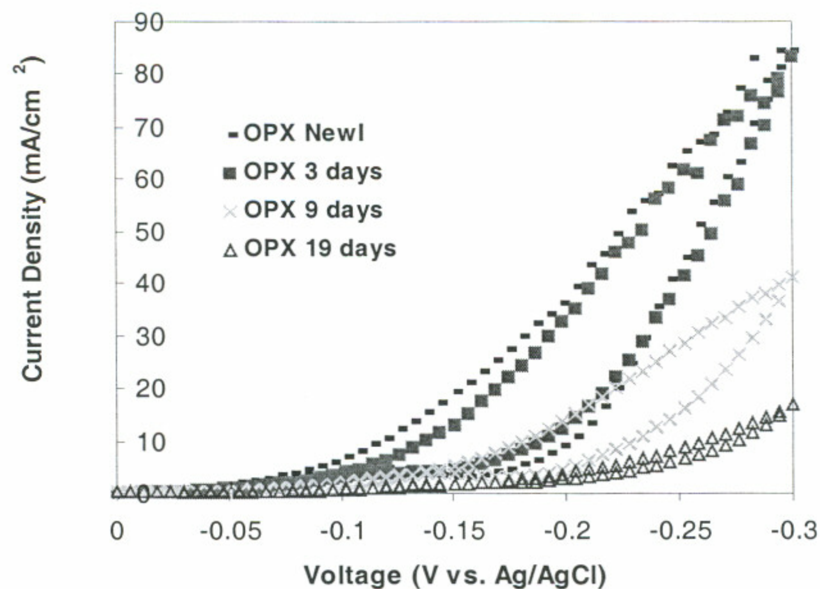

Fig. 5.5 Influence of aging of 12 ppm OPX on the current-potential curves at Pt RDE. The base solution contains 1.8 M H_2SO_4, 0.24 M $CuSO_4$, 50 ppm Cl, and 300ppm PEG (MW 4600)

Chronoamperometry Responses

The CA response curve of OPX bath aging under –0.15 V vs. Ag/AgCl overpotential is shown in Fig. 5.6. It indicates a major degradation of accelerating capability in the first three days. After 6 days, the accelerating capability of OPX bath totally disappeared and electrodeposition reaction is suppressed. This is very similar to SPS bath degradation characteristic.

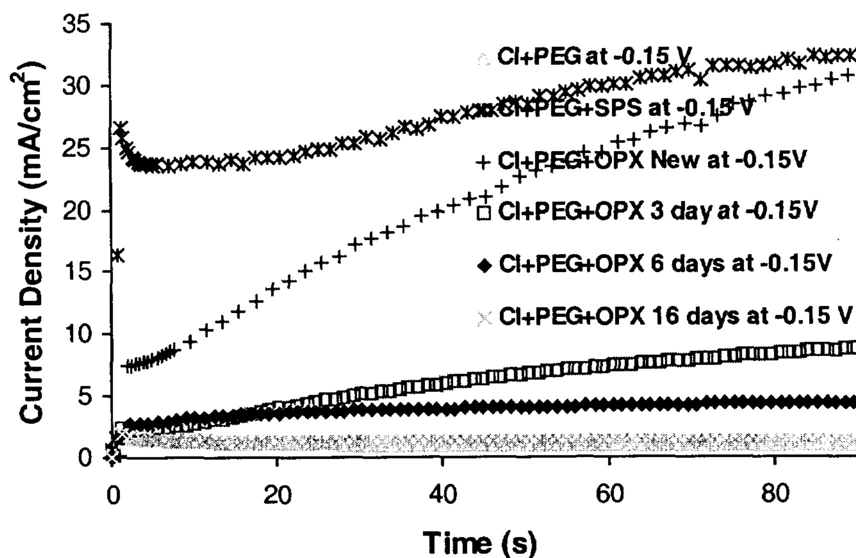

Fig. 5.6 Influence of aging of 12 ppm OPX on the chronoamperometry curves at Pt RDE. The base solution contained 1.8 M H_2SO_4, 0.24 M $CuSO_4$, 50 ppm Cl, and 300ppm PEG (MW 4600)

5.4 DPS Degradation Evaluation in Cl-PEG-DPS Bath

Cyclic Voltammetry

The i-E hysteresis of Cu electrodeposition reaction of DPS aging bath is shown in Fig. 5.7. It is seen that there is very little degradation after 3 days aging for DPS bath. After seven days, the bath is stabilized and there is no change after sixteen days. It still has a moderate hysteresis loop even after sixteen days. Compared to benchmark electrolyte of SPS bath, this is a unique characteristic of the DPS electrolyte.

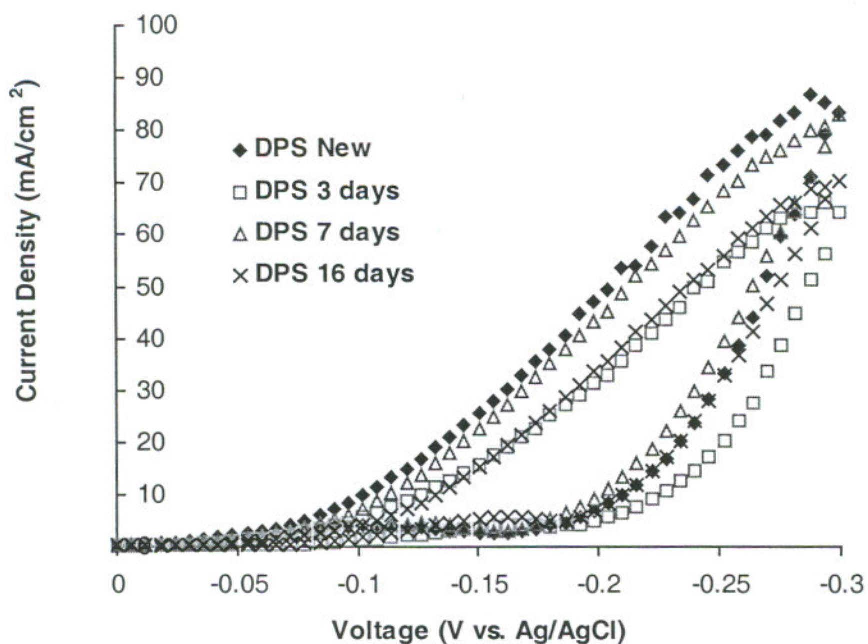

Fig. 5.7 Influence of aging of 12 ppm DPS on the current-potential curves at Pt RDE. The base solution contained 1.8 M H_2SO_4, 0.24 M $CuSO_4$, 50 ppm Cl, and 300ppm PEG (MW 4600)

Chronoamperometry Responses

The chronoamperometry curves of DPS aging bath is shown in Fig. 5.8. It shows that DPS degraded in first three days then stabilized over two weeks. This result is consistent with hyesteresis CV result presented above.

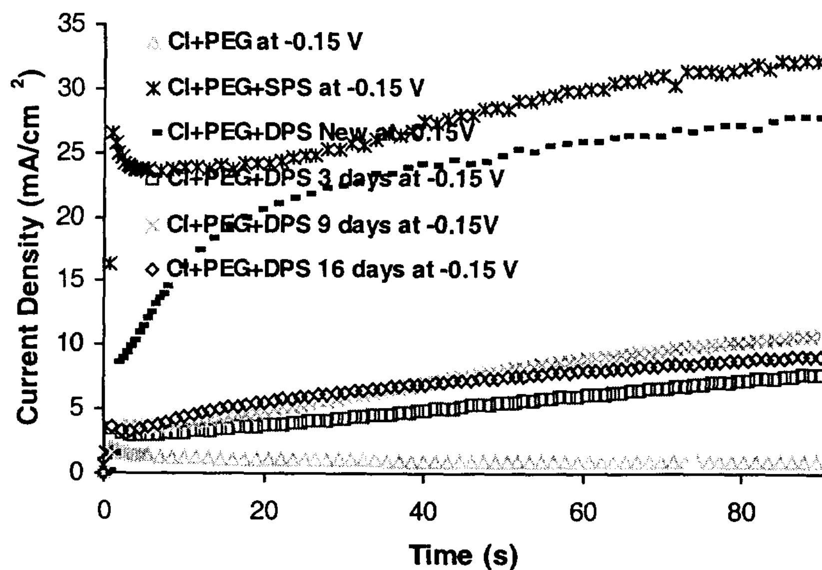

Fig. 5.8 Influence of aging of 12 ppm DPS on the chronoamperometry curves at Pt RDE. The base solution contained 1.8 M H_2SO_4, 0.24 M $CuSO_4$, 50 ppm Cl, and 300ppm PEG (MW 4600)

5.5 ZPS Degradation Evaluation in Cl-PEG-ZPS Bath

Cyclic Voltammetry

As discussed in Chapter 4, ZPS behaves more like a suppressor and retards the electrodeposition reaction. This is confirmed by the hysteresis curves shown in Fig. 5.9. Although it has a little degradation over time, the hysteresis curves did not change too much after seven days. However, after sixteen days, the hysteresis curve did show a different shape compared with previous curves. This shape change could be the indication of by-production generation.

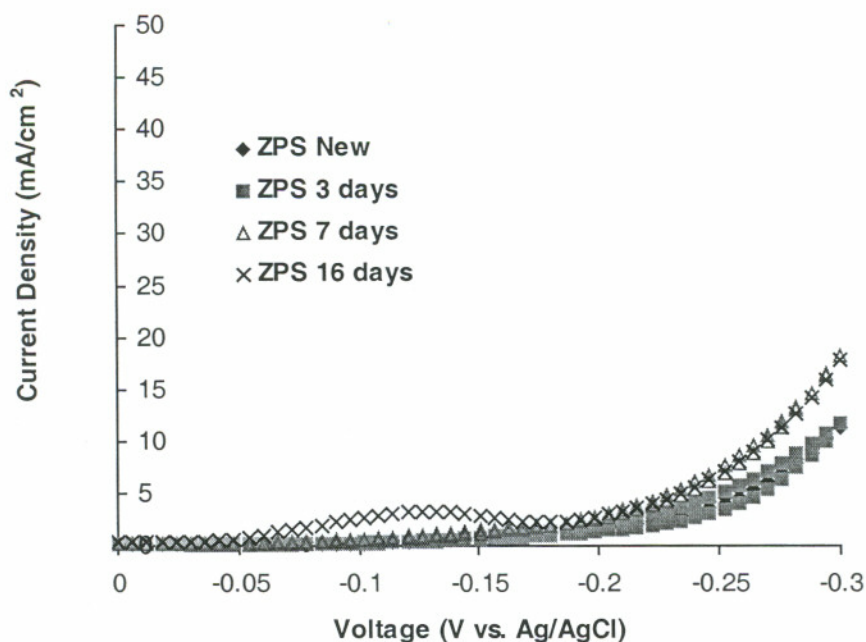

Fig. 5.9 Influence of aging of 12 ppm ZPS on the current-potential curves at Pt RDE. The base solution contained 1.8 M H_2SO_4, 0.24 M $CuSO_4$, 50 ppm Cl, and 300ppm PEG (MW 4600)

Chronoamperometry Responses

The chronoamperomety curves of ZPS bath is shown in Fig. 5.10. It clearly has a suppressing characteristic. This suppressing characteristic changed very little over time, which is in consistent with hysteresis measurement result.

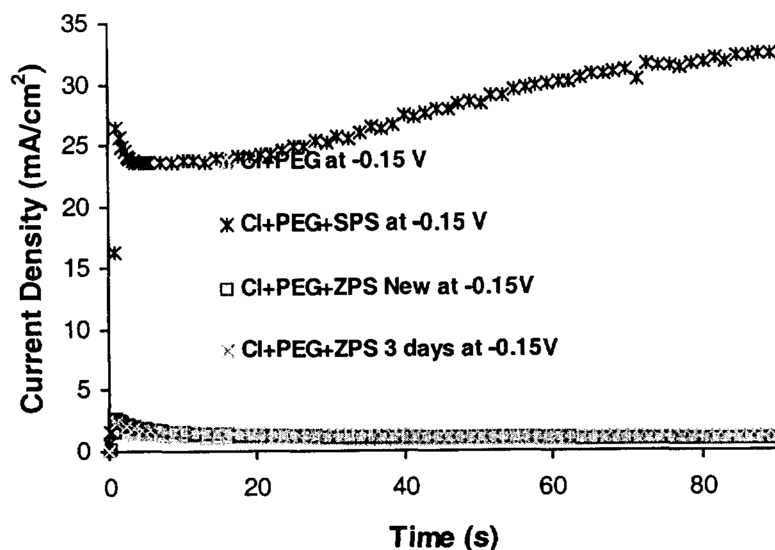

Fig. 5.10 Influence of aging of 12 ppm ZPS on the chronoamperometry curves at Pt RDE. The base solution contained 1.8 M H_2SO_4, 0.24 M $CuSO_4$, 50 ppm Cl, and 300ppm PEG (MW 4600)

5.6 MPS Degradation Evaluation in Cl-PEG-MPS Bath

Cyclic Voltammetry

The hysteresis measurement of Cl+PEG+MPS bath is shown in Fig. 5.11. It shows a stronger accelerating capability than the fresh bath after three days bath aging. Then the bath gradually degrades into a totally suppressed bath in sixteen days. This increase of acceleration in the first few days can be explained by accelerator's special characteristics. The accelerator is known to decompose to other strongly accelerating species. However, after sixteen days, it degraded to something without any accelerating capability. MPS demonstrates a different characteristic than SPS bath for its aging. This is the unique property of MPS bath.

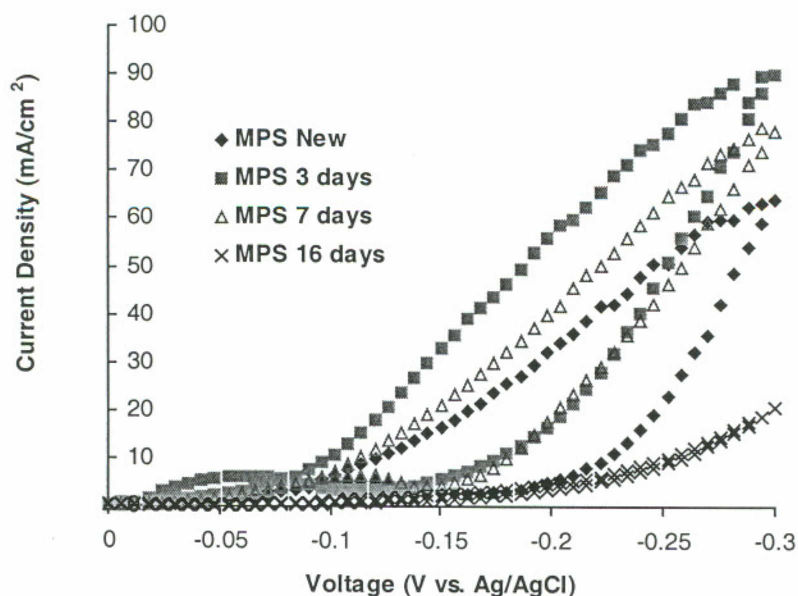

Fig. 5.11 Influence of aging of 12 ppm MPS on the current-potential curves at Pt RDE. The base solution contained 1.8 M H_2SO_4, 0.24 M $CuSO_4$, 50 ppm Cl, and 300ppm PEG (MW 4600)

Chronoamperometry Responses

Fig. 5.12 shows current-time CA curves for Cl+PEG+MPS electrolyte. It indicates a minor degradation of MPS accelerating capability in the first three days. After sixteen days, the accelerating capability totally disappeared. The CA characteristic of MPS bath is not consistent with its hysteresis characteristic, and needs further investigation.

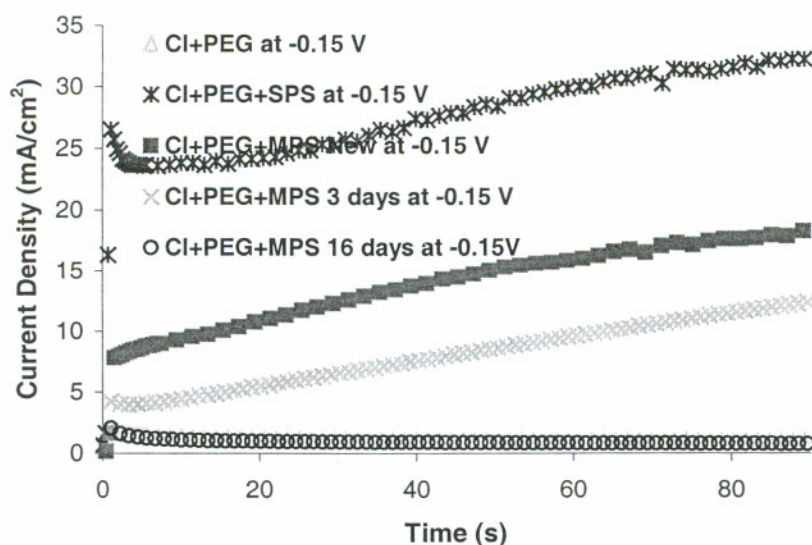

Fig. 5.12 Influence of aging of 12 ppm MPS on the chronoamperometry curves at Pt RDE. The base solution contains 1.8 M H_2SO_4, 0.24 M $CuSO_4$, 50 ppm Cl, and 300ppm PEG (MW 4600)

5.7 Thiols degradation mechanism in an acid copper electroplating bath

Several mechanisms for the decomposition of the additive have been proposed.

Heatly et al.[3], investigated the instability of SPS in an acid copper electroplating bath by electrochemistry methods and UV-visible spectra on samples of solution. He suggested that SPS is not stable in the acid copper electroplating bath even when it is at open circuit. The decomposition of the additive occurs whenever the solution contains cupric ion and it is in contact with copper metal. Oxygen is not essential for SPS to be unstable, hence, the decomposition cannot be initiated by oxygen reduction. Moreover, the rate of decomposition of SPS is not influenced by other common additives to the bath, e.g. chloride ion and polyethylene glycol. Since both Cu2+ and Cu appear necessary for "rapid" decomposition, he proposed that the first step in the mechanism must be

$$Cu^{2+} + Cu \longleftrightarrow 2Cu^{+} \quad (5\text{-}1)$$

The details of the following steps remain speculative but it is clear that a Cu(I)-thiolate complex is the stable product in the absence of oxygen. One possible reaction is

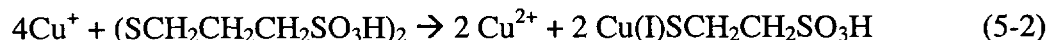

$$4Cu^{+} + (SCH_2CH_2CH_2SO_3H)_2 \rightarrow 2\,Cu^{2+} + 2\,Cu(I)SCH_2CH_2SO_3H \qquad (5\text{-}2)$$

The reduction of SPS is possible because of the strong interaction of the thiolate anion with copper(I). In the normal operating conditions of the plating bath in contact with air, the final step will be

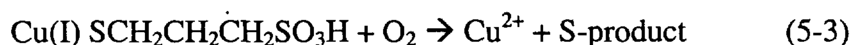

$$Cu(I)\,SCH_2CH_2CH_2SO_3H + O_2 \rightarrow Cu^{2+} + S\text{-product} \qquad (5\text{-}3)$$

Where the S-product is certainly not SPS and is probably a more oxidized product such as propane-1,3-disulphonic acid.

When no cupric ion is present or can be formed in solution, a very much slower decomposition still occurs. It is thought that the reducing agent is now copper metal

$$2Cu + (SCH_2CH_2CH_2SO_3H)_2 \rightarrow 2\,Cu(I)SCH2CH_2CH_2SO_3H \qquad (5\text{-}4)$$

And that although Cu is a stronger reducing reagent than Cu^{+}, this decomposition route is slower because the reproportionation process (5-1) is much faster than this alternative heterogeneous reaction. In the practical situation this mechanism is too slow to contribute significantly to the loss of SPS.

When MPS is used as additive, it is identical to that from the reaction of SPS with Cu^{2+} +Cu, and MPS is oxidized to a complex Cu(I)-thiolate ligand as reviewed [4].

Other thiols decomposition may follow the same mechanism as SPS and MPS. UPS, OPX, DPS, and ZPS could be oxidized to Cu(I)-thiolate complex by Cu^{+}. If SPS could not be regenerated in this process, and Cu(I)-thiolate is further oxidized to S-product, they lose their accelerating capability for electroplating.

Reference

[1] G. Fabricius, K. Kontturi, G. Sundholem. "Influence of thiourea and thiourea aging on the elecrodeposition of copper film from acid sulfate solutions studied by the ring-disc technique," J. Appl. Electrochem., 26, 1996, pp.1179-1183.

[2] K. R. Hebert. "Analysis of current-potential hysteresis during electrodeposition of copper with additives," J. Electrochem. Soc., 148 (11), 2001, pp.726-732.

[3] J.P. Healy, D. Pletcher, M. Goodenouth. " The chemistry of the additives in an acid copper electroplating bath, Part II. The instability of 4,5-dithiaoctane-1,8-disuphoneic acid in the bath on open circuit," J. Electroanal. Chem., 338, 1992, pp.167-177.

[4] J.P. Healy, D. Pletcher, M. Goodenouth. " The chemistry of the additives in an acid copper electroplating bath, Part III. The mechanism of brightening by 4,5-dithiaoctane-1,8-disulphonic acid," J. Electroanal. Chem., 338, 1992, pp.179-187.

Chapter 6

Summary and Conclusions

The copper electrodeposition on ULSI interconnects was studied in the absence of and in the presence of different organic additives. Six different model thiols: SPS, UPS, DPS, OPX, ZPS, and MPS in a Cl-PEG-thiol electrolyte package were characterized for their electrochemical characteristics and aging degradation in acid bath. Each electrolyte package's electrodeposition kinetic and trench fill capability were examined. The microstructure of electroplated Cu film from each electrolyte package was studied. Thiol degradation in acidic copper solution was evaluated by electrochemical methods. The electrochemical methods employed include linear sweep voltammetry(LSV), chronoamperometry(CA), and cyclic voltammetry (CV) on a rotating disk electrode using a EG&G M270 Potentiostat. Copper deposition was carried out in a modified Hull cell under a well-mixed condition. Fill was examined on a coupon wafer plated under DC conditions that corresponded to blanket films grown galvanostatically at a three steps of $3mA/cm^2$, $9.5mA/cm^2$, and $23\ mA/cm^2$.

Cu electrodeposition in the absence of organic additive showed no sign of i-E hysteresis for the reverse plating. The lack of hysteresis of VMS indicated no irreversible changes of the surface chemistry. The Tafel slope of electrodeposition log(i) – E curve indicated a two step reaction mechanism with Cu^{2+} to Cu^{+} as the rate controlling step. The lack of polarization of plating reaction resulted in a conformal fill growth, which formed consistent center voids. Electroplated Cu film from VMS bath was predominately (111) oriented. The microstructure of Cu film electrodeposited from additive free electrolyte was primarily influenced by plating current density. However, when organic additives are added to the electrolyte, they showed a dominated effect on

Cu film roughness as shown in Table 6.1. In the table, the film roughness was measured and calculated with a 10 μm field of view. To compute the RMS roughness, a two dimensional plane is fit to the AFM height data. The resulting standard deviation of the fit is reported as the RMS surface roughness. The mean roughness (Ra), is also listed.

Table 6.1 Roughness of Cu films electrodeposited with various electrolytes

Electrolyte	RMS (nm)	Ra (nm)
Additve-free (VMS)	105	68
Cl+PEG	79	60
Cl+PEG+SPS	55	44
Cl+PEG+UPS	83	59
Cl+PEG+OPX	46	30
Cl+PEG+DPS	53	35
Cl+PEG+ZPS	49	39
Cl+PEG+MPS	46	36

Cu electrodeposition with the addition of PEG provided significant inhibition of the deposition reaction compared to the polarization characteristics for copper deposition from the bath containing only chloride ions. When chloride, PEG, and SPS are all present, the combined action of all three additives yields net inhibition relative to a additive-free electrolyte, but an acceleration relative to Cl-PEG electrolyte, which reflects the competition between the effects of PEG and SPS. Tafel kinetics for copper deposition from solutions containing organic additives showed marked changes compared with additive-free electrolytes. The observed changes in the cathodic Tafel slope and the corresponding decrease in charge transfer coefficient α_c in the presence of organic additives suggests that the process taking place on the electrode surface is no longer a simple one electron transfer. This may be attributed to complex formation between organic additives and cuprous ions at the electrode surface. Further more, the

presence of PEG gives the lower exchange current density, i.e., makes charge transfer reaction more difficult than the additive-free electrolyte. On the other hand, the addition of SPS increases the exchange current density compared to PEG only electrolyte. Significant i-E hysteresis is apparent in the case of Cl-PEG-SPS electrolyte, although little or no hysteresis is observed for the binary combination of Cl-PEG, or the additive-free electrolyte. The fill study results showed that when SPS and PEG ratio reached a certain point, strong superfill was observed and good trench fill was achieved. The Cu film microstructure of Cl+PEG bath is smoother than Cu film electroplated from additive free electrolyte. However, Cu film from Cl+PEG+SPS bath showed a very shiny surface which was much smoother than Cu film from Cl+PEG bath (see table 6.1). The degradation of SPS in acidic solution showed a major bath aging in 3-7 days. After sixteen days, the accelerating capability of SPS bath totally disappeared.

Electrodeposition with Cl+PEG+UPS electrolyte showed very similar i-E relationship with Cl+PEG bath with deposition rate totally suppressed. UPS bath showed no i-E hysterisis. This characteristic was very similar to behavior of a suppressor, and showed no acceleration and resulted in a conformal trench growth. Consistent center voids were observed for fill study. Based on these characterizations, UPS acted more like a suppressor and retarded the Cu deposition. The Cu film electrodeposited from UPS bath showed a very different reddish color with no shiny surface. The roughness of the film is much higher than Cu film from SPS electrolyte bath, even worse than Cu film from Cl+PEG electrolyte bath. UPS was not stable in acidic solution and showed a major degradation in first seven days.

Electrodeposition with Cl+PEG+OPX electrolyte showed a moderately suppressed current, but more accelerated than Cl-PEG bath. OPX bath demonstrated a moderate i-E hysteresis. The fill result showed a center void, which indicated not strong enough bottom-up fill or superfilling capability. The Cu film microstructure electroplated from OPX bath showed a shiny surface with equivalent roughness to Cu film from SPS bath. OPX bath showed a major aging in the seven days. After sixteen days, OPX bath became equivalent to a Cl+PEG bath.

Electrodeposition with Cl+PEG+DPS bath showed a very a strong i-E hysteresis similar to SPS bath. However, the exchange current density of DPS bath is the lowest among all electrolytes with organic additives, which indicates the high activation barrier to start the reaction. The chronoamperometry curve showed a depressed current response in the first twenty seconds of deposition that is consistent with low exchange current density of DPS electrodeposition reaction. A good fill result was not observed for Cl+PEG+DPS bath. The microstructure of Cu film electrodeposited from Cl+PEG+DPS bath showed a shiny film surface with similar film roughness as Cu film electrodeposited from SPS bath. The aging study of DPS bath indicated that DPS is the most stable thiol in the acid bath among all six thiols. It still had moderate i-E hysteresis even after sixteen days.

Electrodeposition with Cl+PEG+ZPS bath showed ZPS bath has a similar i-E relationship as PEG and UPS bath with a total suppression of electrodeposition reaction. No i-E hysteresis was observed for this bath, which indicated ZPS acted more like a suppressor and retarded electrodeposition. Continuous center voids were observed for fill results. However, the microstructure of Cu film electrodeposited from ZPS bath showed a shiny surface with a film roughness equivalent to Cu film from SPS bath. This is significantly different from Cu films electroplated from PEG and UPS bath. ZPS did show degradation over time, but with a small value since it did not have accelerating capability in the beginning.

Finally, the electrodeposition with Cl+PEG+MPS bath showed less accelerating capability compared with SPS and DPS bath. MPS bath had a moderate i-E hysteresis similar with OPX bath. The fill result showed center voids similar to OPX bath fill result. The microstructure of Cu film from MPS bath showed a shiny surface with similar film roughness as Cu film from SPS bath. MPS degraded in the similar speed as OPX. By the end of sixteen days, the accelerating capability totally disappeared.

In summary, SPS has high exchange current density with a strong accelerating behavior and a strong i-E hysteresis. DPS has strong accelerating characteristic and i-E hysteresis but low exchange current density. OPX and MPS are next to SPS and DPS with moderate accelerating capability and i-E hysteresis. Finally, UPS and ZPS act more

like suppressor and retard copper electrodeposition reaction. Among six model thiols, DPS is the most stable thiol in acidic copper solution.

Although this investigation has done a very extensive research for these model thiols, several issues need to be investigated in the future for this study. Fill result can be affected by many factors such as structure of the trench, seed condition, electroplating current waveform, mass transfer of electrolyte (flow/rotation), and organic additive concentrations and their ratios. Good i-E hysteresis has been observed for DPS, OPX, and MPS. However, good gapfill was not observed from these electrolytes. Further investigation is needed to optimize these plating conditions before conclusion can be reached.

The aging of thiols in contact with metal copper anode should be investigated and the effect of aging of thiols on gapfill and film microstructure needs to be investigated for future study.

Finally, leveler is gaining its popularity for Cu electrodeposition for ULSI interconnects. Future study needs to investigate the electrolyte package that contains PEG, thiol, and leveler for the final application of this electrolyte package to next generation ULSI metallization.

Vita

The author, Charlie Chunxing Zhi, was born in Xian, Shanxi, China, in April, 1963. He enrolled in South China University of Technology in 1981 and received a B.E. in Chemical Engineering in 1985. Then he continued his study in the same school and received his M.S. in Pulp and Paper Engineering in 1988. After working in a International Investment firm in Guangzhou for four years, he came to US and enrolled in the Department of Chemical Engineering at Oregon State University in 1992. He received his M.S. in Chemical Engineering in 1995. He entered the Department of Electrical and Computer Engineering at Oregon Graduate Institute in 1998 and received his Ph.D. in 2002.

He worked in Boise Cascade Inc. for a year and half. In 1997, he start to work in Intel Corp. for Cu electrodeposition for IC chip metallization. This cutting-edge technology brought a lot of challenge and excitement to his job. The strong desire to learn and study more about this new technology pushed him to Oregon Graduate Institute to start the research in this field since 1998. With the help from his adviser and other researchers, he has done a very extensive research in the field.

He has published three research papers for his Master Degree research in Oregon State University. More papers for this research are waiting to be published.